Draft version October 1, 2008
Preprint typeset using LaTeX style emulateapj v. 10/09/06

THE PALOMAR/KECK ADAPTIVE OPTICS SURVEY OF YOUNG SOLAR ANALOGS: EVIDENCE FOR A UNIVERSAL COMPANION MASS FUNCTION

Stanimir A. Metchev*
Department of Physics and Astronomy, 430 Portola Plaza, University of California, Los Angeles, California 90095–1547
and
Lynne A. Hillenbrand
Department of Physics, Mathematics & Astronomy, MC 105–24, California Institute of Technology, Pasadena, California 91125
Draft version October 1, 2008

ABSTRACT

We present results from an adaptive optics survey for substellar and stellar companions to Sun-like stars. The survey targeted 266 F5–K5 stars in the 3 Myr to 3 Gyr age range with distances of 10–190 pc. Results from the survey include the discovery of two brown dwarf companions (HD 49197B and HD 203030B), 24 new stellar binaries, and a triple system. We infer that the frequency of 0.012–0.072 $M_\odot$ brown dwarfs in 28–1590 AU orbits around young solar analogs is $3.2^{+3.1}_{-2.7}$% (2σ limits). The result demonstrates that the deficiency of substellar companions at wide orbital separations from Sun-like stars is less pronounced than in the radial velocity "brown dwarf desert." We infer that the mass distribution of companions in 28–1590 AU orbits around solar-mass stars follows a continuous $dN/dM_2 \propto M_2^{-0.4}$ relation over the 0.01–1.0 $M_\odot$ secondary mass range. While this functional form is similar to the that for <0.1 $M_\odot$ isolated objects, over the entire 0.01–1.0 $M_\odot$ range the mass functions of companions and of isolated objects differ significantly. Based on this conclusion and on similar results from other direct imaging and radial velocity companion surveys in the literature, we argue that the companion mass function follows the same universal form over the entire range between 0–1590 AU in orbital semi-major axis and ≈0.01–20 $M_\odot$ in companion mass. In this context, the relative dearth of substellar versus stellar secondaries at *all* orbital separations arises naturally from the inferred form of the companion mass function.

Subject headings: stars: binaries: visual—stars: imaging—stars: low-mass, brown dwarfs—stars: mass function

1. INTRODUCTION

The properties of brown dwarf companions to stars are important for understanding the substellar companion mass function (CMF), the formation of brown dwarfs, and the formation and evolution of low-mass ratio binary systems. Widely-separated brown dwarf companions, in particular, are an important benchmark for studying the properties of substellar objects because of their accessibility to direct spectroscopic characterization and their relative ease of age-dating—from assumed co-evality with their host stars.

However, brown dwarf companions have been an elusive target for direct imaging. The main challenge has been the need to attain sufficient imaging contrast to detect secondaries that are $>10^3$ fainter than their host stars at angular separations spanning solar system-like scales (<40 AU = 0.″4 at 100 pc).

The problem is alleviated at young ages when brown dwarfs are brighter. In addition, nearby stars offer an additional advantage because the relevant angular scales are correspondingly wider and more accessible to direct imaging. Young nearby stars are thus the preferred targets for substellar companion searches through direct imaging.

Nevertheless, early surveys for substellar companions, performed with seeing-limited or first-generation high-contrast imaging technology (Oppenheimer et al. 2001; Hinz et al. 2002; McCarthy & Zuckerman 2004) had very low detection rates, $\lesssim 0.5$%. This low brown dwarf companion detection rate was similar to that inferred from precision radial velocity surveys (< 0.5% over 0–3 AU; Marcy & Butler 2000), and prompted McCarthy & Zuckerman (2004) to conclude that the so-called "brown dwarf desert" extends far beyond the orbital separations probed by radial velocity surveys, out to at least ≈1200 AU.

Over the past few years, advances in adaptive optics (AO) technology and high-contrast imaging methods have improved the chances for the direct imaging of substellar secondaries. Modern AO systems, with >200 corrective elements spread across the beam of a 5–10 m telescope, are able to deliver high order rectification (<250 nm r.m.s. residual error) of wavefronts perturbed by Earth's turbulent atmosphere at up to kHz rates. In addition, our empirical appreciation of the local young stellar population has improved over the past decade, as demonstrated by the recent discoveries of a large number of young (< 500 Myr) stellar associations within 200 pc from the Sun (e.g., Kastner et al. 1997; Mamajek et al. 1999; Zuckerman & Webb 2000; Zuckerman et al. 2001; Montes et al. 2001; Zuckerman & Song 2004, and references therein). These have allowed us to select more suitable targets for direct imaging searches for substellar companions.

Several recent direct imaging surveys of nearby

*Author's current address is: Department of Physics & Astronomy, State University of New York, Stony Brook, New York 11794–3800; metchev@astro.sunysb.edu
Electronic address: metchev@astro.ucla.edu

young stellar associations conducted on high-order AO-equipped telescopes (Neuhäuser & Guenther 2004, 25 A–M stars; Chauvin et al. 2005a,b, 50 A–M stars) or with the *Hubble Space Telescope* (*HST*; Lowrance et al. 2005, 45 A–M stars) have enjoyed higher detection rates (2–4 %) than the first generation of surveys. In addition, at very wide (>1000 AU) separations, where the detection of brown dwarf companions to solar-neighborhood stars is not hindered by contrast, Gizis et al. (2001) have found that the frequency of substellar companions to F–K dwarfs is fully consistent with that of stellar companions to G dwarfs (Duquennoy & Mayor 1991). Thus, while the radial velocity "brown dwarf desert" remains nearly void within 3 AU even after the discovery of numerous extra-solar planets over the past decade, brown dwarf secondaries at >100–1000 AU separations seem to not be as rare.

The precise frequency of substellar companions in direct imaging surveys remains controversial. Several highly sensitive surveys performed with the *HST* (Schroeder et al. 2000, 23 A–M stars; Brandner et al. 2000, 28 G–M stars; Luhman et al. 2005, 150 B–M stars) and with high-order AO (Masciadri et al. 2005, 28 G–M stars; Biller et al. 2007, 54 A–M stars) have reported null detections of substellar companions. Given the low (few per cent) detection rate of substellar companions in direct imaging surveys, it is now clear that, with < 50 targets per sample, some of these surveys were too small to expect to detect even a single brown dwarf companion. However, the non-detection of substellar secondaries in two largest surveys (Luhman et al. 2005; Biller et al. 2007) is potentially significant.

Given current understanding of the importance of stellar mass for (1) stellar multiplicity rates (see review in Sterzik & Durisen 2004) and (2) binary mass ratio distributions (see review in Burgasser et al. 2007), it is imperative that any study of the substellar companion frequency is considered in the context of the mass distribution of primary stars in the sample. Indeed, a large survey sample comprising primaries with identical masses is ideal.

The problem of the brown dwarf companion frequency is perhaps most comprehensively dealt with in the context of solar mass primaries. For these a uniquely large body of stellar and substellar multiplicity data exist on all orbital scales. On one hand, the exhaustive spectroscopic and imaging study of G dwarf multiples by Duquennoy & Mayor (1991) provides an important anchor to the properties of 0.1–1.0 $M_\odot$ stellar companions to Sun-like stars. On the other hand, the results from more than a decade of precision radial velocity surveys for planets around G and K stars allow a comparison with the planetary-mass end of the substellar companion mass range.

A large uniform sample of young Sun-like stars has been compiled by the Formation and Evolution of Planetary Systems (FEPS) *Spitzer* Legacy team. The purpose of the FEPS Legacy campaign with *Spitzer* was to study circumstellar disk evolution in the mid-IR. However, the sample is also well-suited for a high-contrast imaging survey for substellar companions. Seventy percent of the FEPS stars are younger than ∼500 Myr, and all are within 200 pc.

As an auxiliary component to the FEPS program, we imaged most of the northern FEPS sample with the high-order AO systems on the Palomar 5 m and the Keck 10 m telescopes. We further expanded our AO survey by observing several dozen additional nearby and mostly young solar analogs. Preliminary results from the project were published in Metchev & Hillenbrand (2004) and in Metchev & Hillenbrand (2006), including the discoveries of two brown dwarf companions: HD 49197B and HD 203030B. The survey has now been completed, and no further brown dwarf companions have been found. The results were analyzed in Metchev (2006). Here we present the AO survey in its entirety and focus on the statistical interpretation of the data.

The paper is organized as follows. A full description of the survey sample is given in § 2. The Palomar and Keck AO observing campaigns and the data reduction and calibration techniques are described in § 3. The candidate companion detection approach and the survey detection limits are discussed in § 4. The various methods used for bona fide companion confirmation are presented in § 5. Section 6 summarizes the results from our survey, including all of the newly-discovered and confirmed substellar and stellar secondaries. Section 7 contains a brief discussion of the various sources of incompleteness and a full discussion of the biases in the survey. (A full-fledged incompleteness analysis is presented in the Appendix.) In § 8 we estimate the frequency of wide substellar companions to young solar analogs, and present evidence for trends in the companion mass and companion frequency with semi-major axis and primary mass. In § 9 we consider the results of the current investigation in the broader context of stellar multiplicity, and suggest the existence of a universal CMF. Section 10 summarizes the findings from our study.

2. TARGET SAMPLE

The main criteria used for selecting stars for the survey were Sun-like mass, youth, proximity, and visibility from the Northern hemisphere. In this Section we describe how they were applied to generate our AO survey sample.

2.1. *Selection*

The selection of the AO survey sample was largely based on the target selection criteria employed in the construction of the FEPS program sample (Meyer et al. 2006). The FEPS selection criteria will not be reproduced here. The final FEPS target list comprises 328 F5–K5 stars within 200 pc distributed uniformly in logarithmic age intervals between 3 Myr and 3 Gyr. Approximately a third of these are members of open clusters and stellar associations, and the remainder are field stars. We observed 228 of the 240 FEPS stars north of $\delta = -30°$ with AO at Palomar or Keck.

A further 38 solar analogs were added to the AO survey toward the end of the first epoch of observations to bolster the sample size, mirroring FEPS target-selection policy. The additional stars were selected from three sources: (1) the broader compilation of FEPS candidate targets, including stars that had been eliminated from the final FEPS sample based on infrared background or age redundancy considerations; (2) the compilations of nearby young stars by Montes et al. (2001) and Wichmann et al. (2003); and (3) our own Palomar echelle survey of nearby stars (White et al. 2007). The

final set of 266 targets in our AO sample has spectral type and age distributions similar to those of the FEPS sample.

2.1.1. *Deep and Shallow Samples*

To optimize sensitivity to substellar companions, we chose to observe a portion of the youngest and nearest AO sample stars with deep coronagraphic exposures. We applied the following additional guidelines to select stars for the deep coronagraphic sub-sample:

1. stellar activity and lithium levels indicating ages less than 500 Myr;

2. no $\Delta K_S < 4$ objects between $0\farcs8$ and $13\farcs0$, as determined from real-time flux ratio measurements during survey observations;

3. nearby stars were given priority over more distant stars;

4. isolated stars, not belonging to one of the young open clusters or stellar assocciations, were given priority for deep observations.

The first criterion was motivated by the fact that substellar companions should be intrinsically brightest at the youngest ages. The second constraint was aimed at avoiding the loss of sensitivity to faint objects over a large portion of the detector field of view (FOV) because of the presence of a bright neighboring star.[1] Binaries with separations $\leq 0.8''$ had both their components sufficiently well-covered by the $1''$ coronagraphs in the Palomar and Keck AO cameras that they were allowed in the deep sample. The motivation for the third constraint was to optimize sensitivity to substellar companions at the smallest physical separations. The last criterion was applied to avoid duplication with previous sensitive high-angular resolution studies of open clusters: Bouvier et al. (1997, the Pleiades, AO), Köhler et al. (Upper Scorpius; 2000, speckle), and Patience et al. (2002, α Persei, speckle).

Based on the additional criteria outlined above, 84 of the 228 stars selected from the final FEPS sample and 16 of the 38 additional targets were included in our deep sample. The deep sub-sample thus consists of 100 F5–K5 stars with ages less than 500 Myr.

All remaining stars were observed primarily in short sequences of non-coronagraphic images to establish stellar multiplicity. These will be referred to as the "shallow" sample. The shallow sample includes 11 stars older than 500 Myr that were also observed with long coronagraphic exposures: 2 Hyades (∼600 Myr) members and 9 other stars whose subsequent age-dating showed that they were older than originally estimated. Although these 11 stars were observed coronagraphically, for the purpose of limiting our deep sample only to the observations with the highest sensitivity to substellar mass, they are not considered as part of the deep sample.

[1] Following more accurate post-reduction photometry, a $3\farcs1$ companion to one of the stars in our deep sample, HD 31950, was found to be only $\Delta K_S = 3.70$ mag fainter (Table 8). Although this companion violates criterion 2, we have chosen to keep HD 31950 as a member of the deep sample.

The deep and shallow sample stars and their characteristics are listed in Tables 1 and 2. Median age, distance, and spectral-type statistics for the deep, shallow, and complete (deep+shallow) samples are given in Table 3.

2.2. *Stellar Properties*

Our sample stars are near-solar (G2 V) analogs, ranging in spectral type between F5 and K5 ($6300\ \mathrm{K} > T_{\rm eff} > 4400\ \mathrm{K}$) and, depending on stellar age, between IV and V in luminosity class ($3.4 < \log g \leq 4.5$ in cgs units). The corresponding mass range, based on dynamical mass estimates in binary systems and on stellar thermodynamic models (Baraffe et al. 1998; D'Antona & Mazzitelli 1994) is approximately 0.7–1.3 $M_\odot$, following the design of the FEPS sample (Meyer et al. 2006). For greater detail in the assignment of spectral types, effective temperatures, and surface gravities to FEPS sample stars we refer the reader to Carpenter et al. (2008). Histograms of the distribution of stellar effective temperatures and masses of all stars in our AO survey sample are shown in Figure 1.

Seventy-nine of our sample stars are members of known young stellar associations: Upper Scorpius, α Persei, the Pleiades, and the Hyades. For these we have adopted ensemble ages from the literature: 5 Myr for the Upper Scorpius OB association (Preibisch et al. 2002), 80 Myr for α Persei (Ventura et al. 1998), 120 Myr for the Pleiades (Ventura et al. 1998), and 600 Myr for the Hyades (Perryman et al. 1998). Sample stars that do not belong to any known associations were age-dated following one of two approaches: (1) based on the strength of the chromospheric Ca II H and K (3968Å and 3933Å) line emission for > 30 Myr-old stars, and using the recent activity-age relation of Mamajek & Hillenbrand (2008), or (2) isochrone fitting for < 30 Myr-old pre-main sequence stars using the tracks of Baraffe et al. (1998). Where data from high-dispersion optical spectra were previously available (Strassmeier et al. 2000; White et al. 2007), these were also reviewed for the strength of the lithium 6708 Å absorption line to put additional constraints on the ages. All chromospheric and isochronal ages were assumed uncertain to within a factor of two. Ages for a remaining set of 20 stars not present in the extended FEPS sample were taken from the literature (Barrado y Navascues et al. 1997; Gutiérrez et al. 1999; Montes et al. 2001; Wichmann et al. 2003; Nordström et al. 2004). Histograms of the age distribution of the complete survey sample and of the deep sub-sample are shown in Figure 2.

Distances to 166 sample stars with individual *Hipparcos* parallaxes were taken from the *Hipparcos* catalog (Perryman et al. 1997). For a further 55 known members of young open clusters and OB associations, we adopted the corresponding mean cluster distance, calculated from a combination of trigonometric, orbital, secular, and cluster parallaxes in the literature, as inferred from *Hipparcos* and Tycho-2 (Høg et al. 2000) astrometry, long-baseline interferometry, or high-resolution spectroscopy. The adopted distances for open cluster members were: 133 ± 6 pc for stars in the Pleiades (a weighted mean of the distances to seven members presented in Pan et al. 2004, Munari et al. 2004, Zwahlen et al. 2004, Southworth et al. 2005, and assuming $\sim 1^\circ$ cluster angu-

lar extent from Adams et al. 2001), and 190 ± 11 pc for stars in α Persei (van Leeuwen 1999, assuming 1° cluster radius). For stars belonging to the Upper Scorpius association we adopted 145 ± 40 pc (de Zeeuw et al. 1999; Mamajek et al. 2002). All of these distances agree with estimates from main-sequence fitting for the corresponding clusters. For 18 more stars we adopted secular parallaxes from Mamajek et al. (2002) and Mamajek (2004, 2007). Finally, for 27 remaining >30 Myr-old stars we obtained approximate distances based on a combination of moving group association, secular parallax, and spectroscopic parallax, with care to avoid redundancy in distance and age derivation. The errors on the distances in these cases were conservatively assumed to be 25%–50%. More refined distance and age estimates for these stars will be included in a future publication from the FEPS program.

Accurate proper motions for the sample stars are essential in identifying bona fide companions through multi-epoch astrometry. Proper motions for the 166 stars with individual *Hipparcos* parallaxes were taken from the *Hipparcos* database. For the remaining 100 stars proper motions were adopted from The Second U.S. Naval Observatory CCD Astrograph Catalog (UCAC2; Zacharias et al. 2004) and from the Tycho–2 Catalog (Høg et al. 2000). The three catalogs provided similar astrometric accuracy ($\pm$1.0 mas yr^{-1}) for the sample stars, although the UCAC2 and Tycho–2 catalogs went deeper.

Figure 3 presents histograms of the heliocentric distances (panel a) and total proper motions ($\sqrt{(\mu_\alpha \cos\delta)^2 + \mu_\delta^2}$; panel b) of the stars in the complete sample and in the deep sub-sample. The bi-modal distribution of the distances is a combined effect of the large heliocentric distances (130–190 pc) of the youngest (3–120 Myr) stars in the sample, and of the preference given to closer systems at older ages.

3. OBSERVATIONS, DATA REDUCTION, AND CALIBRATION

3.1. *Observing Strategy*

A complete description of the observing strategy of our AO survey was given in Metchev & Hillenbrand (2004) and in Metchev (2006). Here we briefly review the approach and summarize the survey observations.

The full sample of 266 stars was observed in the near-IR with AO at the Palomar and Keck II telescopes on 47 clear nights over the course of 3 years: between 2002 January 31 and 2005 January 24. Additional astrometric follow-up was obtained during 2006 and 2007 in a few individual cases.

We opted to conduct the entire survey in the K_S band to take advantage of the much better AO performance at >2μm. Although cool T-type brown dwarfs ($T_{\rm eff} \lesssim 1400$ K; Golimowski et al. 2004; Vrba et al. 2004) are faintest at K band in the near-IR, warmer (potentially younger) L-type brown dwarfs are brightest at K. Thus, given superior imaging contrast and the relative youth of our deep sample, the 2μm region was seen as the best choice for optimizing sensitivity to close-in young substellar companions.

The majority of the science targets were observed first at Palomar. Only seven of the targets (all belonging to the deep sample) were observed initially and only at Keck. The Palomar campaign was conducted with the PALAO system (Troy et al. 2000) and the PHARO near-IR camera (Hayward et al. 2001) in its 25 mas pix^{-1} mode, providing a $25.6'' \times 25.6''$ FOV. At Keck, we used the facility AO system (Wizinowich et al. 2000) on Keck II and the NIRC2 near-IR camera in its 40 mas pix^{-1} mode, offering an FOV of $40.6'' \times 40.6''$. To improve overall sensitivity and contrast the 100 targets in the deep sample were observed coronagraphically with the opaque $0\farcs97$-diameter occulting spot in PHARO and the partially transmissive $1\farcs0$-diameter occulting spot in NIRC2. All of the sample stars were sufficiently bright to allow use of the AO systems in NGS mode, i.e., to have the wavefront sensing performed on the primaries themselves.

3.1.1. *First-Epoch Observations at Palomar*

We spent 24 min of net exposure time per target during first epoch at Palomar, attaining an imaging depth of $K_S \approx 19.7$ mag on average for stars in the deep sample. The 24 min of exposure were divided in 4 sets of 6 min taken at different orientations of the telescope Cassegrain ring (CR) rotator. The 6 min of net exposure at each CR rotator angle consisted of two sets of three one-minute on-target exposures, with three one-minute sky exposures in between. The purpose of the CR rotation approach was to improve the quality of point-spread function (PSF) subtractions for data taken with an equatorial-mount telescope (Palomar), in a manner similar to that attained with angular differential imaging (ADI) on altitude-azimuth-mounted telescopes (Marois et al. 2006). Stacking images taken at different CR angles also averages out detector and sky noise, much like mosaicking dithered images. Unfortunately, in addition to being less efficient, the CR rotation approach was later found to also produce notable smearing of the PSF in the co-added de-rotated images at $\gtrsim 5''$ from the star, leading to degradation both in imaging depth and in astrometric precision (Metchev 2006). We have since demonstrated that judicious matching of nearby science targets to use as PSFs for one another—a suitable approach for surveys of target-rich young stellar associations—enhances the contrast attainable with PALAO by 0.5–1.0 mag over the one reported here without incurring the overhead of CR rotations (Tanner et al. 2007).

We used two different undersized Lyot stops to block the secondary obscuration and the secondary mirror support structure at Palomar: the "medium" and the "big" cross, obscuring 40% and 76% of the total telescope aperture, respectively (Hayward et al. 2001). The use of an appropriately sized Lyot stop was expected to noticeably improve the dynamic range achievable in high-order AO coronagraphy by suppressing light diffracted by the edge of the coronagraph (Sivaramakrishnan et al. 2001). Early experiments with the PALAO/PHARO system by Oppenheimer et al. (2000) had suggested that the big cross provided the best contrast in single exposures of up to several seconds, outperforming the medium and "standard" (no undersizing) Lyot masks by up to 0.5 mag between $0.5''$–$2.0''$ from bright stars. However, our experience from observing each star in multiple longer exposures was that the less oversized Lyot stops allowed better real-time monitoring of the star-coronagraph alignment and more accurate post-processing image registra-

tion and astrometry. With the medium and the standard Lyot stops the position of the star behind the coronagraph could be monitored by the location of a Poisson-like spot within the dark area of the coronagraph: the result of constructive interference of high spatial frequency light pushed by the coronagraph to the periphery of the Lyot plane. The big Lyot stop likely shutters incoming starlight too aggressively to allow the formation of a sufficiently bright Poisson spot. Because image registration of multiple exposures was crucial for obtaining greater overall exposure depth, we stopped using the big cross after March 2002. Given the adopted technique of rotating the Cassegrain ring to four mutually orthogonal orientations during the imaging of each star, the medium cross provided the best compromise between registration ability for the final images and consistency with which it would obscure the telescope secondary mirror support at each CR orientation. At the end of our survey, only seven of the 100 stars in the deep sample had their deepest observations obtained with the big Lyot cross setup.

In addition to the long coronagraphic K_S-band exposures, we also observed each deep sample target in short (1.4–10 s) unocculted exposures. These were taken to check for stellar multiplicity within the 0.″5 coronagraph radius and to allow relative photometric calibration of the deep occulted exposures. The short exposures were obtained at J, H, and K_S bands, using a 1% neutral density (ND) filter to prevent saturation whenever necessary. For these observations we used a five-point dither pattern as is standard for infrared imaging.

The 166 targets in the shallow sample were observed only in short dithered JHK_S exposures at Palomar to check for stellar multiplicity. The imaging depth of the shallow survey varied greatly from star to star, depending on whether the ND filter was used or not, and was generally in the $12 < K_S < 17$ mag range.

3.1.2. *Follow-up Observations*

After an examination of the initial Palomar images, target stars which contained other objects in the same image—candidate companions—were followed up with additional imaging at later epochs to test for common proper motion between the candidate companions and the host stars. Upon establishing common proper motion, candidate companions were observed spectroscopically to confirm their physical association with the primary.

The imaging and spectroscopic follow-up was performed at both Palomar and Keck. Imaging at Keck was done in 6×1 min coronagraphic integrations per target, with an additional 3×1 min spent on sky. We used the "inscribed circle" NIRC2 pupil mask (90.7% throughput) to occult the telescope mirror outer edge. (None of the available NIRC2 pupil masks occult the Keck segment edges and the secondary support structure.) In most cases the 6 min-long exposures at Keck were ≈0.5 mag deeper ($K_S \approx 20.2$ mag) than the 24 min Palomar exposures, and occasionally revealed new candidate companions. Nearly half (48/100) of our deep sample stars were observed at Keck in addition to at Palomar, including the seven targets observed only at Keck. Because of the marginal difference in the depths of the Keck and Palomar components of the deep survey, and for the sake of preserving the integrity of our well-defined 100-star deep sample, we analyze the Palomar and Keck AO campaigns together as a single survey.

We obtained near-IR spectra of several bona fide and candidate companions for the purposes of further confirmation of their physical association and characterization of their photospheres. The spectroscopic observations and data reduction were described in Metchev & Hillenbrand (2004, 2006). Here we present spectroscopy of only one additional companion candidate, to ScoPMS 214. The observations and data reduction for that are briefly described in § 6.3.1.

3.2. *Imaging Data Reduction*

The imaging data reduction procedure for the survey, including flat-fielding, sky-subtraction, bad-pixel correction, image registration, and image stacking was detailed in Metchev & Hillenbrand (2004). We have since augmented the procedure to include a correction for the non-linear flux response of the PHARO and NIRC2 detectors. Near-infrared detectors often have non-linear response even at small flux levels, that is important to take into account when seeking accurate photometry. We measured the non-linearity of the PHARO and NIRC2 detectors from series of variable-length exposures of the brightly illuminated telescope dome interiors, interspersed with multiple dark frames to mitigate charge persistence effects. The response of the PHARO camera, which employs an HgCdTe detector that does not support multiple non-destructive reads, was found to be >1% non-linear beyond 10,000 counts/pix and >5% non-linear beyond 45,000 counts/pix. The InSb detector on NIRC2, which supports non-destrictive read-outs, was found to be >1% non-linear beyond 3000 counts/pix/read and >5% non-linear beyond 7000 counts/pix/read. We created custom IDL routines[2] to linearize the PHARO and NIRC2 flux response. The linearization was applied to all images before any other data reduction steps.

To enhance our ability to detect faint candidate companions in the deep coronagraphic exposures we attempted various methods of PSF removal, including: (1) subtracting a median-combined PSF of the star formed from the individual images taken at all four CR angles at Palomar, (2) subtraction of a 180°-rotated version of the image centered on the star from itself, (3) high-pass filtering by subtracting a Gaussian-smoothed (Gaussian FWHM = 1–3×PSF FWHM) version of the image from itself, and (4) simple subtraction of an azimuthally medianed radial profile. We found that (1–3) gave comparable results, while (4) did not perform as well as the rest because of the four-cornered or six-spoked symmetry of the PALAO or Keck AO PSFs. Even though (3) is arguably the most widely used method for PSF subtraction when separate PSF observations are not available and when the observations were not taken using ADI, we found that because of the central symmetry of the brightest AO speckles (Boccaletti et al. 2002; Bloemhof 2003) method (2) worked almost as well. Method (2) also did not alter the photon statistics of the PSF-subtracted image in the spatially correlated manner incurred by Gaussian smoothing. Therefore, for PSF subtraction we relied on

[2] The PHARO and NIRC2 detector linearization routines are available at `http://www.astro.caltech.edu/palomar/200inch/palao/Pharo/pharo.html`

method (2) the most.

3.3. *Precision Astrometry*

Multi-epoch astrometry is essential for demonstrating physical association of bound pairs. This is the principal method employed for candidate companion confirmation here. Below we discuss the calibration steps that we undertook to ensure self-consistent astrometric measurements throughout our campaign.

We calibrated our astrometry by obtaining repeated measurements of the positions of well-known visual binaries at each observing epoch. We selected binary stars with well-known ephemeris from the Sixth Orbit Catalog (Hartkopf et al. 2001; Hartkopf & Mason 2003), combining binaries with grade 1 (accurately determined, short-period) and grade 4 (less accurately known, longer-period) orbital solutions, as recommended for astrometric calibration by Hartkopf & Mason (2003). Despite the lower quality of the orbital solutions for the grade 4 binaries, their periods are generally much longer, so that their motions are predicted with sufficient accuracy for many years into the future. The selected calibration binaries and their orbital parameters are given in Table 4.

The above astrometric calibration was adequate for detecting astrometric signals $\delta\rho/\rho \gtrsim 1\%$ with PHARO. Such accuracy allowed the confirmation of the first brown dwarf companion in our survey, HD 49197B (Metchev & Hillenbrand 2004). However, that initial calibration assumed that the pixel scale and field orientation over the entire PHARO detector were well-determined from measurements taken near the center of the array, ignoring possible image distortion in the focal plane. In reality, the PHARO beam is known to be distorted (Hayward et al. 2001). Accurate characterization of this distortion was necessary before considering the results from our complete survey, which focused on stars with small proper motions (10–100 mas yr^{-1}; Fig. 3b) and detected candidate companions over the entire $25.6'' \times 25.6''$ PHARO FOV.

We arrived at an improved astrometric calibration of the PHARO 25 mas pix^{-1} camera in Metchev (2006, §4), where we determined the full extent of the focal plane distortion over the entire array and solved for its dependence on telescope hour angle, declination, and orientation of the CR rotator. For that calibration we used a custom-made astrometric mask with pinholes distributed on a rectangular grid that we inserted in the telescope beam path at the Cassegrain focus. From exposures taken with the mask in place we measured the variations in the spacing among the pinhole images with changes in the instrument gravity vector. We found that the PHARO pixel scale varied by up to $\delta\rho/\rho = 0.9\%$ from the center to the corner of the array in the 25 mas pix^{-1} camera. After fitting two-dimensional polynomials to the distortion, we calibrated the variation to within 0.15% over the entire chip. The polynomial fits to the focal plane distortion on the PHARO 25 mas pix^{-1} camera and its dependence on telescope pointing are given by Equations 4.1–4.4 and 4.7–4.11, and Tables 4.4–4.5 in Metchev (2006). An IDL program that corrects for the distortion at an arbitrary coordinate on the PHARO 25 mas pix^{-1} camera is available at the PHARO instrument web page `http://www.astro.caltech.edu/palomar/200inch/palao/Pharo`

A similar astrometric calibration has already been performed for all three NIRC2 cameras during the pre-ship testing of the instrument (Thompson et al. 2001). Because NIRC2 sits on the Keck II Nasmyth platform and thus has a constant gravity vector, the distortion of the camera pixel scales does not change with telescope pointing. We implemented the existing astrometric calibration of the NIRC2 cameras in the analysis of our Keck AO imaging data.[4]

3.4. *Photometry*

We used 1–2×PSF FWHM-diameter apertures for object photometry, with the smaller apertures used on fainter sources for higher signal-to-noise measurements. The diffraction-limited FWHM of the K_S-band PSF of PALAO was consistently $\approx 0\farcs1$ while for the Keck AO system it was $\approx 0\farcs05$. The local background was measured around each object in an annulus with a wide enough inner radius so that the halo of the point source did not affect the background measurement. The inner radius was as small as 1.5×PSF FWHM for faint sources embedded in the halos of bright stars, or as large as 25–30×PSF FWHM for the target primaries. The variations in the sizes of the apertures and of the background annuli resulted in photometric uncertainties on the order of 0.10–0.30 mag. Uncertainties of ≥0.5 mag were found in a few isolated cases involving very faint point sources and/or point sources near the edges of the FOV, where the PSF was noticeably distorted by anisoplanatism and circular apertures did not produce accurate photometry.

PSF-fitting, rather than aperture photometry was used to measure the fluxes of closely-separated point sources. The photometric uncertainties in such cases were generally ≤ 0.20 mag.

For absolute calibration we relied on the 2MASS fluxes of the primaries. Photometric measurements were always obtained relative to the fluxes of the target primaries, as measured from the unocculted, short exposures, often taken with the PHARO ND 1% filter in place. We calibrated the near-IR extinction of the ND filter from photometric measurements of three program stars on images taken with and without the filter in place. Images with Keck/NIRC2 were obtained only in coronagraphic mode, using predominantly the $1''$-diameter spot, although the $2''$-diameter spot was used during 16–18 May 2003. Unlike the PHARO coronagraphic spots, the NIRC2 spots are transmissive, offering the possibility to obtain relative photometry with respect to the primary. A measurement of the throughput of the $2''$ spot was given in Metchev & Hillenbrand (2004). Subsequent observations showed that such measurements were dependent on the quality of the AO correction, possibly because of the amount of additive background caused by light from the stellar halo diffracted within the area of the coronagraph. Thus, approximate relative photometry with the NIRC2 coronagraph is likely feasible only with good AO cor-

[3] The PALAO/PHARO astrometric calibration was performed in March 2005. The optics on the PALAO system have since been realigned to accommodate recent and future science instrument upgrades. The astrometric calibration presented here is not applicable to PALAO data taken since 2007.

[4] A more precise astrometric calibration of the NIRC2 cameras has since been obtained by Cameron et al. (2008).

rection (usually at H or K bands), when the amount of scattered ("spill-over") light within the area of the coronagraph is minimized. Table 5 lists the measured near-IR extinction in magnitudes for the PHARO ND 1% filter and for the 1″ and 2″ NIRC2 coronagraphs. The large apparent difference in the J-band transmissivity of the two NIRC2 coronagraphic spots is a probable effect of spill-over (more significant for the smaller spot), aggravated by poorer AO performance at J.

4. OBJECT DETECTION AND DETECTION LIMITS

4.1. *Object Detection*

Object detection is a straightforward matter to automate in point-source-rich images where the PSF is radially symmetric, approximately constant in time, and has a well-characterized dependence on image location. Unfortunately, none of these qualifications describe the sparsely populated high-contrast images in our deep survey, in which the main (and frequently only) point source is occulted by the coronagraph. In addition, automated source finding in AO images of bright stars is hindered by large numbers of speckles. Speckles are individual images of the star that form from uncorrected and/or induced (by the telescope optics) aberrations in the wavefront, and appear indistinguishable from point sources to automated detection routines. As a result, even though certain source detection algorithms have been developed (StarFinder; Diolaiti et al. 2000), or adapted (DAOPHOT II, IDAC; Stetson 1992; Jefferies & Christou 1993), for diffraction-limited image restoration, they did not produce satisfactory results on our images. Our experiments with DAOPHOT, WAVDETECT (Freeman et al. 2002), and StarFinder produced large numbers of spurious detections, the vast majority of which could be identified with speckles around the coronagraph. If the signal-to-noise threshold in the source-finding algorithms was adjusted to a correspondingly higher level, the algorithms would miss bona fide point sources far from the central star. The performance of the automated algorithms did not change whether we used various methods of PSF subtraction (§ 3.2) or not. Similar experiences and conclusions were drawn independently by Carson et al. (2005), who also used the PALAO/PHARO system for their substellar companion search. Therefore, after some experimentation, and despite an understanding that automated source detection has the potential to offer greater repeatability and conceptual clarity, we abandoned the approach.

Instead, we opted for visual point source identification, which, barring subjective factors, produces superior results compared to automated detection. We carefully inspected all of the final coronagraphic images for candidate companions. The visual inspection was repeated multiple times during the steps of image reduction, photometry, and astrometry to reduce the effect of subjective factors to a minimum.

The high-contrast imaging literature abounds with examples where the authors have resorted to by-eye identification of candidate companions (e.g., Tokovinin et al. 1999; Brandner et al. 2000; Schroeder et al. 2000; Luhman & Jayawardhana 2002; McCarthy & Zuckerman 2004; Masciadri et al. 2005; Luhman et al. 2005; Lafrenière et al. 2007). A notable exception is the study of Lowrance et al. (2005), who apply a rigorous custom-made automated detection scheme to their *HST*/NICMOS data. However, the Lowrance et al. survey benefits from the well-behaved PSF of space-borne *HST* imaging. In a separate instance, Shatsky & Tokovinin (2002) use DAOPHOT II for their non-coronagraphic AO data. Still, they do not discuss an application of the approach to their set of coronagraphic data, which are likely to be speckle-dominated.

4.2. *Determination of Detection Limits*

We quantified our ability to visually detect faint objects by introducing artificial point sources in the Palomar and Keck K_S images of one of our targets, HD 172649, for which data were taken under good observing conditions with Strehl ratios of ≈50%. The method was first described in Metchev et al. (2003) and developed more fully in Metchev (2006). We summarize it here briefly.

We introduced 1000–5000 artificial point sources of constant brightness at random locations over the entire $25\farcs6 \times 25\farcs6$ area of the image and counted the fraction of them that were retrievable by eye in 0.25″–1.0″-wide concentric annuli centered on the star. We recorded both the minimum point source K_S magnitude, at which 100% of the artificial point sources were visible at the given angular separation, and the maximum K_S magnitude, at which only a few artificial point sources were visible. We took the mean of the K_S magnitude range as the representative limiting magnitude at the given separation. We repeated the experiment for a range of artificial star magnitudes, at steps of 0.5 mag, on both the coronagraphic and the non-coronagraphic images of HD 172649. The PSF for artificial stars in the coronagraphic image was obtained from a fit to the brightest field object ($\Delta K_S = 6.4$ mag), whereas in the unocculted image the PSF was obtained from a fit to HD 172649 itself.

The inferred detection limits based on the artificial point source experiments are shown in Figure 4. We see that the 6 min long Keck AO coronagraphic images offered 0.5–1.5 mag higher contrast and up to 0.5 mag greater depth than the 24 min PALAO images. The greatest difference in contrast is in the $1\farcs0$–$1\farcs5$ angular separation range, where the presence of waffle-mode distortion in the PALAO PSF limits the attainable contrast.

For the purpose of estimating the completeness of our survey, it was important to determine sensitivity limits on a per-star basis. However, the above approach was too tedious to apply to all observations. Instead, we employed a simpler strategy based on the r.m.s. scatter of the pixel counts in the radial profile of each sample star. To match the approximate spatial correlation scale in the PALAO and Keck AO images, we normalized the r.m.s. scatter to an aperture with radius equal to the $0\farcs10$ FWHM of the PALAO PSF. That is, we multiplied the r.m.s. profile by the square root of the number N of pixels in the photometry aperture; $N = 50.3$ pix for PALAO/PHARO with the 25 mas pix^{-1}camera and $N = 20.0$ pix for Keck AO/NIRC2 with the wide (40 mas pix^{-1}) camera. This procedure imposed a more stringent requirement on the significance of the detec-

tion of a candidate point source by raising the effective multiple of the pixel-to-pixel r.m.s. scatter used as a threshold by an additional factor of 4.5–7.1. We show the thus-obtained 4σ aperture-normalized r.m.s. noise profile of the halo for our PALAO coronagraphic image of HD 172649 in Figure 4. We found that the 4σ line best approximated the visually determined PALAO detection limits. The strongest systematic deviation of the 4σ r.m.s. profile from the visually-determined contrast limits is at angular separations $>7''$. This is to be expected, to some extent, because in this region we have adjusted the visual detection limits to account for CR angle image mis-registration (§ 3.1.1).

The agreement between the detection limits from visual inspection and from r.m.s. statistics is dependent on a number of factors, such as the radius of the normalization aperture, the PSF pixel sampling, the treatment of point source photon statistics (ignored in our r.m.s. analysis), and the appropriate functional treatment of non-Gaussian sources of error (speckles, shape of the PSF core and halo; also ignored here). As a check on whether the adopted r.m.s. detection limit approach was a valid approximation across the range of PSF and image characteristics encountered in our survey, we repeated the artificial point source experiment on six additional images of targets observed both at Palomar and at Keck. These images were taken under a range of seeing conditions, resulting in PSF Strehl ratios between 10% and 50%. We found that, on average, the by-eye detection limits varied between three and five times the level of the aperture-normalized r.m.s. noise profile over the entire range ($0\farcs5$–$12\farcs5$) of probed angular separations. Thus, the additional experiments confirmed that our choice of the 4σ level was an adequate detection threshold.

In closing, we note that because our image noise statistics in the contrast-limited regime are not Gaussian, the adoption of a 4σ threshold does not carry the statistical significance of a confidence level at which 99.997% of random fluctuations are rejected. Only recently have Marois et al. (2007) shown that quasi-Gaussian behavior of the PSF subtraction residuals can be obtained with the ADI technique, allowing such formal estimates on the detection limits. Because our data were not taken in ADI mode, the same formalism can not be applied here.

4.3. *Illustrative Detection Limits for the Deep Sample*

Table 6 lists the attained point-source magnitude sensitivity for each star in the deep sample at angular separations of $1''$, $2''$, and $5''$. Beyond $5''$ the detection limits are constant to within 0.5 mag. In the cases where multiple images of the same star were taken at different epochs, we have listed the sensitivity only for the epoch with the deepest image. We thus formed a set of 58 Palomar and 42 Keck images that represented the deepest observations of the 100 stars in the deep sample.

Figure 5a depicts the range of attained K_S-band contrast for the coronagraphic observations in the entire survey (thick solid line), and from the Palomar (dotted line) and Keck (dashed line) portions of it. Figure 5b uses the same notation to depict the imaging depth of the survey in terms of apparent K_S magnitude (i.e., with the magnitude of the primary added in each case). The median sensitivities of the combined survey range from $\Delta K_S = 8.4$ mag at $1''$ to $\Delta K_S \approx 12.5$ mag over $4''$–$12\farcs5$ in contrast and from $K_S = 15.4$ mag at $1''$ to $K_S \approx 19.7$ mag in depth. These detection limits will be used in the Appendix to estimate the completeness of the deep survey to substellar and stellar companions.

We obtained the detection limits for the shallow sample in a manner similar to that used for the deep sample: from the 4σ dispersion of the radial profile of each star, normalized to an aperture with radius equivalent to the FWHM of the PALAO PSF. The shallow sample detection limits are given in Table 7, where we have in addition listed the sensitivity at $0\farcs5$.

In some cases close binary companions elevate the dispersion in the radial profile of the primary, resulting in unusually low sensitivities at certain angular separations: e.g., for HD 172649 at $5''$ in Table 6 and for HD 224873 at $2''$ in Table 7. We have retained these lower sensitivities in Tables 6 and 7 as an indication that part of the images around the sample stars in question were compromised by a nearby bright companion.

5. CONFIRMATION OF CANDIDATE COMPANIONS

5.1. *Detected Candidate Companions*

In the course of the three year survey we discovered 287 candidate companions brighter than $K_S = 20.6$ mag within $12.5''$ of 130 from the 266 sample stars. Of these candidate companions 196 were around 61 of the 100 stars in the deep sample. The remaining 91 were in the vicinity of 70 of the 166 shallow-sample targets. All candidate companions around stars in the deep and shallow samples are listed in Tables 8 and 9, respectively. Figure 6 shows all detected candidate companions as a function of magnitude difference ΔK_S and angular separation ρ. Thirty-nine stars in the deep sample and 96 in the shallow sample showed no projected companions within $12.5''$.

5.2. *Deciding Physical Association*

The physical association of each candidate companion was decided based on one of the following criteria: (1) common proper motion with the candidate primary, (2) a combination of the position on a $J - K_S$ versus M_{K_S} color—absolute magnitude diagram (CAMD; assuming equi-distance with the primary) and background star density arguments, or (3) extent of the radial profile of the candidate companion beyond that of a point-source PSF (which suggests an extragalactic object). Candidate substellar companions that satisfied the common proper motion test were also observed spectroscopically to confirm that their spectral types were in agreement with their projected substellar masses.

5.2.1. *Proper Motion*

Proper motion is usually the criterion of choice in companion studies, as it provides nearly unambiguous evidence of association between two objects: whether as components of a gravitationally bound system or as members of a multi-star moving group sharing a common origin. We used the common proper motion criterion through the combined application of two requirements: (i) that the change in the position of the candidate companions relative to the primaries was within 3σ of zero in all of right ascension (α), declination (δ), angular separation (ρ), and position angle (θ) , and (ii) that the

expected change in relative positions of the candidate companions, had they been stationary background objects, was more than 3σ discrepant in either α, δ, ρ, or θ from the observed change. Often in cases of candidate close ($\lesssim$20 AU) binaries, criterion (i) was not satisfied because of appreciable orbital motion. In such situations we instead made sure that (iii) the observed change in relative position was much smaller (and less significant) than the expected change if the components of the candidate binary were not gravitationally bound. A detailed example of the implementation of the above astrometric criteria is worked out in Metchev (2006, §5.4.1).

When a relatively bright field star (4 mag $< \Delta K_S \lesssim$ 8 mag) was present in the deep coronagraphic exposures at Palomar, its position in the shallow non-coronagraphic images was used as an additional astrometric reference. In cases where the subsequent astrometric measurements with respect to the primary and to fainter field objects showed such bright field stars to be approximately stationary, they could be used to bootstrap the association of other candidate companions with the primary, and thus circumventing the somewhat higher positional uncertainty associated with locating the primary behind the opaque PHARO coronagraph. This technique was particularly important in determining the association of systems in the distant Upper Scorpius (145 pc) and α Persei (190 pc) regions, where the primaries have small proper motions ($\lesssim$ 40 mas yr^{-1}) and the images contain multiple background stars because of the low galactic latitude ($5^\circ < |b| < 25^\circ$).

5.2.2. *Near-IR CAMD and Background Object Density*

Systems with bright ($\Delta K_S < 5$ mag) close-in candidate secondaries often lacked dual-epoch astrometry in our survey. Such systems were given lower priority in follow-up observations because the companions were considered to be stellar and almost certainly bound. Multi-epoch astrometric analysis was inapplicable in these cases. However, the candidate stellar secondaries in these systems were bright enough to be seen in the shallow non-coronagraphic JHK_S exposures of our targets. Hence, for the majority of the candidate stellar systems lacking astrometric confirmation, physical association could be estimated based on the near-IR colors and expected absolute magnitudes of the components.

In evaluating the association of a candidate companion based on its near-IR photometry, we placed it on a $J-K_S$ versus M_{K_S} CAMD, and checked whether it laid on the same isochrone as the primary. In the substellar regime, especially near the L/T transition ($12 < M_K < 14$) where the isochrones are not well-constrained, we relied on the empirical main sequence as traced by nearby M–T dwarfs (Leggett et al. 2002; Reid et al. 2004) with known parallaxes (from Dahn et al. 2002; Vrba et al. 2004). All candidate companions with available J-band photometry for which the astrometry was inconclusive had their physical associations with their candidate primaries evaluated in this manner (Fig. 7). To limit the probability of misclassifying field stars as bona fide companions, positive associations were adopted only for candidate companions within a 5″-radius field of interest from the primary.

This approach was successful mostly for stellar-mass companions bluer than $J - K_S = 0.8$ mag, i.e., earlier than spectral type M0. The main sequence for redder M0–M6 dwarfs is nearly degenerate in $J - K_S$ over nearly 4 mag in M_{K_S} (see Fig. 7) and does not allow reliable association estimates from the $J - K_S$ color. At even later spectral types, potentially representative of young brown dwarf companions, the higher photometric uncertainties and the larger empirical color scatter at substellar masses prevented the conclusive determination of physical association in all but a handful of faint projected companions. H-band photometry, where available, did not improve the analysis because of the smaller wavelength range sampled by the $H - K_S$ vs. $J - K_S$ colors. Thus, no candidate substellar companions were confirmed through near-IR photometry. However, a few could be rejected.

In addition to using near-IR colors, it was also possible to obtain a probabilistic estimate of the physical association for a candidate companion to its corresponding primary by comparing the number of detected objects within the 12.″5 survey radius to the surface density of stars at the relevant galactic coordinates down to the limiting magnitude of the survey. Because of the lack of large-area deep ($K_S \lesssim 20$ mag) near-IR survey data, we limited this type of analysis only to candidate companions in the shallow survey. Although the depth of the shallow survey varied depending on the use of the ND filter at Palomar, it was roughly comparable to the 99% completeness limit of the 2MASS catalog: $K_S < 14.3$ mag in unconfused regions of the sky. Therefore, for all candidate companions brighter than $K_S = 14.3$ mag, an empirical estimate of the association probability was possible based on 2MASS. Given that the faintest primaries in the sample have K_S magnitudes of 9.6, such a probabilistic analysis could be performed on all candidate companions with $\Delta K_S \leq 4.7$ mag.

To estimate the contamination from $K_S \leq 14.3$ mag field stars, we counted the number of 2MASS objects within a 5′-radius circular area offset by 12′ from each sample star (to avoid bright artifacts), and from that obtained the expected number of background objects in the 5″-radius field of interest. We used this as an estimate of the purely geometrical chance alignment probability (CAP):

$$\mathrm{CAP} = (\text{number of 2MASS sources within } 5') \times \frac{\pi(5'')^2}{\pi(5')^2}. \quad (1)$$

Table 10 lists the separations, ΔK_S and K_S magnitudes, and the CAPs for all sample stars with color companions (i.e., the ones with "yes(c)" entries in Tables 8 and 9). Most color companions have chance alignment probabilities $\lesssim$2%, with the exception of HD 155902B and HE 935B. However, both of these are very close (< 0.″1) to their candidate primaries, and are thus almost certainly physical companions. (These two systems are in fact below the resolution limits of the 95 mas PALAO K_S-band PSF. Their binarity was only appreciated from PALAO J-band images, where the PSF is 50 mas wide.) The ensemble probability of at least one of the 17 color companions being a false positive is 33%, or 16% if HD 155902 and HE 935 are excluded.

5.2.3. *Source Extent*

Any bona fide companions to our sample stars were expected to be point sources. Apparent source exten-

sion could in principle be used to exclude background galaxies seen in projection. However, the determination of source extent is not a trivial task when the quality of the AO correction and hence, the size and shape of the PSF change throughout the course of a single night depending on guide star brightness and on atmospheric stability. In addition, anisoplanatism may radially elongate point sources PSFs far away from the central AO guide star. Therefore, departures from the nominal, diffraction-limited PSF size and from a centrally symmetric PSF shape were regarded with caution. These were used to classify an object as an extended source only when they were in disagreement with the size and radial behavior of the profiles of other point sources in the same image, if such were present.

5.2.4. *Physical Association Summary*

Using the above criteria, we were able to determine the physical association for 198 of the 287 companion candidates. The proper motion criterion (§ 5.2.1) was used to establish the majority of associations or non-associations: 166 out of 197 (84.3%). These included 55 bona fide common proper motion companions and 111 non-common proper motion background objects seen in projection.

The CAMD and chance alignment criteria (§ 5.2.2) are not conclusive in proving physical association. They were invoked only when astrometric follow-up was not obtained or the proper motion data were ambiguous, and when additional J-band images were taken (§ 5.2.2). These criteria were used in tandem to establish with high fidelity the physical association of candidate *stellar* companions in the 18 cases listed in Table 10. The CMD criterion alone was used in seven cases to exclude background interlopers.

The source extent criterion (§ 5.2.3) was used to weed out faint galaxies, which may otherwise have red near-IR colors, partially due to line-of-sight extinction, and may thus pose as candidate substellar objects for the preceding criterion. This criterion was applied in four cases.

None of the above criteria were applicable to 89 candidate companions (31.0% of the total) that remained "undecided." The vast majority of these were faint objects in the fields of distant (> 100 pc) stars with small apparent proper motions (< 50 mas yr^{-1}), often at low galactic latitudes ($b < 15°$). These were often discovered only in follow-up deeper imaging with Keck and thus lack the full time-span of astrometric observations. Judging by the large number of such candidate companions per star, and based on expectations of the background star contamination rate at low galactic latitudes, probably none of these candidate companions are associated. Throughout the rest of the analysis, we shall assume that all 89 of the undecided candidates are unassociated field stars.

6. SURVEY RESULTS

Preliminary results from the survey were already published in Metchev & Hillenbrand (2004, 2006), including the discovery of two brown dwarf companions, HD 49197B and HD 203030B. In this paper we report the results from the full survey. We found no more substellar companions in our sample. We summarize the findings on the two previously discovered substellar companions in § 6.1. We also report 21 new stellar companions, in addition to three (HD 129333B, HE 373B, and RX J0329.1+0118B) already announced in Metchev & Hillenbrand (2004). Four of the newly-discovered stellar companions, HD 9472B, HE 373B, HD 31950B, PZ99 J161329.3–231106B, in addition to RX J0329.1+0118B announced previously, have masses of only $\approx$0.1 $M_\odot$, and reside in very low mass ratio $q = M_2/M_1 \approx 0.1$ systems. The results on the stellar companions are detailed in § 6.2.

A proper motion companion to the star ScoPMS 214, considered to be a brown dwarf based on its apparent K_S magnitude in Metchev (2006), was found to most probably be an unasociated foreground M star after spectroscopic follow-up. This companion, ScoPMS 214"B", is discussed in § 6.3 as an example of a pathological case where spectroscopic analysis argues against the physical association in an apparent common proper motion system.

Independently of the unbiased survey for substellar companions, we also observed and established the physical association of a previously known (Bouvier et al. 1997) candidate companion to HII 1348. The estimated mass of HII 1348B is near the limit for sustained hydrogen burning. Because of our deliberate inclusion of HII 1348 in our observing program based on known binarity, it is excluded from the present analysis. HII 1348B will be the subject of a future publication.

6.1. *Brown Dwarf Companions*

Both brown dwarf companions, HD 49197B and HD 203030B, were found in the 100-star deep survey. The observed photometric and astrometric properties of the two and their inferred masses are listed in Table 11 alongside those of the stellar secondaries observed in our survey. The spectral types of HD 49197B and HD 203030B are L4 $\pm$ 1 and L7.5 $\pm$ 0.5, respectively, and their masses are estimated at $0.060^{+0.012}_{-0.020}$ $M_\odot$ (Metchev & Hillenbrand 2004) and $0.023^{+0.008}_{-0.011}$ $M_\odot$ (Metchev & Hillenbrand 2006).

Because of their association with main sequence stars, the ages of HD 49197B and HD 203030B are known with relative certainty. Their moderate youth (250–500 Myr) makes them valuable as benchmarks for substellar properties at $\log g \approx 5$ surface gravities, $\sim$0.5 dex lower than the gravities expected of $\sim$3–5 Gyr-old brown dwarfs in the field.

At the time of its discovery, HD 49197B was only the fifth known L dwarf younger than 1 Gyr. At a projected separation of only 43 AU from its host star, HD 49197B was also one of the closest-in resolved substellar companions, second only to HR 7672B (14 AU; Liu et al. 2002). Both HR 7672B and HD 49197B provided early indication that the brown dwarf desert may not extend much outside of 3 AU (Metchev & Hillenbrand 2004).

HD 203030B was the first young brown dwarf with a spectral type unambiguously as late as the L/T transition. Its surprising underluminosity, by $\approx$0.5 dex compared to theoretical predictions for $\sim$1400 K brown dwarfs at its age, indicated that its effective temperature was $\approx$200 K cooler (i.e., $\approx$1200 K) than expected at the L/T transition. That is, the spectrophotometric properties of HD 203030B indicated that either the effective temperature at the L/T transition had a hereto-

fore unappreciated dependence on surface gravity, or that the entire population of field substellar objects had had their effective temperatures and ages significantly overestimated.

In fact, underluminosity and <1400 K expected effective temperatures are observed in all known substellar companions near the L/T-transition (Metchev & Hillenbrand 2006), including both the recently discovered T2.5 dwarf HN PegB (Luhman et al. 2007a) and the presumed planetary mass 2MASS J1207334–393254B (L5–L9; Chauvin et al. 2005a; Mohanty et al. 2007). With the mean ages of their respective primaries ranging between 8 Myr and 2 Gyr, all six known L/T-transition companions (GJ 584C, Kirkpatrick et al. 2001; GJ 337CD, Wilson et al. 2001; Burgasser et al. 2005; 2MASS J1207334–393254B, Chauvin et al. 2005a; HD 203030B, Metchev & Hillenbrand 2006; HN PegB, Luhman et al. 2007a) are likely younger than the 2.9 Gyr model-dependent mean age of L/T-transition dwarfs in the solar neighborhood (Allen et al. 2005). Therefore, the theory may indeed be overestimating the ages of field brown dwarfs, by a factor of at least 1.5. This hypothesis has now been independently reinforced by the first measurement of the dynamical mass of a binary field T dwarf. Liu et al. (2008) find that the components of the T5.0+T5.5 dwarf binary 2MASS J15344984–2952274AB are about 100 K cooler than derived for similar field objects: a fact that they interpret as evidence for a factor of $\approx 6 \pm 3$ overestimate in the adopted ages of field brown dwarfs. Future high-contrast imaging and astrometric observations and discoveries of benchmark brown dwarfs with known ages and dynamical masses will shed important light on these surprising results.

6.2. *Stellar Secondaries*

The entire survey produced 24 new stellar companions, including the three already announced in Metchev & Hillenbrand (2004, HD 129333B, HE 373B, and RX J0329.1+0118B). HD 129333 had previously been identified as a probable long-period single-lined spectroscopic binary by Duquennoy & Mayor (1991), and was independently resolved by König et al. (2005). Four other new binaries have since been independently confirmed in analyses of *Hipparcos* "problem" stars by Makarov & Kaplan (2005, HD 26990 and HD 135363), Goldin & Makarov (2006, HD 152555), and Goldin & Makarov (2007, HD 155902). In addition, PZ99 J161329.3–231106, resolved by us, has since been suggested as a possible spectroscopic binary by Guenther et al. (2007).

In addition to the 24 new systems, the physical association of 51 known binary stars was confirmed astrometrically. The star HD 91962, a previously known binary (Mason et al. 2001, and references therein), was resolved into a triple system. No higher-order multiples were resolved. A higher fraction of multiple systems might have been expected, especially given the high rate of occurrence (34–96%) of visual companions to close (spectroscopic) binary systems (Tokovinin et al. 2006). The visual companions in such multiple systems must have either fallen outside of our 12.″5 survey radius, or been removed from our AO sample by the design of the FEPS target list, which discriminates against visual companions (see § 7.2).

The majority (57 out of 74) of the binaries plus the triple system are members of the shallow survey, as a result of the requirement that no $\Delta K_S < 4.0$ mag candidate companions were present at $> 0.''8$ from deep sample stars (§ 2.1). Hence, the binaries found in the deep survey either have very low mass ratios, such that the secondary is >4 mag fainter than the primary at K_S, or have high mass ratios but $<0.''8$ angular separations, so that both components were fit under the $1''$ coronagraph.

We derive K_S-band absolute magnitudes M_{K_S} for the companions using the known distances to the primaries (Tables 1 and 2). We estimate the stellar companion masses directly from M_{K_S} and from the primary star age using stellar evolutionary models from Baraffe et al. (1998). The mass ratios of the resolved stellar binaries ranged between 0.1 and 1.0. Including the two substellar companions, the mass ratios covered the full 0.02–1.0 range. Table 11 lists M_{K_S} and the mass for each bona fide companion, along with projected separations and system mass ratios.

6.3. *The Apparent Proper Motion Companion to ScoPMS 214*

We detected seven projected companions within 12.″5 of ScoPMS 214 (Fig. 8; Table 8). Among these, candidate companion 1 (CC1) is brightest and closest to the star, and shares the proper motion of ScoPMS 214 to within 3σ limits over the course of 4.8 years (specifically, $\Delta\alpha/\sigma(\Delta\alpha) = 0.7, \Delta\delta/\sigma(\Delta\delta) = 2.4, \Delta\rho/\sigma(\Delta\rho) = 0.7, \Delta\theta/\sigma(\Delta\theta) = 2.3$). The apparent proper motion of CC1 is significantly different from the remaining three candidate companions (2, 3, and 4) to ScoPMS 214 for which we have sufficiently precise astrometric solutions. The proper motion of ScoPMS 214 is predominantly to the south ($\mu_\alpha \cos\delta = -5.6$ mas yr^{-1}, $\mu_\delta = -22.1$ mas yr^{-1}), and candidate companions 2–4 systematically lag behind in their declination motion $\Delta\delta$, at a level of 4.5–5.3$\sigma(\Delta\delta)$ over 4.8 years. These three candidates, along with candidate companion 6, for which the astrometry is insufficiently precise to decide its proper motion association status, are consistent with being stationary distant objects seen in projection (Fig. 9). Astrometric data for candidate companions 5 and 7 does not exist over the entire 4.8-year period, and hence they are not plotted on the proper motion diagram in Figure 9. However, they are also consistent with being background stars.

In summary, CC1 satisfies all of the proper motion association criteria established in § 5.2.1, whereas none of the other candidate companions to ScoPMS 214 do. Therefore, CC1 has a high likelihood of being a bound companion to ScoPMS 214, although it could also be an unrelated member of Upper Scorpius—the parent association of ScoPMS 214—seen in projection.

It is in principle possible to distinguish between the above two possibilities in a probabilistic manner, by following a two-point correlation function analysis, as done for Upper Scorpius by Kraus & Hillenbrand (2007). We find that the probability to find at least one chance alignment among our 23 deep sample targets that belong to young stellar associations with an unrelated ≥M4 dwarf ($\lesssim$0.1 $M_\odot$) within the same association is ∼2.5%. That

is, if CC1 is a member of Upper Scoprius, then there is a 97.5% probability that it is physically bound to ScoPMS 214. Similar reasoning lead us to conclude in Metchev (2006) that CC1 was a bona-fide companion to ScoPMS 214, which we named ScoPMS 214B.

However, as we shall see in § 6.3.2, the spectroscopic evidence argues against membership of CC1 (ScoPMS 214"B") in Upper Scorpius.

6.3.1. *Spectral Type and Effective Temperature of ScoPMS 214"B"*

We obtained a $R \approx 1200$ K-band spectrum of ScoPMS 214"B" (CC1) with Keck AO/NIRC2 on 14 July 2005. We used the 80 mas-wide slit and the medium (20 mas pix^{-1}) NIRC2 camera. We integrated for a total of 7.5 min on the companion, following an ABC pointing sequence with 2.5 min integrations per pointing. We observed a nearby A0 star for telluric correction. Exposures of Ne and Ar lamps were obtained for wavelength calibration. The individual 2.5 min exposures were pair-wise subtracted and the spectrum of ScoPMS 214"B" was traced and extracted from each exposure in a 280 mas-wide (≈ 5.6 PSF FWHM) aperture. The three individual spectra were median-combined and smoothed to the resolution set by the instrument configuration using a Savitsky-Golay smoothing algorithm.

The resultant K-band spectrum of ScoPMS 214"B" is shown in Figure 10, where it is compared to IRTF/SpeX K-band spectra of field M dwarf and M giant standards from the IRTF Spectral Library[5] (Cushing et al. 2005; Rayner et al. 2008), smoothed to the same resolution. The dominant atomic and molecular absorption features due to Na I, Ca I, and CO are identified.

The overall K-band continuum slope of ScoPMS 214"B" is much closer to the continuum slopes of the M dwarfs than to those of the M giants, although ScoPMS 214"B" is redder than both sets of standards. With an extinction of $A_V \sim 2$ mag towards Upper Scorpius the expected reddening of ScoPMS 214"B" at K band is negligible. Instead, the discrepancy between the continuum slopes of ScoPMS 214"B" and the M standards may be due to instrumental systematics between the Keck AO/NIRC2 and IRTF/SpeX spectra. In particular, accurate continuum slopes are difficult to extract from classical AO spectroscopy (Goto et al. 2003; McElwain et al. 2007) because of the chromatic behavior of the AO PSF and because of the narrow slits (here 80 mas) used to match the width of the AO PSF. Nevertheless, an independent indication that ScoPMS 214"B" has a dwarf-like surface gravity ($\log g \sim 5$) comes from the relatively shallow depth of the CO bandheads in the spectrum of ScoPMS 214"B": comparable in strength to the CO bandheads of the M dwarfs and weaker than the CO bandheads of the M giants. This is not unusual despite the possibility that ScoPMS 214"B" may still be contracting toward the main sequence. Even at 5 Myr ages M stars are expected to have surface gravities that are much more similar to those of dwarfs than to those of giants ($\log g \sim 1$).

From a visual examination of the spectra in Figure 10 we estimate that ScoPMS 214"B" has an M3–M5 spectral type, based on the relative strengths of the Na I and Ca I absorption features compared to the other M dwarfs. Unfortunately, a more accurate classification based on the K-band spectrum alone is not possible. On one hand, the Na I 2.21 μm doublet is known to be sensitive to both effective temperature and surface gravity (Gorlova et al. 2003). On the other hand, while the Ca I 2.26 μm triplet is considered to be a good temperature indicator for G and K stars (Ali et al. 1995), the scatter at early- to mid-M spectral types is significant (Gorlova et al. 2003). This is evidenced by the non-monotonic change in the depth of the Ca I triplet in the M3–M6 spectral type sequence in Figure 10. Therefore, we adopt M3–M5 as our final estimate of the spectral type of ScoPMS 214"B."

The effective temperature corresponding to the M3–M5 range is 3250–2800 K (within errors of $\pm$100 K), according to the field M dwarf temperature scale of Reid & Hawley (2005, see their Table 4.1). More recent work on M dwarf effective temperatures, supported by highly accurate photometric and interferometric measurements (Casagrande et al. 2008), finds that the Reid & Hawley scale systematically overestimates the temperatures of <3000 K field M dwarfs by about 100 K. However, Luhman (1999) finds that young M dwarfs specifically are significantly *hotter* than their older field counterparts. Luhman's conclusion is based on the requirement that all components of the GG Tau quadruple system lie on the same 1 Myr theoretical isochrone from the NextGen models of Baraffe et al. (1998), and is supported by population age analyses in other young associations, such as IC 348 (Luhman 1999) and the Orion Nebular Cluster (Slesnick et al. 2004). Although Luhman's conclusion relies on theoretical isochrones from Baraffe et al. (1998), the models in question have been shown to most successfully and, on average, fairly accurately predict the fundamental properties of pre-main-sequence stars (Hillenbrand & White 2004). The effective temperature range of 1 Myr M3–M5 dwarfs found by Luhman (1999) is 3415–3125 K.

Such disagreement at these low effective temperatures is not unusual, given the increasing complexity of stellar spectra at <3000 K. The problem is even more aggravated at young ages, when the lower surface gravities of the objects further affect their photospheric appearance. Because of its specific pertinence to young M dwarfs, when considering the possibility below that ScoPMS 214"B" is a member of Upper Scorpius, we will adopt the temperature scale of Luhman (1999).

We proceed by examining two probable scenarios: (1) a "young" (5 Myr) ScoPMS 214"B" that is a member of Upper Scorpius, probably as a companion to ScoPMS 214, with $3125 \leq T_{\rm eff} \leq 3415$ K, or (2) a "field-aged" (1–10 Gyr) ScoPMS 214"B" that is simply seen in projection along the line of sight toward ScoPMS 214, with 2700 K $\leq T_{\rm eff} \leq 3250$ K.

6.3.2. *Is ScoPMS 214"B" a Member of Upper Scorpius?*

To decide which of the above two scenarios is valid, and by extension, whether ScoPMS 214A and "B" form a physical pair, we compare the locations of ScoPMS 214A and "B" on an HR diagram with respect to the NextGen model isochrones of Baraffe et al. (1998). Mirroring the approach of Luhman (1999), we expect that if

[5] \protecthttp://irtfweb.ifa.hawaii.edu/~spex/spexlibrary/IRTFlibrary.html.

ScoPMS 214A and "B" were bound and hence co-eval, they should lie on the same isochrone. Since the temperature of ScoPMS 214"B" is ∼3000 K regardless of the considered scenario, the use of the dust-free NextGen models is justified. Indeed, the more recent DUSTY models from the Lyon group (Chabrier et al. 2000) do not extend above 3000 K, since dust is not expected to form in stellar photospheres at such high effective temperatures.

The HR diagram analysis is illustrated in Figure 11. In the "young" ScoPMS 214"B" scenario we have adopted the mean distance to Upper Scorpius members, 145 ± 40 pc, for both ScoPMS 214A and "B". The bolometric luminosity of ScoPMS 214"B" is then $\log L/L_{\odot} = -2.37 \pm 0.24$, where we have used bolometric corrections for M3–M5 dwarfs from Tinney et al. (1993) and Leggett et al. (1996). In this scenario, ScoPMS 214"B" lies on the 1 Gyr isochrone (i.e., on the main sequence), in disagreement with the positioning of ScoPMS 214A above the main sequence. Presuming that ScoPMS 214A is itself not an unresolved binary, the discrepancy indicates that the assumed distance range for ScoPMS 214"B" is incorrect, and that probably it is not a member of the Upper Scorpius association. While ScoPMS 214A also lies slightly beneath an extrapolation of the 5 Myr isochrone, its position is not inconsistent with the adopted age for Upper Scorpius, especially given the physical extent (∼40 pc core radius) of the association.

In the "field-aged" ScoPMS 214"B" case, the object is not a member of Upper Scorpius, and hence its heliocentric distance and bolometric luminosity are not constrained. This case is presented by the shaded region in Figure 11. Given the range of luminosities at which the shaded region intersects the main sequence, the distance to ScoPMS 214"B" is between 70–145 pc.

Therefore, we conclude that ScoPMS 214"B" is probably not a member of Upper Scorpius and hence probably not a physical companion to ScoPMS 214. Instead, it is likely to be a foreground M dwarf seen in projection against Upper Scorpius. We arrive at this conclusion despite the apparent agreement between the proper motions of ScoPMS 214 and ScoPMS 214"B" over nearly five years. The reason for the apparent agreement is the relatively small proper motion of ScoPMS 214 (23 mas yr^{-1}), which tests the precision limits of our astrometric calibration even over a five-year period. Ongoing astrometric monitoring of this system and measurements of the individual radial velocities of the two components will allow us to discern the difference in their space motions.

7. SURVEY INCOMPLETENESS AND SAMPLE BIASES

Before addressing the frequency of wide substellar companions in our sample (§ 8), we present a brief summary of the factors that affect the completeness of our survey (§ 7.1), and discuss the various sample biases (§ 7.2). The detailed completeness analysis is relegated to the Appendix.

7.1. *Survey Incompleteness*

The principal factors that influenced the completeness of our deep survey can be divided into three categories: (1) geometrical, defined by the inner and outer working angles (IWA and OWA) of the survey (0.″55 and 12.″5, respectively) and by the distribution of heliocentric distances of the sample targets; (2) observational, defined by the flux limits of the survey relative to the predicted brightness of substellar companions; and (3) orbital, defined by the fraction of orbital phase space observed. For the sake of simplicity in estimating the total survey incompleteness, we have assumed that the distributions of orbital semi-major axis and mass for substellar companions are $dN/d\log a \propto a^0$ and $dN/dM_2 \propto M_2^0$, respectively. Other common distributions for these parameters are explored in § A.4, and are found not to affect the final completeness estimate by more than a factor of 1.24.

We find that the combined completeness of the deep survey to substellar companions in 28–1590 AU semi-major axes ranges from 64.8% at the 0.072 $M_{\odot}$ hydrogen-burning mass limit to 47.0% at the 0.012 $M_{\odot}$ deuterium-burning mass limit. The deep survey is severely incomplete (<30% completeness) to companions below 0.012 $M_{\odot}$ and maximally complete (64.9%) at and above 0.090 $M_{\odot}$. Over the combined 0.012–0.072 $M_{\odot}$ brown dwarf mass range, we estimate that the deep survey is complete to 62% of substellar companions with orbital semi-major axes between 28 AU and 1590 AU (§§ A.3.3–A.5). We combine this estimate with the observational results to obtain the underlying substellar companion frequency in § 8.1.

7.2. *Sample Biases*

Our survey sample carries an important bias against visual binaries, inherited from the FEPS target selection policy. The FEPS sample excluded certain types of visual binaries to minimize photometric confusion in *Spitzer*'s 1.″5–30″ beam at 3.6–70 μm wavelengths (Meyer et al. 2006). In particular:

1. all FEPS sample stars were required to have no projected companions closer than 5″ in 2MASS, and

2. stars older than 100 Myr were also required to have no projected 2MASS companions closer than 15″, unless the companions were both bluer in $J - K_S$ and fainter at K_S by > 3 mag.[6]

The above two criteria create a non-trivial bias against stellar-mass companions in our AO sample. Because of the seeing-limited dynamic range of 2MASS (∼ 4.5 mag at 5″, ∼ 2.5 mag at 3″; see Fig. 11 in Cutri et al. 2003), criterion 1 excludes near-equal magnitude (i.e., near-equal mass) stellar companions. Criterion 2 then further excludes fainter, red (and hence, lower-mass) companions, although only around the >100 Myr-old stars.

Therefore, any analysis of the stellar multiplicity in our survey would tend to underestimate the true stellar companion rate. In particular, if we adopt the median distance for the complete AO sample (Table 3) and the orbital period distribution for solar mass binaries from Duquennoy & Mayor (1991), we find that the above FEPS selection criteria have probably excluded ∼25% of stellar binaries, mostly near-equal mass systems. We do not address this bias further. We only note in § 9.1 that

[6] For reasons of generating a statistically significant sample size, <100 Myr-old stars were allowed to violate this criterion in FEPS.

it has a systematic effect on our estimate of the CMF, in the sense that we have underestimated the relative frequency of near-equal mass binaries.

An additional bias against binary stars, relevant only to the deep portion of our AO survey, is incurred by our on-the-fly selection against $\Delta K_S < 4$ mag projected companions at $0\farcs8 - 13\farcs0$ from our deep-sample coronagraphic targets (criterion 2 in § 2.1). However, by keeping track of which stars were delegated to the shallow sample in this manner, we have accounted for this bias in our analysis of the CMF in § 9.1.

Finally, our AO sample also carries a slight bias against *substellar* secondaries because of the second FEPS selection criterion above. This bias affects only 100–500 Myr-old targets in the deep sample with well-separated ($\geq 5''$) massive brown dwarf secondaries. Fortunately, because of the shallow depth of 2MASS ($K_S \lesssim 15$ mag) and its limited dynamic range ($\Delta K_S \lesssim 6$ mag) within our $12\farcs5$ AO survey radius, the effect of this bias is negligible. Based on the range of assumed semi-major axis distributions for substellar companions considered in § A.4, we find that this criterion would have excluded $\leq$0.5% of detectable $\geq$60 $M_{\rm Jup}$ substellar companions. Over the entire substellar companion mass sensitivity range of our survey (13–75 $M_{\rm Jup}$) the effect of this bias is negligible (<0.1%). We will therefore ignore it in the rest of the discussion.

8. THE FREQUENCY OF WIDE SUBSTELLAR COMPANIONS

Throughout the remainder of this paper we will use the general terms "substellar companion" and "brown dwarf companion" to refer to a 0.012–0.072 $M_\odot$ (13–75 $M_{\rm Jup}$) brown dwarf secondary in a 28–1590 AU orbit around a young Sun-like star, unless otherwise noted.

8.1. *Results from the Present Survey*

Having discovered two bona fide brown dwarf companions among the 100 stars in the deep sample, we estimate the range of true substellar companion fractions that these detections represent. We do so by following a Bayesian approach to derive confidence ranges for the implied frequency of detectable substellar companions, and by applying the incompleteness correction derived in § A.5.

Strictly speaking, the probability of obtaining x successful outcomes (e.g., brown dwarf companion detections) from a number of repetitions of an experiment with a binary outcome is governed by a binomial distribution. In practice, the large number of experiments (100) and the small number of successful outcomes in our case ($x = 2$) mean that the probability of detecting x brown dwarfs given an expected mean rate μ is well approximated by a Poisson probability distribution:

$$P(x|\mu) = \frac{\mu^x \mathrm{e}^{-\mu}}{x!}. \quad (2)$$

We are interested in finding what is the probability distribution for the actual mean rate μ given x detections, i.e., we seek the probability density function (p.d.f.) $P(\mu|x)$.

The result follows from Bayes' Theorem (Rainwater & Wu 1947; Papoulis 1984):

$$P(\mu|x) = \frac{P(x|\mu)P(\mu)}{P(x)}, \quad (3)$$

where the P's denote "probability distributions" rather than identical functional forms. $P(\mu)$ is the "prior" and summarizes our expectation of the state of nature prior to the observations. $P(x|\mu)$ is the "likelihood" that x positive outcomes are observed given a mean of μ. $P(\mu|x)$, the distribution of interest, is the "posterior" probability that the state of nature is μ, given x positive outcomes. $P(x)$ is a normalization factor equal to the sum of all probable outcomes $P(x|\mu)$, given the distribution of the prior $P(\mu)$:

$$P(x) = \int_0^\infty P(x|\mu)P(\mu)d\mu. \quad (4)$$

We assume no previous knowledge of the state of nature, and adopt a prior that minimizes the introduction of subjective information, imposing only a condition of nonnegativity: $P(\mu) = 1$ for $\mu \geq 0$, $P(\mu) = 0$ for $\mu < 0$. That is, we assume that all positive substellar companion detection rates are equally probable. Inserting Equation 2 into Equations 3 and 4, we obtain

$$P(\mu|x) = P(x|\mu) = \frac{\mu^x \mathrm{e}^{-\mu}}{x!}. \quad (5)$$

That is, the p.d.f. of μ is a Gamma distribution that peaks at the observed detection rate x (Fig. 12). Due to the asymmetry of the Gamma distribution, the mean value $\langle\mu\rangle$ is higher than the most likely value $\mu_{\rm ML}$: $\langle\mu\rangle = x + 1 = 3 > \mu_{\rm ML}$.

We determine the confidence interval $[\mu_l, \mu_h]$ of the frequency of substellar companions μ at a desired confidence level CL by integrating $P(\mu|x)$ between μ_l and μ_h. We set the lower and upper bounds μ_l and μ_u of the confidence interval CL so that (see Fig. 12)

$$\int_{\mu_l}^{\mu_u} P(\mu'|x)d\mu' = \mathrm{CL} \quad (6)$$

and

$$P(\mu_l|x) = P(\mu_u|x). \quad (7)$$

Equations (6) and (7) define the minimum size confidence interval $[\mu_l, \mu_u]$ for confidence level CL (Kraft et al. 1991). The system of equations can not be inverted analytically, and has to be solved for μ_l and μ_u numerically. We do so for the equivalent to the 1, 2, and 3 Gaussian sigma (68.2%, 95.4%, and 99.7%) confidence intervals. The respective confidence ranges for μ are 0.9–3.9, 0.3–6.5, and 0.07–9.9 detectable brown dwarf companions for a survey of 100 stars.

Having thus addressed the statistical uncertainties associated with the small number of companion detections, we now apply the estimated survey completeness correction (62%) to $\mu_{\rm ML}$ and to the confidence interval limits of μ. We find that the most likely rate of occurrence of brown dwarf companions in 28–1590 AU orbits around 3–500 Myr-old F5–K5 stars is $\mu_{\rm ML} = 2\%/0.62 = 3.2\%$. The confidence intervals on this estimate are 1.5–6.3% at the 1σ level, 0.5–10.5% at the 2σ level, and 0.1–16.0% at the 3σ level, and are not a strong function of the prior (Kraft et al. 1991). The mean frequency, $3\%/0.62 = 4.8\%$, is higher than the most likely value, but the exact value of the mean frequency is dependent on the Bayesian prior. The higher mean frequency of wide brown dwarf companions (6.8%) that we reported in Metchev (2006) was due to the inclusion of

ScoPMS 214"B" as a substellar companion. We have now shown that ScoPMS 214"B" is most probably an unrelated foreground star seen in projection along the line of sight towards ScoPMS 214 (§ 6.3.2).

Our results for the frequency of substellar companions are built upon simple assumptions for the semi-major axis and mass distributions of substellar secondaries (§ 7.1; for greater detail, see § A.2). However, our conclusions do not depend strongly on these assumptions. As we show in § A.4, when either or both distributions are varied within empirically reasonable limits, the substellar companion frequency remains unchanged to within a factor of 1.24. If, as we argue in § 9.2, the orbital period distribution of substellar companions is the same as for stellar companions, our frequency estimate is accurate to within a factor of 1.06.

8.2. *Comparison to Previous Companion Searches*

8.2.1. *Radial Velocity Surveys*

Precision radial velocity surveys for extrasolar planets have revealed that brown dwarf secondaries are unusually rare ($< 0.5\%$) in 0–3 AU orbits from G and K stars: a phenomenon termed "the brown dwarf desert" (Marcy & Butler 2000). The dearth of brown dwarfs in radial velocity surveys is evident with respect to the observed 0–3 AU frequencies of both extra-solar planets (5–15%; Marcy & Butler 2000; Fischer et al. 2002) and stellar secondaries (11%; Duquennoy & Mayor 1991) around Sun-like stars. That is, brown dwarfs are $\approx$ 20 times rarer than planets and stellar companions in 0–3 AU orbits.

We found that $3.2^{+7.3}_{-2.7}\%$ (2σ confidence interval) of young Sun-like stars have 0.012–0.072 $M_\odot$ companions with semi-major axes between 28 and 1590 AU (§ 8.1). The much wider orbits probed in the present survey prevent a direct parallel with the radial velocity results. Nevertheless, at face value the evidence indicates that the frequency of wide brown dwarf companions to Sun-like stars is, on average, a factor of ~ 3 smaller than that of 0–3 AU extrasolar planets, and a factor of ~ 6 greater than the frequency of 0–3 AU brown dwarfs. The difference with the exoplanet frequency is not statistically significant. The frequencies of 28–1590 AU and 0–3 AU brown dwarfs differ at the 98.6% significance level. That is, wide brown dwarf companions to Sun-like stars are roughly comparable in frequency to radial velocity extrasolar planets, and are probably more common than radial velocity brown dwarfs.

8.2.2. *Wide Stellar Companions*

Based on the Duquennoy & Mayor (1991) orbital period distribution and multiplicity of Sun-like stars, the frequency of 28–1590 AU stellar companions is $\approx$24%. Our estimated frequency of brown dwarfs is a factor of ~ 8 smaller, and significantly (at the $1 - 10^{-8}$ level) so. Therefore, brown dwarf secondaries are indeed less common than stellar secondaries in the 28–1590 AU orbital range.

8.2.3. *Other Direct Imaging Surveys for Substellar Companions*

A large number of direct imaging surveys have been completed to date, covering a wide range in primary mass and in sensitivity to substellar companions. Despite the disparate characteristics of these surveys, there are now enough data to analyze the ensemble of the results.

We compare our AO survey to all previously published direct imaging surveys for substellar companions to $\geq$0.2 $M_\odot$ primaries. We include only surveys targeting $\geq$15 stars that also contain at least a cursory reference to the parent sample statistics and to the substellar companion discovery rates. All such surveys, to our present knowledge, are listed in Table 12. Additional direct imaging surveys certainly exist. However, any published results from these have tended to report only individual detections. To this list of direct imaging surveys we have also added the radial-velocity results of Marcy & Butler (2000) for comparison. For each published survey, Table 12 lists the number, median spectral type, age, primary mass, and heliocentric distance of the sample stars. For most surveys, these values have been inferred from the description or listing of the sample in the referenced publication. For some surveys, however, these parameters have been inferred based on the stated focus of the survey (e.g., Sun-like stars), or where appropriate, based on the properties of stars in the solar neighborhood. Table 12 also lists the maximum probed projected separation, the sensitivity to companion mass, the number of detected brown dwarf companions, and the rate of detection of brown dwarf companions.

Although an incompleteness analysis is crucial for the correct interpretation of survey results, the majority of published results do not contain such. Therefore, any comparison among surveys has to be based solely on the mean or median survey sample statistics and sensitivities. Taking the ensemble statistics of all direct imaging surveys for substellar companions at face value, without accounting for their varying degrees of incompleteness, we find that the mean detection rate is 1.0 substellar companions per 100 stars. Given the very low number of detections per survey (0–2), the results from all imaging companion surveys are fully consistent with each other.

We have plotted the substellar companion detection rates of all surveys on a primary mass versus outer probed separation diagram in Figure 13. The outer probed separation is defined simply as the product of the survey angular radius (generally, the half-width of the imaging detector) and the median heliocentric distance for the survey sample. The diagram reveals that the surveys with the highest detection rates of substellar companions reside in a distinct locus in the upper right quadrant of the diagram, delimited by the dotted line. All surveys outside of this region have detection rates $\leq 0.6\%$, whereas all surveys within the region have generally higher, 0.5–5.0% detection rates. This fact transcends survey sensitivity considerations. Some of the most sensitive companion surveys with the smallest likely degrees of incompleteness, such as the radial velocity survey of Marcy & Butler (2000) and the simultaneous differential imaging (SDI) surveys of Masciadri et al. (2005) and Biller et al. (2007), lie outside of the dotted region and have detection rates well below 1%. That is, unless all of these highly sensitive surveys did not detect brown dwarf companions through some improbable happenstance, a significant population of brown dwarf companions apparently exists at $\gtrsim$150 AU separations from $\gtrsim$0.7 $M_\odot$ stars. Brown dwarf companions appear

to be less frequent both at smaller orbital separations from Sun-like stars, and at wide separations from lower-mass stars. The dearth of brown dwarf companions to 0.2–0.6 $M_\odot$ stars is likely due to a combination of the lower multiplicity rate of low mass stars and the tendency of low mass binaries to exist predominantly in close-in near-equal mass systems (e.g., Burgasser et al. 2007; Allen 2007, and references therein). The surveys with the highest detection rates are those targeting very wide companions to ~ 1 $M_\odot$ stars.

It is important to re-iterate again that none of the detection rates for any of the surveys in Figure 13 have been corrected for systematic or incompleteness effects. In particular, there is a strong bias against the detection of substellar companions in narrow orbits in all direct imaging surveys because of contrast limitations. In addition, the position of each survey along the abscissa is based on the median *outer* probed separation, whereas most companions are detected at smaller projected separations. Therefore, the increase in the frequency of substellar companions to $\gtrsim$0.7 $M_\odot$ stars probably begins well within 150 AU. In the § 9.2 we argue that the peak of the brown dwarf companion projected separation distribution may in fact occur at ∼25 AU, as would be expected from the Duquennoy & Mayor (1991) binary orbital period distribution.

9. DISCUSSION

9.1. *The Sub-Stellar and Stellar Companion Mass Function*

The salient characteristic of the present imaging survey is its high sensitivity to low-mass ($M_2 \leq 0.1 M_\odot$) companions to solar analogs, i.e., to systems with mass ratios $q \lesssim 0.1$. We found only seven such companions among 74 binary and one triple systems: the two brown dwarfs HD 49197B and HD 203030B, and the 0.08–0.14 $M_\odot$ stars HD 9472B, HE 373B, RX J0329.1+0118B, HD 31950B, and PZ99 J161329.3–231106B (Table 11). A naïve expectation from the MF of isolated objects (Kroupa 2001; Chabrier 2001) would require approximately as many < 0.1 $M_\odot$ companions as there are > 0.1 $M_\odot$ companions. Therefore, it appears that there is a dearth of widely-separated *both substellar and low-mass stellar* companions to Sun-like stars.

To assess the reality and magnitude of this effect we need a uniform survey of a well-characterized sample of binaries. Unfortunately, our full survey sample is not adequate for such an analysis because the imaging depths of the deep and the shallow sub-surveys are vastly different, and because the sample is subjected to the combined effect of three different biases against binary stars (§ 7.2). We could, in principle, focus only on the deep survey of 100 young stars, for which we have a well-characterized completeness estimate. However, doing so would not avoid any of the binarity biases. Furthermore, the deep survey sample contains only 19 of all 75 binaries and triples, only six of which are in the 0.″55–12.″5 angular separation range, for which we estimated incompleteness (§ 7.1). This number is too low for a meaningful analysis of the CMF.

Nevertheless, we can un-do some of the binarity biases and recover certain rejected stellar secondary companions by re-visiting how binaries were removed from the deep sample during survey observations. We discuss this procedure and reconstruct a sample that is minimally biased against binaries in the following.

9.1.1. *Defining a Minimally Biased Sample*

We construct a less biased, larger sample of stars by adding to our 100-star deep sample all other ≤500 Myr-old stars that were initially selected to be in the deep sample but for which no coronagraphic exposures were taken because of the discovery of a close-in (0.″8–13.″0) $\Delta K_S < 4$ mag companion (see § 2.1). Since we did not inherit this bias from the larger FEPS program sample, but rather imposed the criteria ourselves, we knew the parent sample and were able to un-do the bias exactly. The resulting "augmented" deep (AD) sample is minimally biased against binaries to the extent to which we controlled the sample generation.

There are 28 binaries excluded in this manner, that contribute to a total of 128 young stars in the AD sample. Among these are a total of 46 binaries and one triple, of which 30 systems (including the triple) have companions between 0.″55 and 12.″5 from the primary. Members of the AD sample are distinguished in the last column of Table 11, where the 30 members with 0.″55–12.″5 companions are marked with "AD_{30}".

We assume that the young binaries added from the shallow sample do not have additional fainter tertiary companions between 0.″55–12.″5 that would have been detectable had we exposed them to the depth of the longer coronagraphic images. Given the ≈10% ratio of double to triple systems in the study of Duquennoy & Mayor (1991), and the fact that the 28–1590 AU orbital range ($\approx 10^{4.7} - 10^{7.3}$ days at 1 $M_\odot$ total mass) includes approximately 42% of all companions (0–10^{10}-day periods) probed in Duquennoy & Mayor (1991), we would expect that $\approx 0.10 \times 0.42 \approx 4\%$ of systems have a tertiary component in a 28–1590 AU orbit. In comparison, the $1:46 \approx 2\%$ ratio of triples to binaries in our sub-sample indicates that such an assumption is not unreasonable: on average, we may have missed one low-mass (possibly substellar) tertiary component. Therefore, we have potentially suffered only a small loss in completeness by including stars for which we do not have deep coronagraphic exposures.

The AD and the AD_{30} samples remain biased against binaries, although mostly against near-equal mass systems (§ 7.2). Because we have placed an upper age limit of 500 Myr for membership in these samples and because of the logarithmically uniform distribution of stellar ages in the parent FEPS sample, the bias against lower mass stellar secondaries (FEPS binarity criterion 2; § 7.2) affects less than a quarter of the stars in the AD sample: only those that are 100–500 Myr old.

The detectability of the AD_{30} secondaries within the greater AD sample is subject to the same set of target selection criteria and to the same geometrical, observational, and orbital incompleteness factors (see § A.3) as for the deep survey. Therefore we can estimate the completeness of the AD sample to the detection of secondaries in 28–1590 AU semi-major axes in the same manner as done for the deep survey.

The completeness to 0.012–0.072 $M_\odot$ substellar companions in 28–1590 AU semi-major axes in the deep survey ranges from 47.0% to 64.8%, depending on companion mass (see § A.3). For masses ≥0.090 $M_\odot$ the deep

survey is maximally complete at 64.9%. The integrated completeness to 0.01–1.0 $M_\odot$ companions is $\approx 64\%$ (cf., 62% integrated completeness to 0.012–0.072 $M_\odot$ substellar companions; § 7.1). Given the 30 0.″55–12.″5 binaries in the AD_{30} sample, we would expect a total of $30/0.64 \approx 47 \pm 9$ binaries with 28–1590 AU semi-major axes in the 128-star AD sample, where the error on that estimate is propagated as $\sqrt{30}/0.64$. (By pure coincidence, this is exactly how many multiple systems (47) are present in the AD sample.) The incompleteness-corrected frequency of 0.01–1.0 $M_\odot$ companions in 28–1590 AU orbits in the AD sample is thus $47/128 = 37 \pm 7\%$. This is somewhat higher than the 24% integrated over the corresponding $10^{4.7}$–$10^{7.3}$-day orbital period from Duquennoy & Mayor (1991). Despite the bias against binaries, the higher multiplicity fraction of stars in our survey is not unexpected because of our superior sensitivity to very low mass companions and our focus on young stars, which tend to more often be found in multiples (e.g., Ghez et al. 1993, 1997).

9.1.2. *The Distribution of Companion Masses*

In their G dwarf multiplicity study, Duquennoy & Mayor (1991) found that the MFs of isolated field stars and of 0.1–1.0 $M_\odot$ stellar companions to solar-mass primaries were indistinguishable. We now re-visit this conclusion in light of our more sensitive imaging data and in the context of more recent determinations of the field MF.

The mass ratio distribution for our selection of 30 young binaries in the AD_{30} sample is shown in Figure 14. The distribution is fit well by a power law of the form

$$\log\left(\frac{dN}{d\log q}\right) = \delta \log q + b, \tag{8}$$

equivalent to $dN/d\log q \propto q^\delta$, or $dN/dq \propto q^{\delta-1} \equiv q^\beta$. The best-fit value for the power law index is $\delta = 0.61$, or equivalently, $\beta = 0.39 \approx 0.4$. The reduced χ^2 of the fit is adequate, 1.5, and given only three of degrees of freedom a higher-order functional fit is not warranted. The χ^2 contours of β and b indicate that the parameters are correlated. By integrating over all possible values for b, we find that the 68% (one Gaussian σ) and 95% confidence intervals for β are $-0.75 < \beta < -0.03$ and $-0.93 < \beta < 0.14$, respectively.

We compare this mass ratio distribution to the known MF of isolated field objects from Chabrier (2003). Because the masses of the primary stars in our sample are distributed closely around 1 $M_\odot$ (Fig. 1b), we can directly compare the distribution of the (unitless) mass ratios to the field MF (in units of $M_\odot$). That is, the mass ratio distribution of our sample is essentially equivalent to the CMF in units of $M_\odot$ since $q = M_2/M_1 \approx M_2/M_\odot$. The power law index β of the CMF is analogous to the linear slope α (Salpeter value -2.35) of the field MF. As is evident from Figure 14, the CMF of our sample of young binaries is very different (reduced $\chi^2 = 7.6$) from the MF of field objects.

A potentially more sensitive comparison between the observed mass ratio distribution and any model MFs (e.g., log-normal, power law) could be obtained using a Kolmogorov-Smirnov (K-S) test. We do not perform Monte Carlo simulations to degrade the MF models to match the observed data, as would be necessary in the rigorous sense, but instead compare the models to the incompleteness-corrected data. Although the K-S test is not strictly applicable with such an approach, the results from the test are nevertheless illustrative. Thus, a one-sample Kolmogorov-Smirnov test finds only a 2×10^{-8} probability that the observed CMF originates from the log-normal field MF of Chabrier (2003). The K-S probability that the fitted power law in Equation 8 with $\beta = -0.39$ is the correct parent CMF is 7%. Ostensibly the best agreement (58% K-S probability) with the incompleteness-corrected data is reached by a log-normal mass ratio distribution with a mean and standard deviation of 0.39. A similar log-normal CMF was inferred independently by Kraus et al. (2008) in their analysis of resolved binaries in Upper Scorpius. However, we note that in our case the difference between the probabilities of the power-law and log-normal parent CMFs (7% versus 58%) is not statistically significant in the context of the K-S test. Therefore, given the already adequate reduced χ^2 of the power law fit from Equation 8, we disregard the potentially better, but statistically less well motivated, agreement with the data of the higher-order log-normal parameterization (three free parameters), in favor of the lower-order (two free parameters) power law.

A value near zero for our CMF power law exponent β is consistent with the MF of < 0.1 $M_\odot$ objects in the field ($-1.0 < \alpha \lesssim 0.6$; Chabrier 2001; Kroupa 2002; Allen et al. 2005) and in young stellar associations ($-1 \lesssim \alpha \lesssim 0$; Hillenbrand & Carpenter 2000; Slesnick et al. 2004; Luhman 2004). However, the monotonic rise of the CMF throughout the entire 0.01–1.0 $M_\odot$ mass range and the lack of a turnover near 0.1 $M_\odot$ disagree with MF determinations for stars in the 0.1–1.0 $M_\odot$ interval, where α ranges between -0.5 and -2 (Kroupa 2002). That is, in the stellar mass regime, the CMF and the MF of isolated stars are distinctly different.

We should note that the results from our companion survey may not be ideally suited for determining the CMF of both brown dwarf and stellar companions. Indeed, we recall that our AD sample is biased against various types of visual binaries (§ 7.2). However, as we discussed in § 9.1.1, the bias against binarity in the AD sample is mostly against near-equal mass systems, the secondaries in which would populate the highest mass ratio bin in Figure 14. That is, the power-law index β of the CMF would only further increase in value if the bias against near equal-mass binaries in our survey sample were taken into account, and the CMF would become even more disparate from the field MF.

Our conclusion counters the established view that the MF of 0.1–1.0 $M_\odot$ binary components is indistinguishable from the MF of isolated objects. In arriving at the original result, Duquennoy & Mayor (1991) had compared the $0.1 < q \leq 1.0$ binary mass ratio distribution of their sample stars to an earlier form of the field MF from Kroupa et al. (1990). Since the mass ratio distribution of $q > 0.1$ binaries in our sample is consistent with that of Duquennoy & Mayor (see Fig. 14b), the difference in the results stems from our superior sensitivity to $q \leq 0.1$ binaries and from the recently improved knowledge of the MF of low-mass (< 0.2 $M_\odot$) stars in the field.

Similar conclusions were reached independently by Shatsky & Tokovinin (2002) and by Kouwenhoven et al.

(2005) in their direct imaging studies of the visual multiplicity of intermediate mass (2–20 $M_\odot$) B and A stars. These two surveys found that the mass ratio distribution of 45–900 AU intermediate mass binaries follows an $f(q) \propto q^\beta$ power law, where β is -0.5 (Shatsky & Tokovinin 2002) or -0.33 (Kouwenhoven et al. 2005). Our determination that $\beta = -0.39 \pm 0.36$ for companions to solar mass stars indicates that the shape of the CMF found by Shatsky & Tokovinin (2002) and Kouwenhoven et al. (2005) is not specific to intermediate mass stars. Considered together, these three sets of results provide a strong evidence for a significant difference between the MFs of wide secondaries and of isolated field objects. That is, the mass ratio distribution of 28–1590 AU binaries is inconsistent with random pairing of stars drawn from the IMF over a vast range of primary and companion masses. We discuss the implications of this conclusion on shaping the dearth of brown dwarf secondaries to stars below.

9.2. *The Brown Dwarf Desert as a Result of Binary Star Formation*

The inferred 0.01–1.0 $M_\odot$ CMF (§ 9.1.2) naturally explains the scarcity of wide brown dwarf companions without the need to invoke formation or evolutionary scenarios specific to substellar companions. The functional form of the wide-binary CMF is also consistent with results from radial velocity studies. Thus, Mazeh et al. (2003) found that the CMF of K-dwarf binaries in 0–4 AU orbits is also a rising function of mass over the 0.07–0.7 $M_\odot$ range. Their data are consistent with a power-law index of $\beta \approx -0.4$, in full agreement with the $-0.3 \leq \beta \leq -0.5$ values for 28–1590 AU binaries found by Shatsky & Tokovinin (2002), Kouwenhoven et al. (2005, 2007), and here.

It may be argued perhaps that, given the disparate sensitivity systematics and statistical treatments in these diverse samples, such an overall agreement is merely coincidental. Indeed, *differences* in the mass ratio distributions of short- vs. long-period binaries within *single* uniform samples have been previously suggested, with dividing periods of 1000 days ($\sim$ 2 AU; Duquennoy & Mayor 1990) or 50 days ($\sim$ 0.3 AU; Halbwachs et al. 2003). However, subsequent analyses by Duquennoy & Mayor (1991) and Mazeh et al. (2003) have shown that the evidence for such discontinuities was inconclusive because of relatively small number statistics. At the same time, the combined set of direct imaging and spectroscopic data referenced here point to an approximately uniform functional form for the CMF over 1.5 orders of magnitude in primary mass (0.6–20 $M_\odot$), 3.3 orders of magnitude in companion mass (0.01–20 $M_\odot$), and 4.7 orders of magnitude in physical separation (0.03–1590 AU). That is, we see strong evidence for a universally uniform shape of the CMF.

Given such universality, it is interesting to consider whether the CMF can explain the very low frequency of brown dwarfs not only in direct imaging, but also in radial velocity surveys. Because stellar and substellar companions to Sun-like stars appear to be derived from the same CMF (§ 9.1.2), we can presume that the Duquennoy & Mayor (1991) period distribution of $\geq$0.1 $M_\odot$ stellar secondaries also holds for substellar companions. Based on this period distribution, the fraction of all secondary companions in 0–3 AU orbits is $\approx$22%. Brown dwarfs account for $\leq 0.5\%/22\% = 2.3\%$ of these. For comparison, brown dwarfs account for $\sim 3.2\%/42\% = 7.6\%$ of all secondaries in 28–1590 AU periods. In the context of our inferred power-law CMF, we find that the value of the index β would need to be as high as 0.2 to reproduce the $\sim$3 times smaller relative frequency of radial velocity brown dwarfs. This does not agree well with our 95% confidence limits on β ($-0.93 < \beta < 0.14$; § 9.1.2). However, we also noted that our estimate for β is systematically underestimated because of the bias against near-equal mass binaries in our AO sample. It is therefore conceivable that the radial velocity brown dwarf desert around G stars represents just the low-mass, narrow-orbit end of a CMF that spans 3.3 dex in secondary mass and 4.7 dex in orbital semi-major axis. *The problem that would need to be addressed then is not why brown dwarf companions specifically are so rare, but why the CMF differs so significantly from the MF of isolated substellar and stellar objects over all orbital ranges.*

In such a universal CMF scenario, brown dwarfs would be expected to peak in frequency at semi-major axes determined by the binary period distribution: at $\approx$ 31 AU from solar mass stars, or at projected separations of $\approx 31/1.26 = 25$ AU (see § A.2 for explanation of factor of 1.26). At first glance, this is not consistent with the diagram of survey detection rates in Figure 13, where we found that (prior to correction for survey incompleteness) the highest detection rates occurred in surveys probing projected separations $\gtrsim$ 150 AU. However, we pointed out that Figure 13 compares only the median *outer* projected separations probed by the various surveys, whereas most companions tend to be discovered at smaller projected separations (§ 8.2.3). In addition, we need to consider that projected separations of 25 AU are usually well within the contrast-limited regime of existing direct imaging surveys of young nearby (50–100 pc) stars. Our own survey is less than 40% complete to objects at the hydrogen-burning mass limit in 31 AU semi-major axis orbits (see § A.3). That is, a number of $\sim$ 30 AU brown dwarfs around solar-mass stars may have simply been missed in direct imaging surveys because of insufficient imaging contrast.

Unfortunately, neither of the two most sensitive direct imaging surveys that probe well within 150 AU (Masciadri et al. 2005; Biller et al. 2007) detect any substellar companions. However, their sample sizes are not large (54 and 28, respectively), and the null detection rates do not place significant constraints on the universal CMF hypothesis. Conversely, the recent discovery of several probable radial velocity brown dwarfs in $>$ 3 AU orbits by Patel et al. (2007) lends support to the idea that brown dwarfs are more common at wider separations, as would be inferred by extrapolation from the Duquennoy & Mayor (1991) orbital period distribution for higher-mass, stellar companions.

Finally, the $\approx$0.012 $M_\odot$ ($\approx$13 $M_{\rm Jup}$) deuterium-burning mass, above which we limit our analysis, does not necessarily mark the bottom of the MF of isolated objects. Based on results from three-dimensional smoothed particle hydrodynamic simulations, Bate et al. (2002) and Bate & Bonnell (2005) estimate that the opacity limit for gravo-turbulent fragmentation may be as low

as 3–10 $M_{\rm Jup}$. Adopting 3 $M_{\rm Jup}$ as the limit and extrapolating the inferred CMF to <13 $M_{\rm Jup}$ masses, we find that sub-deuterium-burning "planetary-mass" companions, if able to form through gravo-turbulent fragmentation, exist in ≥30 AU orbits around only $\lesssim$1% of Sun-like stars.

10. CONCLUSION

We have presented the complete results from a direct imaging survey for substellar and stellar companions to 266 Sun-like stars performed with the Palomar and Keck AO systems. We discovered two brown dwarf companions in a sub-sample of 100 3–500 Myr-old stars imaged in deep coronagraphic observations. Both were already published in Metchev & Hillenbrand (2004, 2006). In addition, we discovered 24 new stellar companions to the stars in the broader sample, five of which are in very low mass ratio $q \sim 0.1$ systems.

Following a detailed consideration of the completeness of our survey, we found that the frequency of 0.012–0.072 $M_\odot$ brown dwarf companions in 28–1590 AU orbits around 3–500 Myr-old Sun-like stars is $3.2^{+3.1}_{-2.7}$% (2σ limits). This frequency is marginally higher than the frequency of 0–3 AU radial velocity brown dwarfs, and is significantly lower than the frequency of stellar companions in 28–1590 AU orbits. The frequency of wide substellar companions is consistent with the frequency of extrasolar giant planets in 0–3 AU orbits. A comparison with other direct imaging surveys shows that substellar companions are most commonly detected at $\gtrsim$ 150 AU projected separations from $\gtrsim$ 0.7 $M_\odot$ stars. However, because of bias against the direct imaging of faint close-in companions, brown dwarf secondaries are likely also common at smaller projected separations.

Considering the two detected brown dwarf companions as an integral part of the broader spectrum of stellar and substellar companions found in our survey, we infer that the mass ratio distribution of 28–1590 AU binaries, and hence, the MF of 28–1590 AU secondary companions to solar-mass primaries, follows a $dN/dM_2 \propto M_2^\beta$ power law, with $\beta = -0.39 \pm 0.36$ (1σ limits). This distribution differs significantly from the MF of isolated objects in the field and in young stellar associations, and is inconsistent with random pairing of individual stars with masses drawn from the IMF. In this context, the observed deficiency of substellar relative to stellar companions at wide separations arises as a natural consequence of the shape of the CMF, and does not require explanation through formation or evolutionary scenarios specific to the substellar or low-mass stellar regime.

Comparing our CMF analysis to results from other direct imaging and radial velocity surveys for stellar and substellar companions, we find tentative evidence for universal behavior of the CMF across the entire 0–1590 AU orbital semi-major axis and the entire 0.01–20 $M_\odot$ companion mass range. Such a universal CMF is not inconsistent with the marked dearth of brown dwarfs in the radial velocity brown dwarf desert around Sun-like stars. That is, the properties of brown dwarf companions at any orbital separation are conceivably an extension of the properties of stellar secondaries. Hence, we predict that the peak in semi-major axes of brown dwarf companions to solar-mass stars occurs at ≈ 30 AU. Extrapolating the inferred CMF to masses below the deuterium burning limit, we find that if 0.003–0.012 $M_\odot$ "planetary-mass" secondaries can form through gravo-turbulent fragmentation, they should exist in ≥ 30 AU orbits only around less than 1% of Sun-like stars.

We would like to thank Richard Dekany, Mitchell Troy, and Matthew Britton for sharing with us their expertise on the Palomar AO system, Rick Burress and Jeff Hickey for assistance with PHARO, Randy Campbell, Paola Amico, and David Le Mignant for their guidance with using Keck AO, Keith Matthews and Dave Thompson for help with NIRC2, and our telescope operators at the Palomar Hale and Keck II telescopes. We are also grateful to Keith Matthews for loaning us a pinhole mask for the astrometric calibration of PHARO, and to both Richard Dekany and Keith Matthews for key insights into the design of the calibration experiment.Use of the FEPS Team database has proven invaluable throughout the course of our survey. We thank John Carpenter for building and maintaining the database. For the target selection, age-dating, and determination of distances to the FEPS sample stars, we acknowledge the tremendous amount of work performed by Eric Mamajek. This publication makes use of data products from the Two Micron All Sky Survey, funded by the NASA and the NSF. The authors also wish to extend special thanks to those of Hawaiian ancestry on whose sacred mountain of Mauna Kea we are privileged to be guests. Support for S.A.M. was provided by NASA through the *Spitzer* Legacy Program under contract 1407 and through the *Spitzer* Fellowship Program under award 1273192. Research for this paper was also supported by the NASA/Origins R&A program.

Facilities: Keck II Telescope, Palomar Observatory's 5 meter Telescope

APPENDIX

INCOMPLETENESS OF THE DEEP SURVEY

Here we examine the factors affecting the sensitivity of the deep survey to substellar companions (§ A.1), and, based on several assumptions about the semi-major axis and mass distributions of wide substellar companions (§ A.2), we estimate the completeness of the survey (§ A.3). We find that variations in the parameters of the semi-major axis and mass distributions have little effect (§ A.4) on the final completeness estimate. This final estimate (§ A.5) is used in § 8 in combination with the observational results from our survey to obtain the actual frequency of substellar companions.

Factors Affecting Survey Completeness

Several factors need to be taken into account when estimating the detectability of substellar companions to our stars. These include: (i) possible sample bias against stars harboring substellar secondaries, (ii) choice of substellar cooling

models, (iii) observational constraints (i.e., survey radius, imaging contrast, and depth), and (iv) physical parameters of the stellar/substellar systems (flux ratio, age, heliocentric distance, orbit).

As discussed in § 7.2, the deep sample is largely unbiased toward substellar companions, i.e., factor (i) can be ignored. For the basis substellar cooling models (ii) we rely on the DUSTY and COND models of the Lyon group (Chabrier et al. 2000; Baraffe et al. 2003). These have been used, either alone or in parallel with the models of the Arizona group (Burrows et al. 1997), in all other studies of substellar multiplicity. Our choice therefore ensures that our results will be comparable with the existing work on the subject. The remaining factors (iii and iv) motivate the rest of the discussion here.

Assumptions

We will base our incompleteness analysis on three assumptions: (1) that the distribution of semi-major axes a of substellar companions to stars is flat per unit logarithmic interval of semi-major axis, $dN/d\log a \propto a^0$ (or equivalently, $dN/da \propto a^{-1}$) between 10 AU and 2500 AU, (2) that this implies a logarithmically flat distribution in *projected* separations ρ: $dN/d\log\rho \propto \rho^0$ (i.e., $dN/d\rho \propto \rho^{-1}$), and (3) that the mass function of substellar companions is flat per linear mass interval ($dN/dM_2 \propto M_2^\beta = M_2^0$) between $0.01M_\odot$ and $0.072M_\odot$. These assumptions, albeit simplistic, have some physical basis into what is presently known about binary systems and brown dwarfs. We outline the justification for each of them in the following.

Assumption (1).— Adopting a total (stellar+substellar) system mass of 1 $M_\odot$, the 10–2500 AU range of projected separations corresponds approximately to orbital periods of $10^4 - 10^{7.5}$ days. This range straddles the peak (at $P = 10^{4.8}$ days; $a = 31$ AU), and falls along the long-period slope of the Gaussian period distribution of G-dwarf binaries (Duquennoy & Mayor 1991). If we were to assume a similar formation scenario for brown dwarfs and stars, brown dwarf secondaries would also be expected to fall in frequency beyond ∼30 AU separations. However, our limited amount of knowledge about brown dwarf companions suggests the opposite: brown dwarf secondaries may appear as common as stellar secondaries at >1000 AU separations (Gizis et al. 2001), whereas a brown dwarf desert exists at <3 AU semi-major axes (Marcy & Butler 2000; Mazeh et al. 2003). A smattering of brown dwarfs have been discovered in between. A logarithmically flat distribution of semi-major axes for substellar companions, $dN/d\log a \propto a^0$, or equivalently $dN/da \propto a^{-1}$, represents a middle ground between the known distribution of stellar binary orbits and the possible orbital distribution of known brown dwarf companions. The assumption is also attractive because of its conceptual and computational simplicity. As we discuss in § A.4, varying the linear exponent on the semi-major axis distribution between 0 and −1, or adopting a log-normal semi-major axis distribution as motivated by the Duquennoy & Mayor (1991) binary period distribution, changes the overall completeness estimate by a factor of ≤ 1.20.

Assumption (2).— For a random distribution of orbital inclinations i on the sky, the true and apparent physical separations are related by a constant multiplicative factor: the mean value of $\sin i$. However, a complication is introduced when relating the projected separation to the true semi-major axis because of the need to consider orbital eccentricity. Because an object spends a larger fraction of its orbital period near the apocenter than near the pericenter of its orbit, the ratio of the semi-major axis to the apparent separation will tend to values >1. Analytical treatment of the problem (Couteau 1960; van Albada 1968) shows that this happens in an eccentricity-dependent manner. Yet, when considering the eccentricity distributions of observed binary populations (Kuiper 1935a,b; Duquennoy & Mayor 1991; Fischer & Marcy 1992), both analytical (van Albada 1968) and empirical Monte Carlo (Fischer & Marcy 1992) approaches yield the same identical result: $\langle\log a\rangle \approx \langle\log\rho\rangle + 0.1$. That is, the true semi-major axis and the measured projected separation are, on average, related by a multiplicative factor of 1.26, such that $\langle a\rangle = 1.26\langle\rho\rangle$. Given assumption (1), this then confirms the appropriateness of the current assumption that $dN/d\log\rho \propto \rho^0$. Furthermore, it allows us to relate the projected separations of an ensemble of visual companions to their expected semi-major axes in a mean statistical sense.

Assumption (3).— The assumption for a linearly flat substellar mass distribution ($dN/dM_2 \propto M_2^\beta$; $\beta = 0$) parallels results from spectroscopic studies of the initial mass function (IMF) of low-mass objects in star-forming regions (Briceño et al. 2002; Luhman et al. 2003a,b; Slesnick et al. 2004; Luhman et al. 2004), which are broadly consistent with $\alpha \sim 0$ (where α is the exponent in $dN/dM \propto M^\alpha$). Independently, in a recent analysis of the field substellar mass function (MF), Allen et al. (2005) find $\alpha = 0.3 \pm 0.6$, also consistent with zero. Therefore, assuming that the *substellar* MFs in young stellar associations and in the field are representative of the MF of wide *substellar* companions, we adopt a linearly flat $dN/dM_2 \propto M_2^0$ CMF for our analysis. This is consistent with our subsequent fit to the CMF in § 9.1.2, where we determine that β is in fact -0.39 ± 0.36 over the entire 0.01–1.0 $M_\odot$ substellar and stellar companion mass range.

The latter result may seem circuitous, since the derivation that β is near zero is in fact dependent on the initial assumption that β is zero. Nevertheless, we find that the initial guess for the CMF exponent is largely unimportant. As we discuss in § A.4, initial values for β ranging between −1 and 1 change the overall completeness estimate by ≤ 1.08, and as a result have negligible effect on the final value for β.

Incompleteness Analysis

Adopting the preceding set of assumptions, we now return to the discussion of the remaining factors affecting survey incompleteness: factors (iii) and (iv) from § A.1. We address the individual factors in three incremental steps, as

pertinent to: geometrical incompleteness, defined solely by the IWA and OWA of the survey and by the distribution of stella heliocentric distances; observational incompleteness, defined by the flux limits of the survey and by the predicted brightness of substellar companions; and orbital incompleteness, defined by the fraction of orbital phase space observed. These are the same incompleteness categories as already mentioned in § 7.1. Throughout, we adopt the aperture-normalized r.m.s. detection limits determined for each star in § 4.3 and assume that the primary ages and distances are fixed at their mean values listed in Table 1.

Geometrical Incompleteness

In deciding the range of projected separations that the study is most sensitive to, we consider the full range of separations that have been explored between the IWA and OWA of the deep survey. For the IWA we adopt 0.″55, i.e., approximately one half width of the 0.″1 PALAO K_S-band PSF wider than the 0.″49 radius of the PHARO coronagraph. For the OWA, we adopt 12.″5, which is 0.″3 less than the half-width of the PHARO FOV. Figure 15 shows the fraction of the deep sample stars (solid line) around which successive 1 AU intervals are probed as a function of projected separation. It is immediately obvious that only a very narrow range of orbital separations, between 105 AU and 125 AU, is probed around 100% of the stars. All other projected separations carry with them some degree of incompleteness that needs to be taken into account. From a purely geometrical standpoint, i.e., ignoring imaging sensitivity, the limitations imposed by the choice of IWA and OWA amount to a factor of 1.96 incompleteness (for a $dN/d\log a \propto a^0$ semi-major axis distribution) between 6 AU and 2375 AU: the projected separation range contained between the IWA for the nearest star and the OWA for the farthest star in the deep sample. That is, provided that substellar companions are detectable regardless of their brightness anywhere between 0.″55 and 12.″5 from each star, and provided that their distribution of semi-major axes a is logarithmically flat, only about half of the companions residing in the 6–2375 AU projected separation range would be detected.

As is evident from Figure 15, such a wide range of orbital separations includes regions probed around only a small fraction of the stars. Consideration of the full 6–2375 AU range will thus induce a poorly substantiated extrapolation of the companion frequency. Instead, we choose to limit the analysis to projected separations explored around at least one-third (i.e., 33) of the stars in the deep sample. The corresponding narrower range, 22–1262 AU, is delimited by the dashed lines in Figure 15. The region has a geometrical incompleteness factor of 1.40 (compared to 1.96 for the full 6–2375 AU range above). That is, $1/1.40 = 71.4\%$ of all companions with projected separations between 22 and 1262 AU should be recovered in our deep survey, if they are sufficiently bright.

Observational Incompleteness

Following an approach analogous to the one described in the preceding discussion, we infer the projected separation range over which our survey is sensitive to a companion of a given mass. That is, we now take into account that not all companions are sufficiently bright to be detected at all probed projected separations. Rather their visibility is determined by their expected brightness and the attained imaging contrast.

Because mass is not an observable, we use the absolute K-band magnitude of a substellar object as a proxy for its mass, and employ the Lyon suite of theoretical models to convert between absolute magnitude and mass at the assumed stellar age.

We calculate the observational incompleteness of the deep survey for a grid of 11 discrete companion masses (0.005, 0.010, 0.012, 0.015, 0.020, 0.030, 0.040, 0.050, 0.060, 0.072, and 0.090 $M_\odot$) and over the entire 3–500 Myr age range of our deep sample. We use the DUSTY models from Chabrier et al. (2000) when the predicted companion effective temperature is above 1400 K (i.e., for spectral types L or earlier), and the COND models from Baraffe et al. (2003) at lower effective temperatures (spectral type T). We compare the estimated companion fluxes at the age of each of our sample stars to the corresponding flux limits for each star (see Table 6), and obtain a minimum projected separation at which a companion of a given mass would be visible around each star. Thus, summing over all stars in the deep sample, we estimate the observational incompleteness of the entire deep survey to companions of this mass.

The observational completeness estimates for each of the discrete set of 0.005–0.090 $M_\odot$ companion masses are shown by the filled circles in Figure 16a. The geometrical completeness limit (i.e., if companion brightness were not a limiting factor) is shown by the horizontal continuous line. Figure 16a demonstrates that the deep survey is nearly as complete as is theoretically possible to stellar-mass companions at angular separations between the IWA and OWA, since the observational completeness reaches the geometrical limit at 0.090 $M_\odot$, just above the minimum hydrogen-burning mass. Figure 16a also illustrates that the observational completeness of the deep survey is >50% for all substellar objects above the deuterium-burning limit. The survey completeness drops rapidly below the deuterium-burning limit because of the significantly fainter luminosities expected of non-deuterium fusing objects (e.g., Burrows et al. 2001).

With the aim to minimize our incompleteness correction, we limit our analysis to substellar companions in the 0.012–0.072 $M_\odot$ range, i.e., between the deuterium- and hydrogen-burning mass limits. The sum of the geometrical + observational completeness in this mass range is between 53.0% and 71.3%. Adopting a $dN/dM_2 \propto M_2^0$ (i.e., $\beta = 0$) MF for substellar companions (§ A.2), we find that the observational survey is 68.2% complete to 0.012–0.072 $M_\odot$ substellar companions at projected separations of 22–1262 AU from their host stars.

Orbital Incompleteness

The analysis so far has dealt only with the projected separation of substellar companions. We now consider the effect of realistic orbital semi-major axes, inclinations, and eccentricities.

We first adopt the multiplicative factor of 1.26 to relate the projected separation ρ to the true semi-major axis a: $\langle a \rangle = 1.26\langle \rho \rangle$ (see § A.2). That is, the orbital semi-major axes probed by the survey are on average a factor of 1.26 further from the star, at 28–1590 AU, than the range of probed projected separations.

The multiplicative transformation from $\langle \rho \rangle$ to $\langle a \rangle$ does not exhaust the discussion of orbital incompleteness. Because companions on orbits with non-zero inclinations and eccentricities spend most of their time at projected separations $\rho \neq a/1.26$, they may still be missed in the survey. The most likely scenarios in which this can occur are for companions on highly inclined and/or eccentric orbits.

With a small number of positive substellar companion detections, orbital incompleteness issues are best addressed through Monte Carlo simulations. Such have been performed for a wide range of realistic orbital inclinations and eccentricities in a study by Brown (2004), the results of which we adopt here. Brown's work investigates the detectability of populations of habitable extra-solar terrestrial planets with a range of orbital distributions by the *Terrestrial Planet Finder–Coronagraph (TPF–C)*. Although the angular scales and the levels of imaging contrast between the present coronagraphic survey and the design specifications for *TPF–C* are vastly different (*TPF–C* projections call for a factor of ≈ 2.5 smaller IWA and $\sim 10^6$ higher contrast), the problem is conceptually the same: to determine the completeness to orbits with a certain semi-major axis, given an opaque coronagraph of a fixed radius. Brown (2004) parameterizes this problem in terms of the ratio ζ (which he defines as α) of the semi-major axis to the obscuration radius, so his results are universally scalable. His analysis does not include treatment of imaging contrast or limiting flux (these are addressed in a follow-up work: Brown 2005), which makes it suitable to apply to results that have already been corrected for these effects, as we have already done for our survey in § A.3.2.

Brown (2004) finds that the detectability of orbiting companions in a single-visit observation, what he terms the "single visit obscurational completeness" (SVOC), is a strong function of ζ between $\zeta = 1$ and 2. The SVOC varies between ≈30% at $\zeta = 1$ and ≈85% at $\zeta = 1.9$ (Fig. 3 in Brown 2004). Higher SVOC, at the 95% and 99% levels, is achieved only for $\zeta = 3.2$ and 7.1, respectively, i.e., far from the coronaghraphic edge. The result is largely independent ($< 10\%$ variation) of the assumed orbital eccentricity e for $0 \leq e \leq 0.35$.

We adopt the results of Brown's analysis and use the SVOC values for a representative orbital eccentricity of 0.35 (Table 4 in Brown 2004)—a value near the peak of the eccentricity distribution of G-dwarf binaries with $> 10^3$ day periods (Duquennoy & Mayor 1991). We calculate the SVOC on the deepest image of each sample star, for each of the discrete candidate companion masses in the 0.005–0.090 $M_\odot$ range considered in § A.3.2. We define the minimum projected separation at which a companion of a given mass is detectable as the effective obscuration radius for that companion mass. The results from the combined treatment of the observational completeness (§ A.3.2) and the SVOC are shown in Figure 16a by filled triangles and in Figure 16b with the dotted lines. The long-dashed lines in Figure 16a,b delimit the maximum attainable SVOC, that is, when the companion brightness is not a limiting factor. Figure 16a shows that the completeness to ≥ 0.072 $M_\odot$ objects is very near (64.8%) the SVOC limit (64.9%). That is, the deep survey is almost maximally complete to stellar companions. The survey is only 47.0% complete to companions at the low end of the brown dwarf mass range at 0.012 $M_\odot$.

The additional consideration of orbital incompleteness does not affect significantly the overall incompleteness of the survey within the posited 22–1262 AU projected separation (28–1590 AU semi-major axis) range. Given the assumed companion mass and orbital semi-major axis distributions (§ A.2), the overall (geometrical + observational + orbital) completeness becomes 62.0%.

We note that the consideration of the SVOC, as defined by Brown (2004), does not address all possibilities for orbital incompleteness. Other than being obscured by the coronagraph or lost in the glare of its host star, a companion on a highly-eccentric orbit may fall outside the OWA, even if its semi-major axis was in the explored range. This additional factor, among possible other sources of orbital incompleteness, is not taken into account here. However, judging by the small decrease ($68.2\% - 62.0\% = 6.2\%$) in the overall incompleteness correction induced by the consideration of the SVOC, it is unlikely that inclusion of the remaining factors affecting orbital incompleteness will decrease the overall survey completeness below 50%.

Effect of Variations in the Assumed Companion Semi-major Axis and Period Distributions

The above final completeness estimate is based on the assumptions for the semi-major axis and companion mass distributions adopted in § A.2. These assumptions are merely guesses, and in reality the companion orbital and mass distributions may take different forms. Indeed, in § 9.2 we argue that the orbital period distribution of substellar and stellar mass companions are probably the same, while in § 9.1.2 we conclude that the MFs of companions and isolated objects are different. Both of these results are at odds with the corresponding assumptions. It is conceivable that other initial guesses for the orbital and mass distributions of the companions may lead to different conclusions.

We therefore analyzed the completeness of the survey to substellar companions under a broader set of functional forms for the companion semi-major axis and mass distributions. For the semi-major axis distribution we also considered: (1) the equivalent of the log-normal orbital period distribution for sun-like binary stars from Duquennoy & Mayor (1991) under the assumption that the total system mass is 1 $M_\odot$, (2) the extrasolar planet period $dN/d\log P \propto P^{0.26}$ distribution from Cumming et al. (2008), which converts to $dN/da \propto a^{-0.61}$ for solar-mass primaries, and (3) a linearly flat $dN/da \propto a^0$ distribution. For the CMF exponent β we tested values in the -1 to 1 range.

The estimates for the completeness to substellar companions for the three different semi-major axis distributions with β fixed at zero were 62.7%, 59.9%, and 51.9% respectively, all within a factor of 1.20 of the one already obtained in § A.3.3. In particular, we note that the assumption of either the star-like log-normal or the planet-like period distribution altered the completeness estimate very little (by a factor of ≤1.04). If we set the CMF index β to either

-1 or 1 but held the assumed semi-major axis distribution fixed at $dN/da \propto a^{-1}$, the completeness became 58.1% or 64.9%, respectively. If we allowed both of the companion orbital and mass distributions to vary, the completeness estimates ranged from 50.2%–66.0%.

Overall, we found that the inferred frequency of wide substellar companions to young solar analogs in § 8.1 would be affected by a factor of ≤ 1.24. In the likely case that the orbital period distributions of substellar and stellar companions are the same, as in Duquennoy & Mayor (1991), our inferred frequency would be accurate to a within factor of 1.06.

Such small changes to the incompleteness estimate of our survey affect the resultant CMF power law index β only minimally. Because the relative changes in the completeness-corrected numbers per mass bin of the CMF are much smaller than the observed trend, the variations in the fitted value for β are well within the derived 1σ range.

Summary of Incompleteness Analysis and Further Considerations

We adopt 62% as the final estimate for the completeness to substellar companions in our deep survey. That is, given two detected brown dwarf companions with semi-major axes in the 28–1590 AU range, on average $0.62^{-1} = 1.6$ more companions with semi-major axes in the same range have been missed. This estimate is based on the combined consideration of the geometrical, observational, and orbital incompleteness factors described in § A.3.

In closing, we recall that because the physical association status of a large fraction (31.4%) of candidate companions discovered in the survey remains undecided (§ 5.2), it is possible that more bona fide substellar companions may be confirmed in this data set in the future. This is not very likely, given that the vast majority of the undecided candidates are faint, reside in relatively high-density fields, and are at wide angular separations from their candidate primaries (Fig. 6), i.e., they have very high probabilities of being background stars. Because of the presently unknown and likely unimportant nature of the additional candidate companions, and for the sake of preserving statistical rigor, we have assumed that none of the remaining candidates are bona fide brown dwarfs, and that the derived value of 62% provides an accurate estimate of the completeness of our deep survey.

REFERENCES

Adams, J. D., Stauffer, J. R., Monet, D. G., Skrutskie, M. F., & Beichman, C. A. 2001, AJ, 121, 2053

Ali, B., Carr, J. S., Depoy, D. L., Frogel, J. A., & Sellgren, K. 1995, AJ, 110, 2415

Allen, P. R. 2007, ApJ, 668, 492

Allen, P. R., Koerner, D. W., Reid, I. N., & Trilling, D. E. 2005, ApJ, 625, 385

Baraffe, I., Chabrier, G., Allard, F., & Hauschildt, P. H. 1998, A&A, 337, 403

Baraffe, I., Chabrier, G., Barman, T. S., Allard, F., & Hauschildt, P. H. 2003, A&A, 402, 701

Barrado y Navascues, D., Fernandez-Figueroa, M. J., Garcia Lopez, R. J., de Castro, E., & Cornide, M. 1997, A&A, 326, 780

Bate, M. R., & Bonnell, I. A. 2005, MNRAS, 356, 1201

Bate, M. R., Bonnell, I. A., & Bromm, V. 2002, MNRAS, 332, L65

Biller, B. A., et al. 2007, ApJS, 173, 143

Bloemhof, E. E. 2003, ApJ, 582, L59

Boccaletti, A., Riaud, P., & Rouan, D. 2002, PASP, 114, 132

Bouvier, J., Rigaut, F., & Nadeau, D. 1997, A&A, 323, 139

Brandner, W., et al. 2000, AJ, 120, 950

Briceño, C., Luhman, K. L., Hartmann, L., Stauffer, J. R., & Kirkpatrick, J. D. 2002, ApJ, 580, 317

Brown, R. A. 2004, ApJ, 607, 1003

Brown, R. A. 2005, ApJ, 624, 1010

Burgasser, A. J., Kirkpatrick, J. D., & Lowrance, P. J. 2005, AJ, 129, 2849

Burgasser, A. J., Reid, I. N., Siegler, N., Close, L., Allen, P., Lowrance, P., & Gizis, J. 2007, in Protostars and Planets V, ed. B. Reipurth, D. Jewitt, & K. Keil, 427

Burrows, A., Hubbard, W. B., Lunine, J. I., & Liebert, J. 2001, Reviews of Modern Physics, 73, 719

Burrows, A., et al. 1997, ApJ, 491, 856

Cameron, P. B., Britton, M. C., & Kulkarni, S. R. 2008, ApJ, submitted, arXiv:0805.2153, 805

Cannon A.J. and Pickering E.C. 1918, Annals of Harvard College Observatory, 91

Carpenter, J. M., et al. 2008, ArXiv:0807.4362, 807

Carson, J. C., Eikenberry, S. S., Brandl, B. R., Wilson, J. C., & Hayward, T. L. 2005, AJ, 130, 1212

Casagrande, L., Flynn, C., & Bessell, M. 2008, MNRAS, accepted; ArXiv:0806.2471, 806

Chabrier, G. 2001, ApJ, 554, 1274

Chabrier, G. 2003, PASP, 115, 763

Chabrier, G., Baraffe, I., Allard, F., & Hauschildt, P. 2000, ApJ, 542, 464

Chauvin, G., Lagrange, A.-M., Dumas, C., Zuckerman, B., Mouillet, D., Song, I., Beuzit, J.-L., & Lowrance, P. 2005a, A&A, 438, L25

Chauvin, G., et al. 2005b, A&A, 438, L29

Couteau, P. 1960, Journal des Observateurs, 43, 41

Cox, A. N. 2000, Allen's astrophysical quantities (4th ed. Publisher: New York: AIP Press; Springer, 2000. Edited by Arthur N. Cox. ISBN: 0387987460)

Cumming, A., Butler, R. P., Marcy, G. W., Vogt, S. S., Wright, J. T., & Fischer, D. A. 2008, PASP, 120, 531

Cushing, M. C., Rayner, J. T., & Vacca, W. D. 2005, ApJ, 623, 1115

Cutri, R. M., et al. 2003, 2MASS All Sky Catalog of point sources. (The IRSA 2MASS All-Sky Point Source Catalog, NASA/IPAC Infrared Science Archive. http://irsa.ipac.caltech.edu/applications/Gator/)

Dahn, C. C., et al. 2002, AJ, 124, 1170

D'Antona, F., & Mazzitelli, I. 1994, ApJS, 90, 467

de Zeeuw, P. T., Hoogerwerf, R., de Bruijne, J. H. J., Brown, A. G. A., & Blaauw, A. 1999, AJ, 117, 354

Diolaiti, E., Bendinelli, O., Bonaccini, D., Close, L., Currie, D., & Parmeggiani, G. 2000, A&AS, 147, 335

Duquennoy, A., & Mayor, M. 1990, Duplicity of solar-like stars in the solar neighbourhood (New Windows to the Universe), 253

Duquennoy, A., & Mayor, M. 1991, A&A, 248, 485

Fabricius, C., & Makarov, V. V. 2000, A&A, 356, 141

Fischer, D. A., & Marcy, G. W. 1992, ApJ, 396, 178

Fischer, D. A., Marcy, G. W., Butler, R. P., Vogt, S. S., Walp, B., & Apps, K. 2002, PASP, 114, 529

Freeman, P. E., Kashyap, V., Rosner, R., & Lamb, D. Q. 2002, ApJS, 138, 185

Gaidos, E. J., Henry, G. W., & Henry, S. M. 2000, AJ, 120, 1006

Ghez, A. M., McCarthy, D. W., Patience, J. L., & Beck, T. L. 1997, ApJ, 481, 378

Ghez, A. M., Neugebauer, G., & Matthews, K. 1993, AJ, 106, 2005

Gizis, J. E., Kirkpatrick, J. D., Burgasser, A., Reid, I. N., Monet, D. G., Liebert, J., & Wilson, J. C. 2001, ApJ, 551, L163

Goldin, A., & Makarov, V. V. 2006, ApJS, 166, 341

Goldin, A., & Makarov, V. V. 2007, ApJS, 173, 137

Golimowski, D. A., et al. 2004, AJ, 127, 3516

Gorlova, N. I., Meyer, M. R., Rieke, G. H., & Liebert, J. 2003, ApJ, 593, 1074

Goto, M., et al. 2003, in Proc. SPIE Vol. 4839, p. 1117-1123, Adaptive Optical Systems Technologies II, Peter L. Wizinowich, Domenico Bonaccini; Eds., 1117

Guenther, E. W., Esposito, M., Mundt, R., Covino, E., Alcalá, J. M., Cusano, F., & Stecklum, B. 2007, A&A, 467, 1147
Gutiérrez, C. M., García López, R. J., Rebolo, R., Martín, E. L., & François, P. 1999, A&AS, 137, 93
Halbwachs, J. L., Mayor, M., Udry, S., & Arenou, F. 2003, A&A, 397, 159
Hale, A. 1994, AJ, 107, 306
Hartkopf, W. I., & Mason, B. D. 2003, http://ad.usno.navy.mil/wds/orb6/orb6c.html
Hartkopf, W. I., Mason, B. D., & McAlister, H. A. 1996, AJ, 111, 370
Hartkopf, W. I., Mason, B. D., & Worley, C. E. 2001, AJ, 122, 3472
Hayward, T. L., Brandl, B., Pirger, B., Blacken, C., Gull, G. E., Schoenwald, J., & Houck, J. R. 2001, PASP, 113, 105
Heckmann, O., Dieckvoss, W., & Kox, H. 1956, Astronomische Nachrichten, 283, 109
Hertzspring, E. 1947, Annalen van de Sterrewacht te Leiden, 19, 1
Hillenbrand, L. A., & Carpenter, J. M. 2000, ApJ, 540, 236
Hillenbrand, L. A., & White, R. J. 2004, ApJ, 604, 741
Hinz, J. L., McCarthy, D. W., Jr., Simons, D. A., Henry, T. J., Kirkpatrick, J. D., & McGuire, P. C. 2002, AJ, 123, 2027
Høg, E., et al. 2000, A&A, 355, L27
Jayawardhana, R., & Brandeker, A. 2001, ApJ, 561, L111
Jefferies, S. M., & Christou, J. C. 1993, ApJ, 415, 862
König, B., Guenther, E. W., Woitas, J., & Hatzes, A. P. 2005, A&A, 435, 215
Kastner, J. H., Zuckerman, B., Weintraub, D. A., & Forveille, T. 1997, Science, 277, 67
Kirkpatrick, J. D., Dahn, C. C., Monet, D. G., Reid, I. N., Gizis, J. E., Liebert, J., & Burgasser, A. J. 2001, AJ, 121, 3235
Köhler, R., Kunkel, M., Leinert, C., & Zinnecker, H. 2000, A&A, 356, 541
Kohler, R., & Leinert, C. 1998, A&A, 331, 977
Kouwenhoven, M. B. N., Brown, A. G. A., & Kaper, L. 2007, A&A, 464, 581
Kouwenhoven, M. B. N., Brown, A. G. A., Zinnecker, H., Kaper, L., & Portegies Zwart, S. F. 2005, A&A, 430, 137
Kraft, R. P., Burrows, D. N., & Nousek, J. A. 1991, ApJ, 374, 344
Kraus, A. L., & Hillenbrand, L. A. 2007, ApJ, 664, 1167
Kraus, A. L., Ireland, M. J., Martinache, F., & Lloyd, J. P. 2008, ApJ, in press, arXiv:0801.2387, 801
Kroupa, P. 2001, MNRAS, 322, 231
Kroupa, P. 2002, Science, 295, 82
Kroupa, P., Tout, C. A., & Gilmore, G. 1990, MNRAS, 244, 76
Kuiper, G. P. 1935a, PASP, 47, 15
Kuiper, G. P. 1935b, PASP, 47, 121
Lafrenière, D., et al. 2007, ApJ, 670, 1367
Lafreniere, D., Jayawardhana, R., Brandeker, A., Ahmic, M., & van Kerkwijk, M. H. 2008, ArXiv e-prints, 803
Leggett, S. K., Allard, F., Berriman, G., Dahn, C. C., & Hauschildt, P. H. 1996, ApJS, 104, 117
Leggett, S. K., et al. 2002, ApJ, 564, 452
Liu, M. C., Dupuy, T. J., & Ireland, M. J. 2008, ApJ, in press; ArXiv:0807.0238, 807
Liu, M. C., Fischer, D. A., Graham, J. R., Lloyd, J. P., Marcy, G. W., & Butler, R. P. 2002, ApJ, 571, 519
Lowrance, P. J., et al. 2005, AJ, 130, 1845
Luhman, K. L. 1999, ApJ, 525, 466
Luhman, K. L. 2004, ApJ, 617, 1216
Luhman, K. L., Briceño, C., Stauffer, J. R., Hartmann, L., Barrado y Navascués, D., & Caldwell, N. 2003a, ApJ, 590, 348
Luhman, K. L., & Jayawardhana, R. 2002, ApJ, 566, 1132
Luhman, K. L., Joergens, V., Lada, C., Muzerolle, J., Pascucci, I., & White, R. 2007a, in Protostars and Planets V, ed. B. Reipurth, D. Jewitt, & K. Keil, 443
Luhman, K. L., McLeod, K. K., & Goldenson, N. 2005, ApJ, 623, 1141
Luhman, K. L., et al. 2007b, ApJ, 654, 570
Luhman, K. L., Peterson, D. E., & Megeath, S. T. 2004, ApJ, 617, 565
Luhman, K. L., Stauffer, J. R., Muench, A. A., Rieke, G. H., Lada, E. A., Bouvier, J., & Lada, C. J. 2003b, ApJ, 593, 1093
Makarov, V. V., & Kaplan, G. H. 2005, AJ, 129, 2420
Mamajek, E. E. 2004, Ph.D. Thesis, University of Arizona, Tucson, Arizona
Mamajek, E. E. 2007, private communication
Mamajek, E. E., & Hillenbrand, L. A. 2008, ArXiv e-prints, 807
Mamajek, E. E., Lawson, W. A., & Feigelson, E. D. 1999, ApJ, 516, L77
Mamajek, E. E., Meyer, M. R., & Liebert, J. 2002, AJ, 124, 1670
Marcy, G. W., & Butler, R. P. 2000, PASP, 112, 137
Marois, C., Lafrenière, D., Doyon, R., Macintosh, B., & Nadeau, D. 2006, ApJ, 641, 556
Marois, C., Lafreniere, D., Macintosh, B., & Doyon, R. 2007, ArXiv:0709.3548, 709
Masciadri, E., Mundt, R., Henning, T., Alvarez, C., & Barrado y Navascués, D. 2005, ApJ, 625, 1004
Mason, B. D., Wycoff, G. L., Hartkopf, W. I., Douglass, G. G., & Worley, C. E. 2001, AJ, 122, 3466
Mazeh, T., Simon, M., Prato, L., Markus, B., & Zucker, S. 2003, ApJ, 599, 1344
McCarthy, C., & Zuckerman, B. 2004, AJ, 127, 2871
McElwain, M. W., et al. 2007, ApJ, 656, 505
Mermilliod, J.-C., Rosvick, J. M., Duquennoy, A., & Mayor, M. 1992, A&A, 265, 513
Metchev, S. A. 2006, Ph.D. thesis, California Institute of Technology, United States – California
Metchev, S. A., & Hillenbrand, L. A. 2004, ApJ, 617, 1330
Metchev, S. A., & Hillenbrand, L. A. 2006, ApJ, 651, 1166
Metchev, S. A., Hillenbrand, L. A., & White, R. J. 2003, ApJ, 582, 1102
Metchev, S. A., Kirkpatrick, J. D., Berriman, G. B., & Looper, D. 2008, ApJ, 676, 1281
Meyer, M. R., et al. 2006, PASP, 118, 1690
Mohanty, S., Jayawardhana, R., Huélamo, N., & Mamajek, E. 2007, ApJ, 657, 1064
Montes, D., López-Santiago, J., Gálvez, M. C., Fernández-Figueroa, M. J., De Castro, E., & Cornide, M. 2001, MNRAS, 328, 45
Mugrauer, M., et al. 2004, A&A, 417, 1031
Munari, U., Dallaporta, S., Siviero, A., Soubiran, C., Fiorucci, M., & Girard, P. 2004, A&A, 418, L31
Neuhäuser, R., & Guenther, E. W. 2004, A&A, 420, 647
Nordström, B., et al. 2004, A&A, 418, 989
Oppenheimer, B. R., Dekany, R. G., Hayward, T. L., Brandl, B., Troy, M., & Bloemhof, E. E. 2000, in Proc. SPIE Vol. 4007, p. 899-905, Adaptive Optical Systems Technology, Peter L. Wizinowich; Ed., 899
Oppenheimer, B. R., Golimowski, D. A., Kulkarni, S. R., Matthews, K., Nakajima, T., Creech-Eakman, M., & Durrance, S. T. 2001, AJ, 121, 2189
Pan, X., Shao, M., & Kulkarni, S. R. 2004, Nature, 427, 326
Papoulis, A. 1984, Probability, Random Variables, and Stochastic Processes (New York: McGraw–Hill, 1984)
Patel, S. G., Vogt, S. S., Marcy, G. W., Johnson, J. A., Fischer, D. A., Wright, J. T., & Butler, R. P. 2007, ApJ, 665, 744
Patience, J., Ghez, A. M., Reid, I. N., & Matthews, K. 2002, AJ, 123, 1570
Patience, J., Ghez, A. M., Reid, I. N., Weinberger, A. J., & Matthews, K. 1998, AJ, 115, 1972
Perryman, M. A. C., et al. 1998, A&A, 331, 81
Perryman, M. A. C., et al. 1997, A&A, 323, L49
Potter, D., Martín, E. L., Cushing, M. C., Baudoz, P., Brandner, W., Guyon, O., & Neuhäuser, R. 2002, ApJ, 567, L133
Pounds, K. A., et al. 1993, MNRAS, 260, 77
Pourbaix, D. 2000, A&AS, 145, 215
Preibisch, T., Brown, A. G. A., Bridges, T., Guenther, E., & Zinnecker, H. 2002, AJ, 124, 404
Preibisch, T., & Zinnecker, H. 1999, AJ, 117, 2381
Pye, J. P., et al. 1995, MNRAS, 274, 1165
Rainwater, L. J., & Wu, C. S. 1947, Nucleonics, 1, 60
Rayner, J. T., Vacca, W. D., & Cushing. 2008, in preparation
Reid, I. N., et al. 2004, AJ, 128, 463
Reid, I. N., & Hawley, S. L. 2005, New light on dark stars : red dwarfs, low-mass stars, brown dwarfs (New Light on Dark Stars Red Dwarfs, Low-Mass Stars, Brown Stars, by I.N. Reid and S.L. Hawley. Springer-Praxis books in astrophysics and astronomy. Praxis Publishing Ltd, 2005. ISBN 3-540-25124-3)
Söderhjelm, S. 1999, A&A, 341, 121
Scardia, M. 1979, Astronomische Nachrichten, 300, 307
Schroeder, D. J., et al. 2000, AJ, 119, 906
Shatsky, N., & Tokovinin, A. 2002, A&A, 382, 92
Sivaramakrishnan, A., Koresko, C. D., Makidon, R. B., Berkefeld, T., & Kuchner, M. J. 2001, ApJ, 552, 397
Skrutskie, M. F., et al. 2006, AJ, 131, 1163

Slesnick, C. L., Hillenbrand, L. A., & Carpenter, J. M. 2004, ApJ, 610, 1045
Southworth, J., Maxted, P. F. L., & Smalley, B. 2005, A&A, 429, 645
Sterzik, M. F., & Durisen, R. H. 2004, in Revista Mexicana de Astronomia y Astrofisica, vol. 27, Vol. 21, Revista Mexicana de Astronomia y Astrofisica Conference Series, ed. C. Allen & C. Scarfe, 58
Stetson, P. B. 1992, in ASP Conf. Ser. 25: Astronomical Data Analysis Software and Systems I, 297
Strassmeier, K., Washuettl, A., Granzer, T., Scheck, M., & Weber, M. 2000, A&AS, 142, 275
Swenson, F. J., Faulkner, J., Rogers, F. J., & Iglesias, C. A. 1994, ApJ, 425, 286
Tanner, A., et al. 2007, PASP, 119, 747
Thompson, D., Egami, E., & Sawicki, M. 2001, The Keck Near-Infrared AO Camera. Preship testing., California Institute of Technology, http://www2.keck.hawaii.edu/inst/nirc2/preship_testing.pdf
Tinney, C. G., Mould, J. R., & Reid, I. N. 1993, AJ, 105, 1045
Tokovinin, A., Thomas, S., Sterzik, M., & Udry, S. 2006, A&A, 450, 681
Tokovinin, A. A., Chalabaev, A., Shatsky, N. I., & Beuzit, J. L. 1999, A&A, 346, 481
Troy, M., et al. 2000, in Proc. SPIE Vol. 4007, Adaptive Optical Systems Technology, Peter L. Wizinowich; Ed., 31
van Albada, T. S. 1968, Bull. Astron. Inst. Netherlands, 20, 47
van Bueren, H. G. 1952, Bull. Astron. Inst. Netherlands, 11, 385
van Leeuwen, F. 1999, A&A, 341, L71
van Leeuwen, F., Alphenaar, P., & Brand, J. 1986, A&AS, 65, 309
Ventura, P., Zeppieri, A., Mazzitelli, I., & D'Antona, F. 1998, A&A, 334, 953
Voges, W., et al. 1999, A&A, 349, 389
Voges, W., et al. 2000, IAU Circ., 7432, 1
Vrba, F. J., et al. 2004, AJ, 127, 2948
Walter, F. M., Vrba, F. J., Mathieu, R. D., Brown, A., & Myers, P. C. 1994, AJ, 107, 692
Whipple, F. L. 1966, Smithsonian Astrophysical Observatory Star Catalog (Smithsonian Astrophysical Observatory Star Catalog, Washington: Smithsonian Institution Press)
White, R. J., Gabor, J. M., & Hillenbrand, L. A. 2007, AJ, 133, 2524
Wichmann, R., Schmitt, J. H. M. M., & Hubrig, S. 2003, A&A, 399, 983
Wilson, J. C., Kirkpatrick, J. D., Gizis, J. E., Skrutskie, M. F., Monet, D. G., & Houck, J. R. 2001, AJ, 122, 1989
Wizinowich, P., et al. 2000, PASP, 112, 315
Zacharias, N., Urban, S. E., Zacharias, M. I., Wycoff, G. L., Hall, D. M., Monet, D. G., & Rafferty, T. J. 2004, AJ, 127, 3043
Zuckerman, B., & Song, I. 2004, ApJ, 603, 738
Zuckerman, B., Song, I., Bessell, M. S., & Webb, R. A. 2001, ApJ, 562, L87
Zuckerman, B., & Webb, R. A. 2000, ApJ, 535, 959
Zwahlen, N., North, P., Debernardi, Y., Eyer, L., Galland, F., Groenewegen, M. A. T., & Hummel, C. A. 2004, A&A, 425, L45

TABLE 1
Deep Sample

Star	α (J2000.0)	δ (J2000.0)	$\mu_\alpha \cos\delta$ (mas yr^{-1})	μ_δ (mas yr^{-1})	d (pc)	K_S (mag)	Sp.T.	Association	log Age/yr
HD 377	00:08:25.74	+06:37:00.50	85.2 ± 1.5	-2.6 ± 1.4	40.0 ± 2.0	6.1	G2V	···	7.6
HD 691	00:11:22.44	+30:26:58.52	209.7 ± 1.0	35.5 ± 1.0	34.0 ± 1.0	6.2	K0V	···	8.5
HD 984	00:14:10.25	−07:11:56.92	104.9 ± 1.3	-67.6 ± 1.2	46.0 ± 2.0	6.1	F7V	···	7.6
HD 1405	00:18:20.78	+30:57:23.76	141.5 ± 2.2	-177.0 ± 2.1	29.0 ± 10.0	6.4	K2V	···	8.0
QT And	00:41:17.32	+34:25:16.77	44.8 ± 0.7	-36.2 ± 0.8	50.0 ± 25.0	7.4	K4	···	7.8
HD 7661	01:16:24.19	−12:05:49.33	134.8 ± 1.1	-5.7 ± 1.1	27.0 ± 1.0	5.7	K0V	···	8.6
HIP 6276	01:20:32.27	−11:28:03.74	116.0 ± 1.1	-140.2 ± 1.1	35.0 ± 1.0	6.5	G0	···	8.5
HD 8907	01:28:34.35	+42:16:03.70	51.7 ± 1.0	-99.2 ± 1.1	34.0 ± 1.0	5.4	F8	···	8.3
HD 12039	01:57:48.98	−21:54:05.32	102.4 ± 1.2	-48.0 ± 1.1	42.0 ± 2.0	6.5	G3/5V	···	7.5
HD 15526	02:29:35.03	−12:24:08.56	42.1 ± 1.3	-12.2 ± 1.1	106.0 ± 26.0	8.0	G5/6V	···	7.6
1RXS J025216.9+361658	02:52:17.59	+36:16:48.14	53.4 ± 1.3	-40.1 ± 0.7	100.0 ± 50.0	7.6	K2IV	···	7.8
HD 17925	02:52:32.14	−12:46:11.18	397.3 ± 1.2	-189.9 ± 1.3	10.0 ± 0.1	4.1	K1V	···	7.9
1RXS J025751.8+115759	02:57:51.68	+11:58:05.83	31.4 ± 1.2	-28.4 ± 1.2	118.0 ± 16.0	8.5	G7V	···	7.8
RX J0258.4+2947	02:58:28.77	+29:47:53.80	17.4 ± 1.2	-40.0 ± 0.6	100.0 ± 50.0	9.1	K0IV	···	8.0
1RXS J030759.1+302032	03:07:59.20	+30:20:26.05	31.2 ± 0.6	-66.6 ± 0.7	75.0 ± 37.5	7.4	G5IV	···	8.3
HD 19668	03:09:42.28	−09:34:46.46	88.0 ± 1.2	-113.3 ± 1.1	40.0 ± 2.0	6.7	G8/K0V	···	8.4
1E 0307.4+1424	03:10:12.55	+14:36:02.90	-4.0 ± 1.2	-25.3 ± 1.2	160.0 ± 80.0	8.8	G6V	···	7.8
V525 Per	03:19:02.76	+48:10:59.61	16.4 ± 4.0	-23.6 ± 1.4	190.0 ± 11.0	9.4	K2	αPer	7.9
1RXS J031907.4+393418	03:19:07.61	+39:34:10.50	27.3 ± 0.9	-25.3 ± 1.7	100.0 ± 50.0	9.5	K0V	···	7.8
HE 622	03:24:49.71	+48:52:18.33	22.3 ± 0.9	-26.3 ± 0.7	190.0 ± 11.0	9.6	G7	αPer	7.9
1E 0324.1−2012	03:26:22.05	−20:01:48.81	25.0 ± 1.6	7.4 ± 1.6	160.0 ± 80.0	8.9	G4V	···	7.8
RX J0329.1+0118	03:29:08.06	+01:18:05.66	4.4 ± 1.3	-4.5 ± 1.3	100.0 ± 50.0	9.2	G0(IV)	···	7.8
HE 1101	03:35:08.75	+49:44:39.59	20.9 ± 1.3	-28.5 ± 0.9	190.0 ± 11.0	9.3	G5	αPer	7.9
HD 22179	03:35:29.91	+31:13:37.45	42.6 ± 0.6	-46.0 ± 0.7	140.0 ± 70.0	7.4	G5IV	···	7.8
HD 23208	03:42:39.80	−20:32:43.80	3.8 ± 1.5	24.1 ± 1.0	57.5 ± 4.7	7.2	G8V	···	6.7
HII 120	03:43:31.95	+23:40:26.61	18.0 ± 0.7	-46.8 ± 0.6	133.0 ± 6.0	9.1	G5	Pleiades	8.1
HII 2147	03:49:06.11	+23:46:52.49	15.9 ± 0.9	-43.8 ± 0.8	133.0 ± 6.0	8.6	G7IV	Pleiades	8.1
1RXS J035028.0+163121	03:50:28.40	+16:31:15.19	26.2 ± 1.3	-23.4 ± 2.1	138.0 ± 21.0	8.6	G5IV	···	7.8
RX J0354.4+0535	03:54:21.31	+05:35:40.77	-1.4 ± 1.3	-7.6 ± 1.3	100.0 ± 50.0	8.7	G2(V)	···	8.3
Pels 191	03:54:25.23	+24:21:36.38	17.1 ± 0.7	-46.8 ± 0.8	133.0 ± 6.0	9.1	G5IV	Pleiades	8.1
RX J0357.3+1258	03:57:21.39	+12:58:16.83	22.7 ± 1.8	-21.9 ± 1.5	149.0 ± 23.0	9.0	G0	···	7.8
HD 285751	04:23:41.33	+15:37:54.87	8.2 ± 1.7	-15.8 ± 1.4	150.0 ± 75.0	8.8	K2(V)	···	6.8
RX J0442.5+0906	04:42:32.09	+09:06:00.86	28.9 ± 2.4	-22.3 ± 2.0	119.0 ± 21.0	9.1	G5(V)	···	7.8
HD 286179	04:57:00.65	+15:17:53.09	-1.8 ± 1.5	-17.3 ± 1.4	140.0 ± 70.0	8.5	G3(V)	···	7.3
HD 31950	05:00:24.31	+15:05:25.28	0.3 ± 1.1	-15.2 ± 1.1	100.0 ± 50.0	8.4	F8	···	7.8
HD 35850	05:27:04.77	−11:54:03.38	17.5 ± 0.7	-49.8 ± 0.8	27.0 ± 1.0	4.9	F7/8V	···	7.5
1RXS J053650.0+133756	05:36:50.06	+13:37:56.22	4.9 ± 1.3	-108.8 ± 1.2	56.0 ± 28.0	8.1	K0V	···	8.3
HD 245567	05:37:18.44	+13:34:52.52	7.5 ± 0.9	-33.2 ± 0.9	119.0 ± 21.0	7.6	G0V	···	6.6
SAO 150676	05:40:20.74	−19:40:10.85	19.2 ± 1.2	-12.9 ± 1.2	78.0 ± 30.0	7.5	G2V	···	7.8
HD 38949	05:48:20.06	−24:27:50.04	-29.8 ± 1.1	-37.8 ± 1.2	43.0 ± 2.0	6.4	G1V	···	8.4
HD 43989	06:19:08.05	−03:26:20.39	10.6 ± 0.9	-43.7 ± 1.0	50.0 ± 2.0	6.6	G0V	···	7.8
HD 49197	06:49:21.34	+43:45:32.87	-37.6 ± 0.6	-50.9 ± 0.6	45.0 ± 2.0	6.1	F5	···	8.7
RE J0723+20	07:23:43.58	+20:24:58.64	-66.2 ± 1.8	-230.2 ± 2.6	24.0 ± 12.0	6.9	K3(V)	···	8.1
HD 60737	07:38:16.44	+47:44:55.34	-14.2 ± 1.0	-165.0 ± 1.0	38.0 ± 2.0	6.3	G0	···	8.2
HD 70573	08:22:49.95	+01:51:33.58	-49.1 ± 1.1	-49.7 ± 1.1	46.0 ± 23.0	7.2	G1/2V	···	8.0
HD 70516	08:24:15.66	+44:56:58.92	-63.1 ± 0.9	-178.4 ± 1.0	37.0 ± 3.0	6.1	G0	···	7.9
HD 72905	08:39:11.62	+65:01:15.14	-28.9 ± 1.0	88.5 ± 1.0	14.0 ± 0.1	4.2	G1.5VB	···	8.3
HD 75393	08:49:15.35	−15:33:53.12	35.8 ± 1.4	-33.6 ± 1.2	42.0 ± 1.0	5.9	F7V	···	8.4
HD 82558	09:32:25.72	−11:11:05.00	-248.3 ± 1.2	35.1 ± 0.6	18.3 ± 0.3	5.4	K3V	···	8.0
HD 82443	09:32:43.92	+26:59:20.76	-147.5 ± 0.9	-246.3 ± 0.5	17.7 ± 0.3	5.1	K0V	···	8.0
SAO 178272	09:59:08.42	−22:39:34.57	-62.8 ± 1.4	-15.6 ± 1.7	58.0 ± 29.0	7.4	K2V	···	8.0
HD 90905	10:29:42.23	+01:29:27.82	-150.4 ± 0.8	-124.1 ± 0.8	32.0 ± 1.0	5.5	G1V	···	8.3
HD 91782	10:36:47.84	+47:43:12.42	-71.4 ± 0.6	-81.7 ± 0.7	56.0 ± 3.0	6.8	G0	···	8.2
HD 92855	10:44:00.62	+46:12:23.86	-268.8 ± 1.1	-61.9 ± 1.2	36.0 ± 1.0	5.9	F9V	···	8.2
HD 93528	10:47:31.20	−22:20:52.80	-122.7 ± 1.1	-29.4 ± 0.8	34.9 ± 1.2	6.5	K0V	···	8.0
HD 95188	10:59:48.28	+25:17:23.65	-126.3 ± 1.4	1.7 ± 1.3	36.0 ± 1.0	6.6	G8V	···	8.4
HD 101472	11:40:36.59	−08:24:20.32	-20.0 ± 0.8	-13.8 ± 0.8	39.0 ± 2.0	6.1	F7V	···	8.4
BPM 87617	11:47:45.73	+12:54:03.31	-71.5 ± 1.9	-0.4 ± 1.8	50.0 ± 25.0	7.8	K5Ve	···	8.1
HD 104576	12:02:39.46	−10:42:49.16	32.7 ± 1.0	-18.4 ± 0.9	49.0 ± 3.0	6.7	G3V	···	8.2
HD 104860	12:04:33.71	+66:20:11.58	-56.1 ± 1.4	49.7 ± 1.4	48.0 ± 2.0	6.5	F8	···	7.6
HD 107146	12:19:06.49	+16:32:53.91	-175.6 ± 0.9	-149.5 ± 1.0	29.0 ± 1.0	5.5	G2V	···	8.0
SAO 15880	12:43:33.36	+60:00:53.28	-125.2 ± 1.4	-66.4 ± 1.5	60.0 ± 20.0	7.3	K0	···	8.0
SAO 2085	12:44:02.88	+85:26:56.40	-129.6 ± 0.8	43.2 ± 0.9	66.0 ± 20.0	7.3	G5	···	8.2
HD 111456	12:48:39.46	+60:19:11.40	107.8 ± 3.1	-30.6 ± 2.7	24.2 ± 1.9	4.6	F5V	···	8.5
HD 132173	14:58:30.51	−28:42:34.15	-99.9 ± 1.5	-93.0 ± 1.7	49.0 ± 2.0	6.2	G0V	···	8.2
HD 139813	15:29:23.61	+80:27:01.08	-218.0 ± 1.2	105.8 ± 1.2	22.0 ± 0.3	5.5	G5	···	8.3
HD 139498	15:39:24.40	−27:10:21.87	-21.8 ± 1.5	-28.1 ± 1.5	127.0 ± 10.0	7.5	G8(V)	ScoCen	7.2
HD 142361	15:54:59.86	−23:47:18.26	-29.3 ± 1.1	-38.8 ± 1.1	101.0 ± 14.0	7.0	G3V	USco	6.7
HD 143006	15:58:36.92	−22:57:15.35	-10.6 ± 1.7	-19.5 ± 1.3	145.0 ± 40.0	7.1	G6/8	USco	6.7
PZ99 J155847.8−175800	15:58:47.73	−17:57:59.58	-14.8 ± 3.5	-18.4 ± 2.8	145.0 ± 40.0	8.3	K3	USco	6.7
ScoPMS 21	16:01:25.63	−22:40:40.38	-9.4 ± 2.8	-23.8 ± 1.7	145.0 ± 40.0	8.5	K1IV	USco	6.7
PZ99 J160158.2−200811	16:01:58.22	−20:08:12.0	-6.8 ± 2.1	-21.7 ± 2.3	145.0 ± 40.0	7.7	G5	USco	6.7
PZ99 J160302.7−180605	16:03:02.69	−18:06:05.06	-11.3 ± 2.9	-22.7 ± 1.7	145.0 ± 40.0	8.7	K4	USco	6.7
ScoPMS 27	16:04:47.76	−19:30:23.12	-14.0 ± 2.3	-20.1 ± 3.1	145.0 ± 40.0	8.0	K2IV	USco	6.7
ScoPMS 52	16:12:40.51	−18:59:28.31	-8.4 ± 2.4	-28.5 ± 4.1	145.0 ± 40.0	7.5	K0IV	USco	6.7
PZ99 J161318.6−221248	16:13:18.59	−22:12:48.96	-9.1 ± 1.2	-21.0 ± 1.4	145.0 ± 40.0	7.4	G9	USco	6.7
PZ99 J161402.1−230101	16:14:02.12	−23:01:02.18	-8.8 ± 1.7	-22.8 ± 1.7	145.0 ± 40.0	8.6	G4	USco	6.7
PZ99 J161411.0−230536	16:14:11.08	−23:05:36.26	-12.1 ± 1.6	-23.8 ± 1.9	145.0 ± 40.0	7.5	K0	USco	6.7
PZ99 J161459.2−275023	16:14:59.18	−27:50:23.06	-12.2 ± 1.6	-30.5 ± 5.0	145.0 ± 40.0	8.7	G5	USco	6.7

TABLE 2
Shallow Sample

Star	α (J2000.0)	δ (J2000.0)	$\mu_\alpha \cos\delta$ (mas yr^{-1})	μ_δ (mas yr^{-1})	d (pc)	K_S (mag)	Sp.T.	Association	log Age/yr	I (
HD 224873	00:01:23.66	+39:36:38.12	-28.7 ± 0.6	-43.3 ± 0.7	49.0 ± 5.0	6.7	K0	···	8.5	
HD 6963	01:10:41.91	+42:55:54.50	-154.6 ± 0.9	-198.5 ± 0.9	27.0 ± 1.0	5.9	G7V	···	9.0	
HD 8467	01:24:28.00	+39:03:43.55	210.6 ± 1.8	-26.6 ± 1.0	31.0 ± 1.0	6.6	G5	···	9.3	
HD 8941	01:28:24.36	+17:04:45.20	118.3 ± 0.7	-34.8 ± 0.7	50.0 ± 2.0	5.4	F8IV–V	···	9.2	
HD 9472	01:33:19.03	+23:58:32.19	0.0 ± 1.0	28.4 ± 0.9	33.0 ± 1.0	6.0	G0	···	8.9	
RE J0137+18A	01:37:39.41	+18:35:33.16	65.8 ± 1.9	-46.0 ± 2.5	64.0 ± 8.0	6.7	K3Ve	···	6.8	
HD 11850	01:56:47.27	+23:03:04.09	-83.8 ± 1.0	-18.1 ± 1.0	33.0 ± 1.0	6.2	G5	···	8.8	
HD 13382	02:11:23.15	+21:22:38.39	273.1 ± 0.8	-12.6 ± 0.7	33.0 ± 1.0	5.8	G5V	···	8.7	
HD 13507	02:12:55.00	+40:40:06.00	56.9 ± 1.3	-99.2 ± 1.3	26.0 ± 1.0	5.6	G5V	···	8.9	
HD 13531	02:13:13.35	+40:30:27.34	57.6 ± 1.0	-96.4 ± 1.0	26.0 ± 1.0	5.7	G7V	···	8.7	
HD 13974	02:17:03.23	+34:13:27.32	1153.8 ± 0.8	-245.1 ± 0.8	11.0 ± 0.1	3.2	G0V	···	9.2	
1RXS J025223.5+372914	02:52:24.73	+37:28:51.83	22.5 ± 0.7	-24.5 ± 1.0	170.0 ± 85.0	9.1	G5IV	···	8.3	
2RE J0255+474	02:55:43.60	+47:46:47.58	79.8 ± 0.6	-76.1 ± 0.7	50.0 ± 25.0	7.2	K5Ve	···	7.9	
HD 18940	03:03:28.65	+23:03:41.19	111.4 ± 0.8	-0.7 ± 0.7	34.0 ± 1.0	5.5	G0	···	8.9	
HD 19019	03:03:50.82	+06:07:59.82	231.8 ± 1.8	50.7 ± 1.7	31.0 ± 1.0	5.6	F8	···	9.2	
HD 19632	03:08:52.45	−24:53:15.55	226.7 ± 1.3	136.3 ± 1.3	30.0 ± 1.0	5.7	G3/5V	···	8.6	
vB 1	03:17:26.39	+07:39:20.90	167.2 ± 1.3	-6.4 ± 1.4	43.1 ± 0.6	6.0	F8	Hyades	8.8	
HE 350	03:17:36.93	+48:50:08.50	23.2 ± 0.8	-23.0 ± 0.9	190.0 ± 11.0	9.3	G2	αPer	7.9	
HE 373	03:18:27.39	+47:21:15.42	29.0 ± 0.7	-26.8 ± 2.0	190.0 ± 11.0	9.4	G8	αPer	7.9	
HE 389	03:18:50.31	+49:43:52.19	22.5 ± 0.9	-23.9 ± 0.7	190.0 ± 11.0	9.5	G0	αPer	7.9	
HE 696	03:26:19.36	+49:13:32.54	19.8 ± 0.7	-25.0 ± 0.7	190.0 ± 11.0	9.7	G3	αPer	7.9	
HE 699	03:26:22.22	+49:25:37.52	22.4 ± 0.8	-24.5 ± 0.7	190.0 ± 11.0	9.4	G3	αPer	7.9	
HE 750	03:27:37.79	+48:59:28.78	22.0 ± 0.7	-25.6 ± 0.7	190.0 ± 11.0	9.1	F5	αPer	7.9	
HE 767	03:27:55.02	+49:45:37.16	21.1 ± 0.6	-26.0 ± 0.6	190.0 ± 11.0	9.2	F6	αPer	7.9	
HE 848	03:29:26.24	+48:12:11.74	22.2 ± 0.6	-26.4 ± 0.6	190.0 ± 11.0	8.5	F9V	αPer	7.9	
HE 935	03:31:28.99	+48:59:28.37	21.3 ± 0.9	-26.6 ± 0.6	190.0 ± 11.0	8.5	F9.5V	αPer	7.9	
HE 1234	03:39:02.91	+51:36:37.11	21.4 ± 0.8	-33.7 ± 0.7	190.0 ± 11.0	8.9	G4	αPer	7.9	
HD 22879	03:40:22.08	−03:13:00.86	691.6 ± 1.1	-212.8 ± 1.1	24.0 ± 1.0	5.2	F7/8V	···	9.3	
HII 102	03:43:24.54	+23:13:33.30	17.1 ± 0.6	-43.7 ± 0.6	133.0 ± 6.0	8.7	G6	Pleiades	8.1	
HII 152	03:43:37.73	+23:32:09.59	19.5 ± 0.7	-46.9 ± 1.0	133.0 ± 6.0	9.1	G4	Pleiades	8.1	
HII 174	03:43:48.33	+25:00:15.83	18.8 ± 1.1	-47.0 ± 0.9	133.0 ± 6.0	9.4	K1	Pleiades	8.1	
HII 173	03:43:48.41	+25:11:24.19	20.4 ± 0.8	-48.4 ± 0.7	133.0 ± 6.0	8.8	K0	Pleiades	8.1	
HII 250	03:44:04.24	+24:59:23.40	20.1 ± 1.0	-49.4 ± 0.7	133.0 ± 6.0	9.1	G3	Pleiades	8.1	
HII 314	03:44:20.09	+24:47:46.16	18.2 ± 0.7	-49.8 ± 0.8	133.0 ± 6.0	8.9	G3	Pleiades	8.1	
1RXS J034423.3+281224	03:44:24.25	+28:12:23.07	46.4 ± 0.7	-50.6 ± 0.6	49.0 ± 10.0	7.2	G7V	···	7.8	
HII 514	03:45:04.01	+25:15:28.23	17.3 ± 0.7	-46.3 ± 0.6	133.0 ± 6.0	9.0	G4	Pleiades	8.1	
HII 571	03:45:15.35	+25:17:22.11	15.1 ± 0.9	-48.5 ± 0.9	133.0 ± 6.0	9.2	G9	Pleiades	8.1	
HII 1015	03:46:27.35	+25:08:07.97	18.6 ± 0.7	-48.5 ± 0.9	133.0 ± 6.0	9.0	G1	Pleiades	8.1	
HII 1101	03:46:38.78	+24:57:34.61	18.4 ± 0.8	-48.1 ± 0.7	133.0 ± 6.0	8.8	G4	Pleiades	8.1	
HII 1182	03:46:47.06	+22:54:52.48	18.4 ± 0.6	-45.6 ± 0.7	133.0 ± 6.0	8.9	G1	Pleiades	8.1	
HII 1200	03:46:50.54	+23:14:21.06	17.3 ± 0.6	-40.2 ± 0.7	133.0 ± 6.0	8.5	F6	Pleiades	8.1	
HII 1776	03:48:17.70	+25:02:52.29	19.0 ± 1.0	-47.1 ± 1.0	133.0 ± 6.0	9.2	G5	Pleiades	8.1	
HII 2106	03:48:58.49	+23:12:04.33	16.5 ± 1.3	-44.9 ± 1.1	133.0 ± 6.0	9.4	K1	Pleiades	8.1	
RX J0348.9+0110	03:48:58.76	+01:10:53.99	35.1 ± 1.6	-22.1 ± 1.2	100.0 ± 50.0	8.3	K3(V)/E	···	8.2	
HII 2278	03:49:25.70	+24:56:15.43	18.4 ± 0.9	-47.0 ± 0.8	133.0 ± 6.0	8.8	K0	Pleiades	8.1	
HII 2506	03:49:56.49	+23:13:07.01	17.6 ± 0.7	-43.9 ± 0.6	133.0 ± 6.0	8.8	F9	Pleiades	8.1	
HII 2644	03:50:20.90	+24:28:00.22	19.8 ± 0.8	-46.8 ± 0.9	133.0 ± 6.0	9.3	G5	Pleiades	8.1	
HII 2786	03:50:40.08	+23:55:58.94	17.6 ± 0.7	-45.2 ± 1.0	133.0 ± 6.0	8.9	F9	Pleiades	8.1	
HII 2881	03:50:54.32	+23:50:05.52	17.7 ± 0.7	-46.9 ± 1.1	133.0 ± 6.0	9.1	K2	Pleiades	8.1	
HII 3097	03:51:40.44	+24:58:59.41	17.5 ± 0.7	-46.1 ± 1.0	133.0 ± 6.0	9.1	G6	Pleiades	8.1	
HII 3179	03:51:56.86	+23:54:06.98	19.2 ± 0.6	-46.5 ± 0.8	133.0 ± 6.0	8.6	F8	Pleiades	8.1	
HD 285281	04:00:31.07	+19:35:20.70	2.7 ± 1.1	-12.9 ± 1.2	49.0 ± 11.0	7.6	K1	···	7.0	
HD 284135	04:05:40.58	+22:48:12.14	6.0 ± 0.6	-14.9 ± 0.6	140.0 ± 70.0	7.8	G3(V)	···	6.8	
HD 281691	04:09:09.74	+29:01:30.55	19.9 ± 0.7	-36.3 ± 1.0	140.0 ± 70.0	8.4	K1(V)	···	7.8	
HD 26182	04:10:04.69	+36:39:12.14	23.8 ± 0.7	-36.7 ± 0.7	100.0 ± 50.0	7.8	G0V	···	7.8	
HD 284266	04:15:22.92	+20:44:16.93	1.8 ± 1.0	-13.6 ± 0.7	140.0 ± 70.0	8.6	K0(V)	···	7.3	
HD 26990	04:16:16.50	+07:09:34.15	-85.6 ± 1.5	-52.1 ± 1.5	35.0 ± 2.0	5.9	G0(V)	···	8.9	
HD 27466	04:19:57.08	−04:26:19.60	-58.6 ± 1.2	-37.0 ± 1.2	36.0 ± 1.0	6.3	G5V	···	9.2	
vB 39	04:22:44.74	+16:47:27.56	173.3 ± 11.5	4.7 ± 10.2	39.3 ± 3.5	6.2	G4V	Hyades	8.8	
vB 49	04:24:12.78	+16:22:44.22	87.6 ± 1.3	-21.9 ± 1.2	57.5 ± 1.0	6.8	G0V	Hyades	8.8	
vB 52	04:24:28.33	+16:53:10.32	113.1 ± 1.4	-23.3 ± 1.2	44.8 ± 0.8	6.3	G2V	Hyades	8.8	
vB 176	04:25:47.56	+18:01:02.20	102.6 ± 2.2	-29.9 ± 3.2	48.0 ± 1.0	6.8	K2V	Hyades	8.8	
vB 63	04:26:24.61	+16:51:11.84	106.7 ± 1.3	-24.5 ± 1.2	46.9 ± 1.0	6.4	G1V	Hyades	8.8	
vB 64	04:26:40.11	+16:44:48.78	107.0 ± 1.1	-26.8 ± 1.1	46.4 ± 0.9	6.5	G2+	Hyades	8.8	
vB 66	04:27:46.07	+11:44:11.07	110.1 ± 1.3	-13.2 ± 1.2	44.6 ± 0.9	6.2	F8	Hyades	8.8	
vB 73	04:28:48.29	+17:17:07.84	110.1 ± 1.1	-28.9 ± 1.0	44.5 ± 0.8	6.4	G2V	Hyades	8.8	
vB 79	04:29:31.61	+17:53:35.46	106.7 ± 1.1	-31.4 ± 1.1	45.6 ± 0.8	7.1	K0V	Hyades	8.8	
vB 180	04:29:57.73	+16:40:22.23	106.2 ± 1.1	-27.1 ± 1.1	46.0 ± 0.8	7.1	K1V	Hyades	8.8	
vB 88	04:31:29.35	+13:54:12.55	90.0 ± 1.2	-16.0 ± 1.2	53.1 ± 1.3	6.5	F9V	Hyades	8.8	
1RXS J043243.2−152003	04:32:43.51	−15:20:11.39	2.3 ± 1.1	14.2 ± 1.1	140.0 ± 70.0	8.6	G4V	···	6.6	
vB 91	04:32:50.12	+16:00:20.96	103.2 ± 1.0	-25.9 ± 1.0	45.9 ± 0.6	6.8	G7	Hyades	8.8	
vB 92	04:32:59.45	+15:49:08.37	99.1 ± 1.2	-24.1 ± 1.2	47.8 ± 0.8	6.9	G7	Hyades	8.8	
vB 93	04:33:37.97	+16:45:44.96	99.0 ± 1.1	-22.9 ± 1.2	48.3 ± 0.7	7.4	G7	Hyades	8.8	
vB 96	04:33:58.54	+15:09:49.04	101.9 ± 1.3	-29.4 ± 1.3	45.4 ± 0.8	6.5	G5	Hyades	8.8	
RX J0434.3+0226	04:34:19.54	+02:26:26.10	18.0 ± 2.0	-16.4 ± 1.9	161.0 ± 24.0	9.5	K4e	···	7.8	
vB 183	04:34:32.18	+15:49:39.23	91.0 ± 1.0	-20.0 ± 1.0	51.7 ± 0.8	7.6	G7	Hyades	8.8	
vB 97	04:34:35.31	+15:30:16.56	98.1 ± 1.0	-26.7 ± 1.1	47.2 ± 0.9	6.4	F8:V:	Hyades	8.8	
vB 99	04:36:05.27	+15:41:02.60	95.0 ± 1.0	-23.1 ± 1.2	48.7 ± 0.7	7.4	G7	Hyades	8.8	
vB 196	04:38:57.31	+14:06:20.16	99.5 ± 0.9	-24.4 ± 1.1	44.6 ± 0.9	6.4	G5	Hyades	8.8	

TABLE 3
Median Sample Statistics

Sample	log (Age/yr) range	log (Age/yr) median	Distance (pc) range	Distance (pc) median	Spectral Type range	Spectral Type median
Deep	6.6–8.7	8.0	10–190	50	F5–K5	G5
Shallow	6.6–10.0	8.8	11–190	45	F5–K5	G7
Complete	6.6–10.0	8.3	10–190	46	F5–K5	G5

TABLE 4
Calibration Binaries and Assumed Parameters of Their Astrometric Orbits

Binary (WDS)	a (arcsec)	P (years)	T_0 (year)	e	i (degrees)	Ω (degrees)	ω (degrees)	grade	Ref.
09006+4147	0.6472 ± 0.0010	21.776 ± 0.017	1993.725 ± 0.023	0.1507 ± 0.0008	131.26 ± 0.13	204.39 ± 0.19	32.52 ± 0.36	1	1
16147+3352	5.927	888.989	1826.949	0.7605	31.795	16.889	72.201	4	2
18055+0230	4.5540 ± 0.0052	88.38 ± 0.02	1895.94 ± 0.02	0.4992 ± 0.0004	121.16 ± 0.08	302.12 ± 0.10	14.0 ± 0.1	1	3
20467+1607	10.22	3249	2305	0.88	148.78	88.06	331.16	4	4

References. — 1. Hartkopf et al. (1996); 2. Scardia (1979); 3. Pourbaix (2000); 4. Hale (1994).

Note. — Explanation of orbital parameters: a—semi-major axis; P—period; T_0—epoch of periastron; e—eccentricity; i—inclination; Ω—longitude of periastron; ω—longitude of the ascending node.

TABLE 5
Extinction Due to PHARO and NIRC2 Optics

Transmissive Optic	ΔJ (mag)	ΔH (mag)	ΔK_S (mag)
PHARO ND 1% filter	4.753 ± 0.039	4.424 ± 0.033	4.197 ± 0.024
NIRC2 $1''$ coronagraph	8.36 ± 0.28	7.78 ± 0.15	7.10 ± 0.17
NIRC2 $2''$ coronagraph	9.26 ± 0.09	7.79 ± 0.22	7.07 ± 0.22

TABLE 6
Deep Sample Observations and Sensitivity Limits

Star	Date (UT)	Observatory	Optic[a]	Limiting K_S-Band Magnitude at[b] 1″	2″	5″
HD 377	2002 Aug 28	Palomar	corona	...	...	...
	2003 Nov 09	Keck	corona	16.7	18.3	20.0
	2004 Oct 07	Keck	corona	...	...	...
HD 691	2002 Aug 31	Palomar	corona	...	...	...
	2002 Nov 18	Palomar	corona	15.1	18.3	20.3
HD 984	2002 Aug 29	Palomar	corona	13.1	16.9	18.5
	2003 Sep 20	Palomar	corona	...	...	...
	2004 Oct 04	Palomar	corona	...	...	...
HD 1405	2004 Jun 06	Keck	corona	16.3	18.3	19.2
QT And	2002 Aug 29	Palomar	corona	...	...	...
	2003 Nov 10	Keck	corona	17.6	19.1	19.9
	2004 Oct 07	Keck	corona	...	...	...
HD 7661	2002 Aug 30	Palomar	corona	...	...	...
	2002 Nov 09	Keck	corona	16.5	18.0	20.0
HIP 6276	2002 Aug 30	Palomar	corona	14.5	18.9	20.7
	2004 Oct 08	Keck	corona	...	...	...
HD 8907	2002 Aug 27	Palomar	corona	13.5	17.3	19.3
HD 12039	2002 Aug 28	Palomar	corona	14.0	18.5	20.0
HD 15526	2003 Sep 20	Palomar	corona	15.5	19.4	20.3
1RXS J025216.9+361658	2002 Nov 18	Palomar	corona	...	...	...
	2003 Nov 10	Keck	corona	17.8	19.3	20.3
	2004 Feb 07	Palomar	corona	...	...	...
HD 17925	2003 Sep 21	Palomar	corona	12.5	15.3	18.6
1RXS J025751.8+115759	2002 Nov 16	Palomar	corona	16.4	19.8	20.5
RX J0258.4+2947	2002 Feb 28	Palomar	corona	17.7	19.5	19.6
1RXS J030759.1+302032	2002 Nov 18	Palomar	corona	15.1	18.2	19.8
HD 19668	2002 Aug 27	Palomar	corona	...	...	...
	2003 Nov 09	Keck	corona	17.0	18.5	20.0
1E 0307.4+1424	2003 Jan 12	Palomar	corona	15.6	18.9	20.5
V525 Per	2003 Sep 20	Palomar	...	...	...	...
	2004 Oct 03	Palomar	...	...	...	...
	2004 Oct 08	Keck	corona	18.7	20.3	20.4
1RXS J031907.4+393418	2002 Aug 29	Palomar	corona	...	...	...
	2003 Nov 10	Keck	corona	19.3	20.5	20.7
	2004 Oct 08	Keck	corona	...	...	...
HE 622	2003 Sep 20	Palomar	...	...	...	...
	2004 Oct 08	Keck	corona	19.2	20.8	20.9
1E 0324.1–2012	2003 Jan 12	Palomar	corona	...	...	...
	2004 Feb 07	Palomar	corona	...	...	...
	2004 Oct 08	Keck	corona	18.1	19.5	19.8
RX J0329.1+0118	2003 Sep 21	Palomar	corona	16.6	19.7	20.1
HE 1101	2003 Sep 20	Palomar	...	...	...	...
	2004 Oct 03	Palomar	...	...	...	...
	2004 Oct 07	Keck	corona	19.2	20.9	21.0
	2006 Dec 12	Keck	corona	...	...	...
HD 22179	2002 Nov 16	Palomar	corona	...	...	...
	2003 Nov 09	Keck	corona	18.1	19.4	20.2
	2004 Feb 07	Palomar	corona	...	...	...
	2004 Oct 08	Keck	corona	...	...	...
HD 23208	2004 Oct 05	Palomar	corona	14.9	19.2	20.1
HII 120	2003 Sep 20	Palomar	...	...	...	...
	2004 Oct 04	Palomar	...	...	...	...
	2004 Oct 08	Keck	corona	18.6	20.0	20.2
	2006 Jan 18	Palomar	...	...	...	...
HII 2147	2003 Jan 13	Palomar	corona	15.2	19.3	20.6
1RXS J035028.0+163121	2002 Nov 17	Palomar	corona	16.7	19.9	20.3
RX J0354.4+0535	2003 Jan 13	Palomar	corona	...	...	...
	2004 Feb 07	Palomar	...	...	...	...
	2004 Oct 07	Keck	corona	18.3	19.9	20.3
HD 283167	2002 Nov 18	Palomar	corona	17.0	19.6	19.8
RX J0357.3+1258	2003 Jan 11	Palomar	corona	...	...	...
	2003 Nov 09	Keck	corona	18.9	20.3	20.5
	2004 Feb 07	Palomar	corona	...	...	...
HD 285751	2002 Jan 31	Palomar	corona	15.7	18.1	19.2
RX J0442.5+0906	2003 Jan 11	Palomar	corona	16.4	19.5	20.0
	2004 Feb 07	Palomar	...	...	...	...
HD 286179	2002 Jan 31	Palomar	corona	...	...	...
	2004 Feb 07	Palomar	...	...	...	...
	2004 Oct 07	Keck	corona	17.8	19.6	20.3
	2006 Dec 12	Keck	corona	...	...	...
HD 31950	2002 Nov 16	Palomar	corona	...	...	...
	2003 Nov 09	Keck	corona	18.1	19.4	19.8
	2004 Feb 07	Palomar	corona	...	...	...
	2004 Oct 08	Keck	corona	...	...	...
HD 35850	2002 Feb 01	Palomar	corona	11.7	14.3	16.9
1RXS J053650.0+133756	2002 Feb 28	Palomar	corona	...	...	...
	2003 Jan 14	Palomar	corona	...	...	...
	2003 Nov 10	Keck	corona	18.4	18.0	20.6
HD 245567	2002 Nov 16	Palomar	corona			

TABLE 7
Shallow Sample Observations and Sensitivity Limits

Star	Date (UT)	Observatory	Optic[a]	Limiting K_S-Band Magnitude at[b] 0.″5	1″	2″	5″
HD 224873	2002 Aug 31	Palomar	ND1	...	...	...	...
	2003 Sep 21	Palomar	ND1	11.8	13.5	10.0	14.7
HD 6963	2004 Jun 04	Palomar	ND1	10.3	11.9	13.8	14.1
HD 8467	2004 Jun 04	Palomar	ND1	10.8	12.4	13.6	13.9
HD 8941	2004 Jun 04	Palomar	ND1	9.8	11.3	13.5	14.0
HD 9472	2002 Nov 18	Palomar	ND1	...	...	...	...
	2003 Sep 20	Palomar	ND1	...	...	...	...
	2004 Oct 05	Palomar	ND1	10.8	12.6	15.1	15.8
RE J0137+18A	2002 Jan 31	Palomar	...	11.7	13.2	12.0	14.9
	2003 Sep 20	Palomar	ND1	...	...	...	...
HD 11850	2003 Sep 21	Palomar	ND1	10.7	12.4	14.8	15.3
HD 13382	2004 Jun 04	Palomar	ND1	10.4	12.2	14.7	15.0
HD 13507	2002 Aug 28	Palomar	corona	11.7	13.8	15.6	18.1
HD 13531	2002 Aug 28	Palomar	ND1	...	...	...	...
	2003 Sep 21	Palomar	ND1	...	...	...	...
	2004 Oct 05	Palomar	ND1	10.4	12.1	14.7	15.6
HD 13974	2004 Jun 04	Palomar	ND1	7.6	9.2	11.8	13.5
1RXS J025223.5+372914	2003 Sep 21	Palomar	...	...	...	...	...
	2004 Oct 05	Palomar	...	14.1	12.8	17.6	18.2
2RE J0255+474	2002 Feb 28	Palomar	...	...	...	...	...
	2004 Oct 05	Palomar	...	12.5	14.9	15.8	16.7
HD 18940	2002 Aug 29	Palomar	ND1	9.9	11.9	14.8	15.1
HD 19019	2004 Jun 04	Palomar	ND1	9.9	12.0	14.6	14.9
HD 19632	2002 Aug 30	Palomar	...	9.8	12.0	14.2	14.5
vB 1	2002 Aug 29	Palomar	ND1	10.3	12.2	14.6	14.8
HE 350	2003 Sep 20	Palomar	...	...	...	...	...
	2004 Oct 04	Palomar	...	13.7	15.9	18.1	18.3
HE 373	2003 Sep 20	Palomar	...	...	...	...	...
	2003 Nov 10	Keck	...	...	...	...	...
	2004 Oct 05	Palomar	...	13.8	16.1	18.0	18.2
HE 389	2003 Sep 20	Palomar	...	...	...	...	...
	2004 Oct 04	Palomar	...	14.3	16.4	18.3	18.5
HE 696	2003 Sep 20	Palomar	...	14.4	15.6	17.5	17.7
HE 699	2003 Sep 20	Palomar	...	14.1	16.2	17.5	17.7
HE 750	2003 Sep 20	Palomar	...	13.8	16.0	17.6	17.8
HE 767	2003 Sep 20	Palomar	...	13.9	16.1	17.5	17.8
HE 848	2003 Sep 20	Palomar	...	13.3	15.3	17.3	17.9
HE 935	2003 Sep 20	Palomar	...	13.2	15.4	17.1	17.7
	2006 Dec 12	Palomar	...	...	...	...	...
HE 1234	2003 Sep 20	Palomar	...	13.2	15.7	16.9	17.4
HD 22879	2004 Jun 04	Palomar	ND1	9.7	11.3	14.4	14.9
HII 102	2003 Sep 20	Palomar	...	...	...	...	...
	2004 Oct 04	Palomar	...	13.3	15.6	17.1	17.3
	2006 Jan 18	Palomar	...	...	...	...	...
HII 120	2003 Dec 10	Palomar	...	13.4	15.3	17.2	17.9
HII 152	2003 Sep 21	Palomar	...	13.5	15.4	16.4	16.7
HII 174	2003 Sep 21	Palomar	...	13.8	15.8	16.8	17.0
HII 173	2003 Sep 21	Palomar	...	13.0	14.9	16.2	16.6
HII 250	2003 Dec 10	Palomar	...	13.3	15.9	17.3	18.0
HII 314	2003 Dec 10	Palomar	...	13.2	15.1	17.0	17.6
1RXS J034423.3+281224	2002 Nov 17	Palomar	ND1	...	...	...	...
	2004 Oct 05	Palomar	ND1	11.5	12.0	15.8	16.3
HII 514	2003 Dec 10	Palomar	...	13.3	15.2	16.9	17.4
HII 571	2003 Dec 10	Palomar	...	...	...	...	...
	2004 Oct 03	Palomar	...	13.8	16.0	17.7	17.8
HII 1015	2003 Dec 10	Palomar	...	13.2	15.2	17.0	17.6
HII 1101	2003 Dec 10	Palomar	...	...	...	...	...
	2004 Oct 05	Palomar	...	13.2	15.4	17.3	17.7
HII 1182	2003 Dec 10	Palomar	...	...	...	...	...
	2004 Oct 03	Palomar	...	...	...	...	...
	2005 Jan 24	Palomar	...	13.8	15.8	17.5	18.0
HII 1776	2003 Dec 10	Palomar	...	13.2	14.4	16.0	16.3
HII 2106	2003 Dec 10	Palomar	...	...	...	...	...
	2005 Jan 24	Palomar	...	13.3	16.7	18.1	18.2
RX J0348.9+0110	2003 Dec 10	Palomar	...	11.8	13.6	15.2	16.0
	2005 Jan 24	Palomar	...	...	...	...	...
HII 2278	2003 Dec 10	Palomar	...	...	...	...	...
	2005 Jan 24	Palomar	...	11.3	14.6	17.1	17.6
HII 2506	2003 Dec 10	Palomar	...	12.8	15.0	17.1	17.8
HII 2644	2003 Dec 10	Palomar	...	13.6	15.7	17.2	17.7
HII 2786	2003 Dec 10	Palomar	...	12.9	15.4	17.0	17.7
HII 2881	2003 Dec 10	Palomar	...	...	...	...	...
	2005 Jan 24	Palomar	...	13.8	15.9	17.6	17.8
HII 3097	2003 Dec 10	Palomar	...	13.6	15.5	17.4	17.9
HII 3179	2005 Jan 24	Palomar	...	13.2	15.4	17.3	17.5
HD 285281	2002 Feb 01	Palomar	...	...	...	...	...
	2004 Feb 07	Palomar	...	12.7	12.7	15.5	17.8
HD 284135	2002 Jan 31	Palomar	...	10.9	12.0	14.8	17.3
	2004 Feb 07	Palomar	ND1				

TABLE 8
Candidate Companions in the Deep Sample

Primary Star	N_C	ρ (arcsec)	θ (deg)	ΔK_S (mag)	K_S (mag)	$J-K_S$ (mag)	t_0 (UT Date)	Tel.	Assoc.	Ref.
QT And	1	7.696 ± 0.019	239.56 ± 0.22	11.56 ± 0.22	18.91 ± 0.22	1.57 ± 0.31	2002-08-29	P	no(a)	
HD 15526	1	0.077 ± 0.004	177.96 ± 0.75	0.00 ± 0.05	8.76 ± 0.06	0.61 ± 0.08	2003-09-20	P	yes(c)	
1RXS J025216.9+361658	1	5.811 ± 0.020	10.63 ± 0.41	10.26 ± 0.09	17.86 ± 0.09	···	2002-11-18	P	no(a)	
RX J0258.4+2947	1	0.086 ± 0.011	220.82 ± 4.14	0.60 ± 0.30	10.15 ± 0.30	0.58 ± 0.42	2002-02-28	P	yes(c)	
HD 19668	1	6.565 ± 0.020	148.98 ± 0.19	10.58 ± 0.03	17.28 ± 0.04	···	2002-08-27	P	no(a)	
V525 Per	1	4.135 ± 0.026	83.86 ± 0.23	7.57 ± 0.30	16.93 ± 0.30	···	2003-09-20	P	no(a)	
	2	12.452 ± 0.021	64.09 ± 0.13	7.23 ± 0.32	16.59 ± 0.32	···	2004-10-03	P	?	
	3	10.680 ± 0.043	126.00 ± 0.20	9.98 ± 0.20	19.34 ± 0.20	···	2004-10-08	K	?	
1RXS J031907.4+393418	1	7.656 ± 0.030	286.56 ± 0.25	8.77 ± 0.09	18.26 ± 0.09	0.87 ± 0.24	2002-08-29	P	no(a)	
	2	10.157 ± 0.024	333.52 ± 0.18	9.69 ± 0.09	19.18 ± 0.09	1.14 ± 0.24	2002-08-29	P	no(a)	
HE 622	1	7.275 ± 0.017	48.24 ± 0.18	6.38 ± 0.22	15.97 ± 0.22	0.66 ± 0.31	2003-09-20	P	?	
	2	9.756 ± 0.024	311.79 ± 0.17	6.51 ± 0.22	16.10 ± 0.22	0.83 ± 0.31	2003-09-20	P	?	
	3	12.478 ± 0.021	107.92 ± 0.12	8.76 ± 0.22	18.35 ± 0.22	1.03 ± 0.31	2004-10-08	K	?	
	4	12.368 ± 0.023	109.57 ± 0.12	9.58 ± 0.22	19.17 ± 0.22	0.98 ± 0.31	2004-10-08	K	?	
	5	10.436 ± 0.017	224.37 ± 0.12	8.10 ± 0.22	17.69 ± 0.22	1.12 ± 0.31	2004-10-08	K	?	
RX J0329.1+0118	1	3.761 ± 0.004	303.35 ± 0.09	3.62 ± 0.08	12.82 ± 0.08	0.90 ± 0.14	2003-09-21	P	yes(c)	MH04
HE 1101	1	5.828 ± 0.025	323.66 ± 0.25	6.58 ± 0.09	15.89 ± 0.09	0.34 ± 0.13	2003-09-20	P	no(a)	
	2	5.911 ± 0.010	276.86 ± 0.12	8.25 ± 0.09	17.56 ± 0.09	0.14 ± 0.13	2004-10-07	K	no(a)	
	3	5.316 ± 0.009	247.23 ± 0.12	9.13 ± 0.09	18.44 ± 0.09	0.53 ± 0.13	2004-10-07	K	no(a)	
	4	10.100 ± 0.017	113.32 ± 0.12	9.63 ± 0.09	18.94 ± 0.09	0.61 ± 0.13	2004-10-07	K	no(a)	
	5	2.173 ± 0.006	29.19 ± 0.14	10.11 ± 0.09	19.42 ± 0.09	1.15 ± 0.17	2004-10-07	K	no(a)	
HD 22179	1	6.536 ± 0.029	236.26 ± 0.24	8.82 ± 0.10	16.24 ± 0.10	···	2002-11-09	P	no(a)	
	2	6.616 ± 0.029	235.44 ± 0.23	9.30 ± 0.11	16.73 ± 0.11	···	2002-11-16	P	no(a)	
	3	9.200 ± 0.027	179.64 ± 0.23	10.20 ± 0.12	17.62 ± 0.12	···	2002-11-09	P	no(a)	
HII 120	1	3.549 ± 0.008	119.15 ± 0.14	5.75 ± 0.21	14.85 ± 0.21	1.21 ± 0.25	2003-09-20	P	no(a)	
	2	10.633 ± 0.023	70.53 ± 0.13	5.43 ± 0.15	14.53 ± 0.15	1.22 ± 0.20	2003-09-20	P	no(a)	
RX J0354.4+0535	1	11.128 ± 0.035	225.82 ± 0.18	7.27 ± 0.10	15.94 ± 0.10	0.62 ± 0.18	2003-01-13	P	no(c)	
	2	0.205 ± 0.004	357.44 ± 0.92	2.10 ± 0.20	10.92 ± 0.20	0.97 ± 0.28	2004-02-07	P	yes(c)	
RX J0357.3+1258	1	10.086 ± 0.025	115.72 ± 0.19	6.56 ± 0.08	15.54 ± 0.08	0.64 ± 0.22	2003-01-11	P	no(a)	
	2	3.831 ± 0.026	338.31 ± 0.26	10.50 ± 0.10	19.48 ± 0.10	···	2003-01-11	P	?	
HD 286179	1	10.124 ± 0.024	237.40 ± 0.19	7.20 ± 0.20	15.66 ± 0.20	···	2002-01-31	P	no(a)	
	2	3.406 ± 0.009	194.68 ± 0.22	10.72 ± 0.18	19.18 ± 0.18	···	2004-10-07	K	no(e)	
HD 31950	1	2.596 ± 0.007	264.22 ± 0.18	4.13 ± 0.04	12.51 ± 0.05	0.67 ± 0.07	2002-11-16	P	yes(a)	
	2	3.106 ± 0.007	137.92 ± 0.18	3.70 ± 0.04	12.08 ± 0.05	0.49 ± 0.07	2002-11-16	P	no(c)	
	3	6.925 ± 0.016	146.81 ± 0.18	6.35 ± 0.04	14.73 ± 0.05	0.89 ± 0.07	2002-11-16	P	?	
	4	3.117 ± 0.015	327.86 ± 0.35	8.53 ± 0.05	16.91 ± 0.06	0.31 ± 0.08	2002-11-16	P	no(c)	
	5	10.013 ± 0.027	351.17 ± 0.16	9.91 ± 0.09	18.29 ± 0.09	···	2002-11-16	P	?	
	6	6.528 ± 0.020	28.55 ± 0.14	10.73 ± 0.11	19.11 ± 0.11	···	2002-11-16	P	?	
	7	6.313 ± 0.019	248.03 ± 0.20	10.36 ± 0.08	18.74 ± 0.08	···	2002-11-16	P	?	
1RXS J053650.0+133756	1	1.839 ± 0.018	37.26 ± 0.54	8.88 ± 0.30	16.95 ± 0.30	···	2002-02-28	P	no(a)	
	2	12.096 ± 0.027	212.16 ± 0.17	8.10 ± 0.10	16.17 ± 0.10	···	2002-02-28	P	no(a)	
HD 245567	1	0.348 ± 0.002	330.66 ± 0.23	1.79 ± 0.04	9.57 ± 0.04	0.52 ± 0.08	2002-11-16	P	yes(c)	
	2	3.185 ± 0.007	198.88 ± 0.17	6.44 ± 0.24	14.03 ± 0.24	0.54 ± 0.34	2002-11-16	P	no(a)	
	3	6.748 ± 0.024	316.18 ± 0.22	8.28 ± 0.24	15.87 ± 0.24	0.97 ± 0.34	2002-11-16	P	no(a)	
	4	10.927 ± 0.024	315.63 ± 0.17	6.21 ± 0.24	13.80 ± 0.24	0.55 ± 0.34	2002-11-16	P	no(a)	
	5	2.724 ± 0.007	21.87 ± 0.13	11.55 ± 0.24	19.14 ± 0.24	···	2003-11-09	K	no(a)	
SAO 150676	1	8.375 ± 0.029	351.31 ± 0.14	9.30 ± 0.20	16.77 ± 0.20	···	2002-11-17	P	no(a)	
HD 49197	1	6.952 ± 0.016	345.82 ± 0.18	6.75 ± 0.06	12.82 ± 0.06	0.15 ± 0.12	2002-02-28	P	no(a)	
	2	0.948 ± 0.032	77.50 ± 1.03	8.22 ± 0.14	14.29 ± 0.14	1.63 ± 1.21	2002-02-28	P	yes(a)	
RE J0723+20	1	8.196 ± 0.013	80.86 ± 0.03	7.80 ± 0.20	14.68 ± 0.20	0.16 ± 0.22	2002-02-28	P	no(a)	
	2	5.532 ± 0.013	329.36 ± 0.09	8.40 ± 0.20	15.28 ± 0.20	1.06 ± 0.22	2002-02-28	P	no(a)	
HD 60737	1	7.657 ± 0.029	127.25 ± 0.18	9.40 ± 0.20	15.65 ± 0.20	···	2002-01-31	P	no(a)	
HD 82443	1	5.459 ± 0.010	190.30 ± 0.23	11.77 ± 0.14	16.89 ± 0.14	···	2004-02-07	P	?	
	2	8.154 ± 0.020	98.76 ± 0.15	12.59 ± 0.21	17.71 ± 0.21	···	2004-02-07	P	?	
	3	7.142 ± 0.027	253.71 ± 0.23	13.84 ± 0.30	18.96 ± 0.30	···	2004-02-07	P	?	
SAO 178272	1	10.082 ± 0.032	356.64 ± 0.18	9.67 ± 0.15	17.06 ± 0.15	···	2003-01-13	P	?	
	2	8.184 ± 0.046	274.53 ± 0.15	10.75 ± 0.22	18.14 ± 0.22	···	2003-01-13	P	?	
HD 90905	1	5.816 ± 0.027	191.77 ± 0.23	11.30 ± 0.10	16.82 ± 0.10	···	2002-02-01	P	no(a)	
	2	12.446 ± 0.031	176.73 ± 0.13	13.49 ± 0.19	19.01 ± 0.19	···	2004-06-05	K	no(e)	
HD 91782	1	1.002 ± 0.008	33.67 ± 0.46	4.30 ± 0.06	11.08 ± 0.06	0.90 ± 0.13	2002-03-02	P	yes(a)	
HD 92855	1	2.934 ± 0.005	291.33 ± 0.13	4.57 ± 0.09	10.46 ± 0.09	0.75 ± 0.15	2002-02-01	P	yes(a)	FM00
	2	12.216 ± 0.022	147.79 ± 0.25	8.90 ± 0.20	14.79 ± 0.20	···	2002-02-01	P	no(a)	
GQ Leo	1	0.248 ± 0.002	273.22 ± 0.11	0.13 ± 0.06	8.58 ± 0.06	1.02 ± 0.08	2003-01-12	P	yes(a)	
	2	10.038 ± 0.009	325.65 ± 0.09	6.40 ± 0.06	14.16 ± 0.06	0.13 ± 0.09	2003-01-12	P	no(a)	
HD 104576	1	10.455 ± 0.028	19.66 ± 0.21	11.00 ± 0.50	17.68 ± 0.50	···	2002-06-22	P	no(e)	
HD 104860	1	3.803 ± 0.027	287.01 ± 0.28	10.92 ± 0.25	17.42 ± 0.25	0.00 ± 0.47	2002-06-23	P	no(a)	
	2	11.961 ± 0.033	260.09 ± 0.19	12.09 ± 0.18	18.59 ± 0.18	···	2004-06-05	K	no(e)	
SAO 15880	1	2.176 ± 0.018	293.93 ± 0.72	8.98 ± 0.17	16.27 ± 0.17	···	2004-02-06	P	no(a)	
HD 111456	1	3.783 ± 0.010	117.45 ± 0.30	12.72 ± 0.16	17.27 ± 0.16	···	2004-02-06	P	?	
HD 139498	1	0.311 ± 0.002	3.39 ± 0.21	0.00 ± 0.02	8.26 ± 0.03	0.50 ± 0.05	2003-07-15	P	yes(a)	WDS
	2	11.246 ± 0.033	123.98 ± 0.19	8.48 ± 0.30	15.98 ± 0.30	···	2004-06-26	P	?	
	3	8.801 ± 0.026	61.50 ± 0.21	10.98 ± 0.30	18.49 ± 0.30	···	2004-06-26	P	?	
HD 142361	1	0.705 ± 0.001	236.41 ± 0.13	2.01 ± 0.10	9.19 ± 0.10	0.85 ± 0.14	2002-06-21	P	yes(a)	G93
	2	11.207 ± 0.046	164.99 ± 0.17	5.85 ± 0.17	12.88 ± 0.17	0.77 ± 0.28	2002-06-21	P	no(a)	
HD 143006	1	8.355 ± 0.026	130.27 ± 0.25	9.28 ± 0.16	16.33 ± 0.16	1.18 ± 0.23	2002-06-23	P	?	
	2	6.626 ± 0.028	0.32 ± 0.23	10.40 ± 0.16	17.45 ± 0.16	1.40 ± 0.23	2002-06-23	P	?	
	3	8.502 ± 0.029	268.41 ± 0.23	10.66 ± 0.16	17.71 ± 0.16	1.27 ± 0.23	2002-06-23	P	no(a)	
	4	7.698 ± 0.023	357.97 ± 0.12	12.11 ± 0.16	19.16 ± 0.16	1.30 ± 0.23	2003-05-18	K	?	
	5	12.879 ± 0.028	102.74 ± 0.13	11.29 ± 0.16	18.34 ± 0.16	0.88 ± 0.23	2003-05-18	K	?	

TABLE 9
Candidate Companions in the Shallow Sample

Primary Star	N_C	ρ (arcsec)	θ (deg)	ΔK_S (mag)	K_S (mag)	$J-K_S$ (mag)	t_0 (UT Date)	Tel.	Assoc.	Ref.
HD 224873	1	1.268 ± 0.002	171.44 ± 0.12	0.25 ± 0.02	7.57 ± 0.03	0.50 ± 0.05	2002-08-31	P	yes(a)	WDS
HD 9472	1	2.793 ± 0.025	343.69 ± 0.30	5.79 ± 0.09	11.83 ± 0.09	1.04 ± 0.14	2002-11-18	P	yes(a)	
RE J0137+18A	1	1.691 ± 0.006	24.60 ± 0.12	0.05 ± 0.01	7.49 ± 0.02	0.76 ± 0.03	2002-01-31	P	yes(a)	WDS
HD 13531	1	0.717 ± 0.003	16.79 ± 0.43	4.20 ± 0.08	9.88 ± 0.08	1.04 ± 0.15	2002-08-28	P	yes(a)	
1RXS J025223.5+372914	1	0.637 ± 0.003	91.28 ± 0.28	1.43 ± 0.08	10.77 ± 0.08	0.67 ± 0.12	2003-09-21	P	yes(a)	
	2	5.255 ± 0.016	76.85 ± 0.18	4.37 ± 0.09	13.45 ± 0.09	0.50 ± 0.13	2003-09-21	P	no(a)	
2RE J0255+474	1	2.131 ± 0.004	272.63 ± 0.16	0.08 ± 0.05	7.29 ± 0.06	0.72 ± 0.08	2002-02-28	P	yes(a)	WDS
	2	11.469 ± 0.033	46.40 ± 0.11	7.00 ± 0.10	14.21 ± 0.10	0.57 ± 0.14	2002-02-28	P	no(a)	
HD 18940	1	0.167 ± 0.002	8.59 ± 1.18	0.78 ± 0.03	6.71 ± 0.04	0.51 ± 0.08	2002-08-29	P	yes(c)	Hip
	2	4.321 ± 0.012	207.38 ± 0.12	4.58 ± 0.03	10.08 ± 0.04	0.92 ± 0.07	2002-08-29	P	?	
	3	4.120 ± 0.010	203.78 ± 0.13	5.21 ± 0.03	10.71 ± 0.04	0.81 ± 0.07	2002-08-29	P	?	
vB 1	1	2.470 ± 0.006	200.63 ± 0.14	2.63 ± 0.03	8.62 ± 0.04	0.91 ± 0.06	2002-08-29	P	yes(c)	WDS
HE 350	1	8.464 ± 0.016	109.22 ± 0.14	5.85 ± 0.21	15.11 ± 0.21	1.50 ± 0.37	2003-09-20	P	no(a)	
	2	6.896 ± 0.011	38.37 ± 0.19	7.66 ± 0.30	16.92 ± 0.30	···	2004-10-04	P	?	
HE 373	1	2.081 ± 0.005	193.77 ± 0.18	5.24 ± 0.10	14.59 ± 0.10	0.98 ± 0.14	2003-09-20	P	yes(a)	MH04
	2	11.598 ± 0.031	265.81 ± 0.25	7.51 ± 0.30	16.86 ± 0.30	···	2003-09-20	P	?	
	3	8.478 ± 0.034	55.82 ± 0.22	8.37 ± 0.30	17.72 ± 0.30	···	2003-09-20	P	?	
HE 389	1	9.023 ± 0.016	133.30 ± 0.12	5.47 ± 0.13	14.96 ± 0.13	1.10 ± 0.18	2003-09-20	P	no(a)	
HE 696	1	0.448 ± 0.001	357.22 ± 0.18	2.72 ± 0.08	12.50 ± 0.08	0.70 ± 0.12	2003-09-20	P	yes(a)	P02
HE 935	1	0.026 ± 0.025	247.44 ± 0.21	0.00 ± 0.20	9.21 ± 0.20	0.40 ± 0.28	2003-09-20	P	yes(c)	P02
	2	3.116 ± 0.025	109.45 ± 0.21	8.70 ± 0.30	17.16 ± 0.30	···	2003-09-20	P	no(a)	
HII 102	1	3.599 ± 0.009	213.29 ± 0.14	3.07 ± 0.10	11.72 ± 0.10	1.05 ± 0.14	2003-09-20	P	yes(a)	B97
	2	9.959 ± 0.027	240.21 ± 0.16	5.75 ± 0.10	14.40 ± 0.10	1.05 ± 0.14	2003-09-20	P	?	
1RXS J034423.3+281224	1	0.425 ± 0.002	202.20 ± 0.10	1.13 ± 0.10	8.62 ± 0.10	0.48 ± 0.22	2002-11-17	P	yes(a)	WDS
	2	5.711 ± 0.006	313.30 ± 0.12	7.11 ± 0.11	14.27 ± 0.11	···	2004-10-05	P	?	
HII 571	1	3.903 ± 0.005	66.10 ± 0.08	3.84 ± 0.08	13.07 ± 0.08	0.95 ± 0.12	2003-12-10	P	yes(a)	B97,M9
HII 1101	1	9.167 ± 0.016	104.93 ± 0.12	5.70 ± 0.09	14.46 ± 0.09	0.40 ± 0.16	2003-12-10	P	no(a)	
HII 1182	1	1.113 ± 0.009	219.69 ± 0.26	4.54 ± 0.19	13.48 ± 0.19	···	2003-12-10	P	yes(a)	B97
HII 2106	1	0.240 ± 0.010	31.09 ± 0.59	1.71 ± 0.12	11.29 ± 0.12	···	2003-12-10	P	yes(a)	B97
RX J0348.9+0110	1	0.047 ± 0.007	41.50 ± 3.64	0.00 ± 0.05	9.02 ± 0.06	···	2003-12-10	P	yes(a)	
HII 2278	1	0.331 ± 0.005	179.20 ± 0.32	0.03 ± 0.02	9.57 ± 0.03	···	2003-12-10	P	yes(a)	B97
HII 2881	1	0.099 ± 0.005	335.73 ± 1.20	0.26 ± 0.09	9.94 ± 0.09	···	2003-12-10	P	yes(a)	B97
HD 285281	1	0.770 ± 0.001	188.34 ± 0.05	1.20 ± 0.10	9.12 ± 0.10	0.66 ± 0.14	2002-02-01	P	yes(a)	KL98
HD 284135	1	0.367 ± 0.002	253.23 ± 0.21	0.12 ± 0.01	8.58 ± 0.02	···	2002-01-31	P	yes(a)	WDS
HD 281691	1	6.768 ± 0.014	138.91 ± 0.13	1.90 ± 0.05	10.30 ± 0.06	0.74 ± 0.08	2002-11-18	P	yes(a)	KL98
HD 26182	1	0.818 ± 0.002	175.11 ± 0.11	0.92 ± 0.08	9.09 ± 0.08	0.42 ± 0.11	2003-12-10	P	yes(c)	WDS
HD 284266	1	0.569 ± 0.006	356.92 ± 0.11	1.90 ± 0.10	10.66 ± 0.10	0.89 ± 0.41	2002-01-31	P	yes(a)	KL98
HD 26990	1	0.123 ± 0.004	163.56 ± 1.40	0.38 ± 0.20	6.81 ± 0.20	0.67 ± 0.36	2003-12-10	P	yes(a)	
vB 49	1	2.139 ± 0.017	256.86 ± 0.16	4.60 ± 0.14	11.40 ± 0.14	···	2003-01-12	P	yes(c)	
vB 52	1	1.115 ± 0.002	236.40 ± 0.18	2.73 ± 0.06	9.10 ± 0.06	0.85 ± 0.08	2003-01-12	P	yes(a)	P98
vB 176	1	0.227 ± 0.003	307.06 ± 0.38	0.28 ± 0.09	7.67 ± 0.09	···	2003-12-10	P	yes(a)	Hip
vB 66	1	9.781 ± 0.023	248.88 ± 0.11	10.75 ± 0.10	16.91 ± 0.10	···	2002-11-17	P	?	
vB 91	1	0.133 ± 0.002	172.98 ± 2.79	0.37 ± 0.14	7.72 ± 0.14	···	2003-12-10	P	yes(a)	WDS
vB 96	1	0.171 ± 0.003	264.05 ± 0.78	0.36 ± 0.10	7.41 ± 0.10	···	2003-12-10	P	yes(p)	P98
RX J0434.3+0226	1	1.340 ± 0.022	271.76 ± 0.30	2.38 ± 0.05	11.99 ± 0.06	0.77 ± 0.11	2003-01-12	P	yes(c)	
vB 106	1	7.230 ± 0.012	76.50 ± 0.44	9.50 ± 0.30	15.94 ± 0.30	···	2003-12-10	P	no(a)	
HD 282346	1	0.461 ± 0.001	272.14 ± 0.18	1.13 ± 0.04	8.91 ± 0.04	0.61 ± 0.17	2002-11-18	P	yes(a)	Hip
vB 142	1	6.070 ± 0.013	123.82 ± 0.16	11.30 ± 0.20	18.04 ± 0.20	···	2002-11-17	P	no(a)	
1RXS J051111.1+281353	1	0.495 ± 0.001	211.51 ± 0.10	0.39 ± 0.04	8.77 ± 0.05	0.69 ± 0.07	2002-02-28	P	yes(a)	
HD 36869	1	8.230 ± 0.014	152.30 ± 0.12	3.10 ± 0.35	9.95 ± 0.35	0.93 ± 0.35	2003-01-14	P	yes(a)	
	2	8.043 ± 0.016	249.72 ± 0.20	7.59 ± 0.15	14.44 ± 0.15	···	2003-01-14	P	?	
HD 61994	1	5.210 ± 0.008	77.00 ± 0.08	7.32 ± 0.13	12.67 ± 0.13	0.28 ± 0.30	2002-11-18	P	no(c)	
HD 69076	1	1.232 ± 0.005	101.06 ± 0.11	3.91 ± 0.05	10.38 ± 0.05	1.04 ± 0.21	2002-11-18	P	yes(a)	
HD 71974	1	0.383 ± 0.014	87.34 ± 0.63	0.42 ± 0.05	6.45 ± 0.06	0.35 ± 0.21	2002-03-03	P	yes(c)	S99
HD 72760	1	0.964 ± 0.007	215.08 ± 0.38	4.84 ± 0.01	10.28 ± 0.02	1.01 ± 0.04	2002-11-16	P	yes(c)	
HD 77407	1	1.659 ± 0.004	353.36 ± 0.04	2.00 ± 0.10	7.60 ± 0.10	0.90 ± 0.14	2002-01-31	P	yes(a)	M04
HD 78899	1	8.174 ± 0.013	75.76 ± 0.12	3.36 ± 0.08	9.17 ± 0.08	0.79 ± 0.13	2003-12-09	P	?	
HD 91962	1	0.842 ± 0.003	176.00 ± 0.11	1.37 ± 0.06	7.03 ± 0.06	0.73 ± 0.13	2002-03-02	P	yes(a)	WDS
	2	0.142 ± 0.004	56.17 ± 1.76	1.25 ± 0.11	6.94 ± 0.11	0.98 ± 0.19	2003-05-10	P	yes(c)	
HD 99565	1	0.408 ± 0.001	6.13 ± 0.18	0.09 ± 0.05	6.55 ± 0.05	0.48 ± 0.06	2003-01-11	P	yes(a)	WDS
HD 108799	1	2.070 ± 0.006	338.46 ± 0.09	1.47 ± 0.02	6.30 ± 0.03	0.80 ± 0.06	2003-05-10	P	yes(a)	WDS
HD 108944	1	1.941 ± 0.006	345.48 ± 0.18	3.49 ± 0.02	9.56 ± 0.03	0.85 ± 0.09	2002-03-03	P	yes(a)	
HD 112196	1	1.501 ± 0.001	55.52 ± 0.09	2.07 ± 0.01	7.77 ± 0.02	0.73 ± 0.04	2002-02-01	P	yes(a)	
HD 115043	1	1.639 ± 0.003	358.61 ± 0.05	4.87 ± 0.08	10.22 ± 0.08	0.86 ± 0.12	2003-12-09	P	yes(a)	L05
HD 129333	1	0.717 ± 0.009	172.77 ± 0.11	2.83 ± 0.05	8.82 ± 0.05	0.81 ± 0.07	2003-01-11	P	yes(a)	DM91,MH
HD 134319	1	5.356 ± 0.020	260.77 ± 0.10	4.00 ± 0.10	10.79 ± 0.10	0.85 ± 0.11	2002-03-02	P	yes(a)	L05
HD 135363	1	0.251 ± 0.003	121.35 ± 0.46	0.68 ± 0.10	7.34 ± 0.10	0.57 ± 0.14	2002-02-01	P	yes(a)	L07
RX J1541.1–2656	1	6.261 ± 0.018	82.05 ± 0.13	3.13 ± 0.02	12.05 ± 0.03	···	2003-07-15	P	?	
	2	6.250 ± 0.015	224.11 ± 0.15	7.19 ± 0.11	16.11 ± 0.11	···	2003-07-15	P	no(a)	
PZ99 J161329.3–231106	1	1.430 ± 0.002	91.41 ± 0.05	2.70 ± 0.05	11.28 ± 0.05	0.87 ± 0.08	2003-05-10	P	yes(a)	
HD 150554	1	11.595 ± 0.023	183.44 ± 0.08	3.06 ± 0.10	9.37 ± 0.10	1.03 ± 0.14	2003-05-10	P	yes(p)	WDS
HD 152555	1	3.819 ± 0.008	56.86 ± 0.15	3.78 ± 0.02	10.14 ± 0.03	0.81 ± 0.05	2002-08-31	P	yes(a)	
HD 155902	1	0.062 ± 0.007	0.28 ± 6.05	0.50 ± 0.30	6.26 ± 0.30	0.39 ± 0.42	2003-09-21	P	yes(c)	
HD 157664	1	0.036 ± 0.002	118.76 ± 3.21	0.00 ± 0.10	7.46 ± 0.10	0.31 ± 0.14	2003-05-10	P	yes(a)	
HD 166435	1	2.653 ± 0.022	273.69 ± 0.26	10.67 ± 0.20	15.99 ± 0.20	-0.15 ± 0.28	2002-06-23	P	no(a)	
	2	10.376 ± 0.030	281.28 ± 0.12	11.90 ± 0.20	17.22 ± 0.20	0.54 ± 0.22	2002-06-23	P	no(a)	
	3	9.496 ± 0.020	183.40 ± 0.19	11.48 ± 0.20	16.80 ± 0.20	0.18 ± 0.28	2002-06-23	P	no(a)	
	4	3.293 ± 0.009	239.04 ± 0.45	13.50 ± 0.30	18.82 ± 0.30	···	2002-08-30	P	no(a)	
HD 175742	1	2.687 ± 0.043	88.98 ± 0.83	10.75 ± 0.09	16.88 ± 0.09		2004-06-28	P	?	

TABLE 10
Color Companions and Their Chance Alignment Probabilities

Companion to	N_C	ρ (arcsec)	ΔK_S (mag)	K_S (mag)	CAP (%)
HD 15526	1	0.0770	0.00	8.01 ± 0.10	0.8
HD 155902	1	0.0620	0.50	5.73 ± 0.10	14.3
HD 18940	1	0.1670	0.78	6.28 ± 0.10	1.5
HD 201989	1	2.0790	3.97	9.70 ± 0.08	0.9
vB 1	1	2.4700	2.63	8.62 ± 0.10	0.9
HD 245567	1	0.3480	1.79	9.38 ± 0.10	0.8
HD 26182	1	0.8180	0.92	8.71 ± 0.10	2.3
vB 49	1	2.1390	4.56	11.36 ± 0.10	1.3
HD 71974	1	0.3830	0.42	5.89 ± 0.10	1.7
HD 72760	1	0.9640	4.84	10.26 ± 0.10	0.9
HD 91962	2	0.1420	1.25	6.64 ± 0.10	0.9
HE 935	1	0.0260	0.30	8.76 ± 0.10	6.7
RX J0329.1+0118	1	3.7610	3.62	12.82 ± 0.10	0.7
RX J0354.4+0535	2	0.2050	2.10	10.77 ± 0.10	1.4
RX J0434.3+0226	1	1.3400	2.38	11.88 ± 0.10	1.2
RX J2313.0+2345	1	1.4060	1.79	10.41 ± 0.10	1.4
ScoPMS 27	1	0.0790	0.60	8.64 ± 0.10	0.7

Note. — Most columns headings are as for Tables 8 and 9. CAP is the chance alignment probability from Equation 1 in § 5.2.2.

TABLE 11
New and Confirmed Secondaries

Companion	M_{K_S} (mag)	Projected Separation (arcsec)	Projected Separation (AU)	M_2 ($M_\odot$)	q	Sample[a]	Ref.
HD 224873B	4.12 ± 0.22	1.27	62.13	0.84	0.98	AD_{30}	WDS
HD 9472B	9.24 ± 0.11	2.79	92.17	0.11	0.10		
RE J0137+18B	3.46 ± 0.27	1.69	108.22	0.63	0.97	AD_{30}	WDS
HD 13531B	7.81 ± 0.12	0.72	18.64	0.19	0.20	AD_{30}	
HD 15526B	3.63 ± 0.54	0.08	8.16	0.90	1.00	AD	
1RXS J025223.5+372914B	4.62 ± 1.09	0.64	108.29	0.71	0.66	AD_{30}	
2RE J0255+474B	3.80 ± 1.09	2.13	106.55	0.91	0.99	AD_{30}	WDS
RX J0258.4+2947B	5.15 ± 1.13	0.09	8.60	0.59	0.78	AD	
HD 18940B	4.05 ± 0.08	0.17	5.68	0.86	0.83		Hip
vB 1B	5.45 ± 0.05	2.47	106.46	0.56	0.47		WDS
HE 373B	8.20 ± 0.16	2.08	395.39	0.10	0.08		MH04
HE 696B	6.11 ± 0.15	0.45	85.12	0.39	0.38		P02
RX J0329.1+0118B	7.82 ± 1.09	3.76	376.10	0.11	0.12	AD_{30}	MH04
HE 935B	2.82 ± 0.24	0.03	4.94	1.20	1.00		P02
HII 102B	6.10 ± 0.14	3.60	478.67	0.43	0.39	AD_{30}	B97
1RXS J034423.3+281224B	5.17 ± 0.20	0.43	20.83	0.57	0.71	AD	WDS
HII 571B	7.45 ± 0.13	3.90	519.10	0.20	0.20		B97, M92
HII 1182B	7.86 ± 0.21	1.11	148.03	0.15	0.14		B97
HII 2106B	5.67 ± 0.15	0.24	31.92	0.51	0.59		B97
RX J0348.9+0110B	4.02 ± 1.09	0.05	4.70	0.87	1.00		
HII 2278B	3.95 ± 0.10	0.33	44.02	0.89	0.99		B97
HII 2881B	4.32 ± 0.13	0.10	13.17	0.79	0.92		B97
RX J0354.4+0535B	5.92 ± 1.10	0.21	20.50	0.48	0.50	AD	
HD 285281B	5.67 ± 0.20	0.77	37.73	0.19	0.42	AD_{30}	KL98
HD 284135B	2.85 ± 1.09	0.37	51.38	0.98	0.93	AD	WDS
HD 281691B	4.57 ± 1.09	6.77	947.52	0.68	0.60	AD_{30}	KL98
HD 26182B	4.09 ± 1.09	0.82	81.80	0.79	0.72	AD_{30}	WDS
HD 284266B	4.93 ± 1.09	0.57	79.66	0.43	0.38	AD_{30}	KL98
HD 26990B	4.09 ± 0.24	0.12	4.31	0.84	0.91		
vB 49B	7.60 ± 0.15	2.14	122.99	0.22	0.19		
vB 52B	5.84 ± 0.07	1.12	49.95	0.49	0.45		P98
vB 176B	4.26 ± 0.10	0.23	10.90	0.80	0.99		Hip
vB 91B	4.41 ± 0.14	0.13	6.10	0.76	0.94		WDS
vB 96B	4.12 ± 0.11	0.17	7.76	0.84	0.97		P98
RX J0434.3+0226B	5.96 ± 0.33	1.34	215.74	0.38	0.39	AD_{30}	
HD 282346B	4.65 ± 0.43	0.46	32.73	0.70	0.73	AD	Hip
HD 31950B	7.51 ± 1.09	2.60	259.60	0.13	0.12	AD_{30}	
1RXS J051111.1+281353B	2.73 ± 0.20	0.50	68.81	0.80	0.76	AD	
HD 36869B	5.66 ± 0.72	8.23	592.56	0.36	0.30	AD_{30}	
HD 245567B	4.19 ± 0.39	0.35	41.41	0.30	0.27	AD	
HD 49197B	11.02 ± 0.17	0.95	42.66	0.06	0.05	AD_{30}	MH04
HD 69076B	7.72 ± 0.08	1.23	41.89	0.20	0.22		
HD 71974B	4.14 ± 0.10	0.38	11.11	0.83	0.92		S99
HD 72760B	8.59 ± 0.05	0.96	21.02	0.13	0.15		
HD 77407B	5.21 ± 0.12	1.66	49.77	0.49	0.48	AD_{30}	M04
HD 91782B	7.34 ± 0.13	1.00	56.11	0.23	0.20	AD_{30}	
HD 91962B	4.19 ± 0.13	0.84	31.15	0.82	0.44[‡]	AD_{30}	WDS
HD 91962C	4.10 ± 0.16	0.14	5.25	0.85	0.76	AD	
HD 92855B	7.68 ± 0.11	2.93	105.62	0.18	0.16	AD_{30}	FM30
HD 99565B	3.83 ± 0.19	0.41	14.28	0.91	0.98		WDS
GQ LeoB	5.09 ± 1.09	0.25	12.40	0.61	0.99	AD	
HD 108799B	4.31 ± 0.09	2.07	51.75	0.79	0.69	AD_{30}	WDS
HD 108944B	6.34 ± 0.10	1.94	85.40	0.41	0.34	AD_{30}	
HD 112196B	5.11 ± 0.13	1.50	51.03	0.59	0.52	AD_{30}	
HD 115043B	8.15 ± 0.09	1.64	42.61	0.16	0.15		L05
HD 129333B	6.16 ± 0.08	0.72	24.38	0.38	0.36	AD_{30}	DM91, MH04
HD 134319B	7.57 ± 0.11	5.36	235.66	0.13	0.13	AD_{30}	L05
HD 135363B	5.03 ± 0.12	0.25	7.28	0.60	0.84	AD	L07
HD 139498B	2.74 ± 0.17	0.31	39.50	1.22	1.00	AD	WDS
HD 142361B	4.17 ± 0.32	0.71	71.21	0.37	0.22	AD_{30}	G93
ScoPMS 27B	3.33 ± 0.63	0.08	11.46	0.65	0.64	AD	
ScoPMS 52B	3.12 ± 0.61	0.14	20.88	0.76	0.62	AD	G93
PZ99 J161329.3−231106B	5.47 ± 0.60	1.43	207.35	0.14	0.14	AD_{30}	
PZ99 J161411.0−230536B	2.51 ± 0.61	0.22	32.19	1.17	0.91	AD	
HD 150554B	6.10 ± 0.14	11.60	521.78	0.45	0.39	AD_{30}	WDS
HD 152555B	6.73 ± 0.14	3.82	183.31	0.31	0.27		
HD 155902B	4.02 ± 0.31	0.06	1.74	0.86	0.90		
HD 157664B	2.84 ± 0.16	0.04	3.02	1.10	0.93		
HD 165590B	3.62 ± 0.11	0.45	16.81	0.90	0.80	AD	Hip
HD 199143B	4.63 ± 0.12	1.05	50.54	0.49	0.39	AD_{30}	JB01
HD 200746B	5.07 ± 0.36	0.23	9.99	0.62	0.60	AD	Hip
HD 201989B	7.31 ± 0.11	2.08	62.37	0.25	0.24		
HD 203030B	13.15 ± 0.14	11.92	488.84	0.02	0.02	AD_{30}	MH06
RX J2312.0+2245B	6.52 ± 1.09	2.86	429.00	0.38	0.28		
RX J2313.0+2345B	4.72 ± 1.09	1.41	210.90	0.35	0.31	AD_{30}	
HD 221613B	4.48 ± 0.12	0.17	5.71	0.74	0.72		WDS

References. — B97: Bouvier et al. (1997); DM91: Duquennoy & Mayor (1991);

TABLE 12
Direct Imaging Surveys for Brown Dwarf Companions

Survey	Sample[a]	Stars	SpT[b]	Age[b] (Gyr)	Mass[b] $M_\odot$	d[b] (pc)	$\rho_{\rm out}$[b] (AU)	Sensitivity[b] ($M_{\rm Jup}$)	$N_{\rm BD}$	$f_{\rm BD}$ (%)	Label	Comm
Marcy & Butler (2000)	field	500	G5 ?	5.0	1.0 ?	···	3	0.5	2	0.40	MB00	
Schroeder et al. (2000)	field	23	M1.5	5.0	0.5	3.5	53	30	0	0	S00	
Brandner et al. (2000)	Cha T, Sco-Cen	24	M1.5	0.005	0.6	150	1500	3	0	0	B00	
Oppenheimer et al. (2001)	field	164	M1	5.0	0.5	5.9	177	35	1	0.61	O01	
Gizis et al. (2001)	field	60 ?	K ?	5.0	0.8 ?	< 25	10000	40	3	5.00	G01	
Potter et al. (2002)	young field	31	G5 ?	0.5	1.1	20 ?	200 ?	30	1	3.22	P02	
Hinz et al. (2002)	field	66	M3.5	5	0.2	5.8	1480	40	0	0	H02	
Neuhäuser & Guenther (2004)	Tuc-Hor	25	G5 ?	0.035	1.2	60	4320	13	1	4.00	NG04	
McCarthy & Zuckerman (2004)	young field	83	M1	0.3	0.5	15	225	30	0	0	MZ04	
Masciadri et al. (2005)	young field	28	M0	0.012	0.8	21	147	5	0	0	M05	
Carson et al. (2005)	field	80	K7	5	0.7	10.3	155	50	0	0	CE05	
Luhman et al. (2005)	IC 348	150	M4.5	0.002	0.2	315	1600	6	0	0	LMG05	
Lowrance et al. (2005)	young field	45	K5	0.15	0.75	30	200	10	1	2.22	L05	
Chauvin et al. (2005b)	young field	50	K ?	0.035 ?	1.0 ?	60 ?	420 ?	5 ?	1	2.00	CL05	
Kouwenhoven et al. (2005, 2007)	Sco OB2	199	A	15	2.0 ?	130	520	30	1	0.50	K05	
Luhman et al. (2007b)	young field	73	G6	0.12	1.1	30	4500	13 ?	1	1.37	$L07_1$	
Luhman et al. (2007b)	field	48	G3	5.0	1.0	22	3300	30 ?	1	2.08	$L07_2$	
Tanner et al. (2007)	Taurus	15	K7	0.002	1.5	140	140	50	0	0.00	T07	
Biller et al. (2007)	young field	54	K2	0.03	1.0	25	50	5	0	0	B07	
Lafrenière et al. (2007)	young field	85	K0	0.1	1.0	22	200	2	1	1.18	LD07	
Lafreniere et al. (2008)	IC 348	126	M2.5	0.002	0.29	160	960	13	0	0	L08	
Kraus et al. (2008)	Upper Sco	82	M0	0.005	0.7	145	435	13	1	1.22	K08	1
This work	young field	100	G5	0.08	1.1	115	1440	13	2	1.98	MH	

Note. — Surveys are listed in approximate chronological order. For $\geq$ 0.3 Gyr-old stars, masses are estimated from the models of Baraffe et al. (1998). For solar neighborhood-aged ($\approx$ 5 Gyr) stars, mass estimates follow the spectral type–mass correspondence from Cox (2000). The median outer projected separation $\rho_{\rm out}$ is obtained as the product of the median sample distance d and the half-width of the FOV (i.e., the OWA) of the imager used in the survey. The sensitivity of each survey, in units of the limiting companion mass, corresponds to the median sensitivity to substellar companions at the widest probed separations, generally well outside the contrast-limited regime. Where this sensitivity was not explicitly stated, it was estimated based on the published survey depth and on substellar evolutionary models from Chabrier et al. (2000) and Baraffe et al. (2003). $N_{\rm BD}$ and $f_{\rm BD}$ are the number of detected brown dwarf companions and the fraction of survey stars with brown dwarf companions, respectively. The label in the penultimate column refers to the survey identifier in Figure 13. The comments on the adopted parameters for each survey from the last column are as follows: **1.** Included for comparison to the radial velocity brown dwarf desert. The median spectral type and stellar mass have been estimated approximately. **2.** The work of Gizis et al. (2001) analyzes brown dwarf companions to $\leq$M0 stars within 25 pc in the 2MASS Second Incremental Data Release (IDR2). The outer probed separation range is likely $> 10^4$ AU. The detection rate has been obtained from the ratio of the number of bound brown dwarf companions to the estimated number of brown dwarfs within 25 pc in 2MASS IDR2, assuming a field mass function that is flat across the stellar/substellar boundary (Metchev et al. 2008). **3.** The median spectral type in the survey of Potter et al. (2002) has been estimated based on the sample of nearby young solar analogs of Gaidos et al. (2000), from which Potter et al. (2002) borrow to form their sample. Also, the detected substellar binary companion, HD 130948B/C, is counted as a single companion object. **4.** We estimate a median spectral type of G5 for the young Sun-like stars in the survey of Neuhäuser & Guenther (2004). **5.** McCarthy & Zuckerman (2004) search for substellar companions only to the 83 apparently single stars in their 102-star Keck survey. **6.** The parameters of the solar analog survey of young southern associations by Chauvin et al. (2005b) have been guessed. **7.** The spectral type distribution of the sample targets in Kouwenhoven et al. (2005, 2007) is approximate. A median primary mass of 2.0 $M_\odot$ has been assumed. The listed brown dwarf companion is a candidate pending astrometric and spectroscopic confirmation. **8.** The work of Luhman et al. (2007b) surveys two distinct populations of Sun-like stars, which have been listed separately here based on the samples of their two *Spitzer* programs (PID=34 and PID=48). The sensitivities of the two sub-surveys are estimated approximately. **9.** The Palomar AO survey sample of Tanner et al. (2007) contains 15 stars in Taurus and 14 stars in the Pleiades. Definitive proper motion associations are available only within $1''$ of the primaries. Here and in Figure 13 we have shown only the Taurus subset because only that attains sensitivity to substellar objects within $1''$ from the primaries. **10.** Half of the sample observations of Kraus et al. (2008) are sensitive to companions below the 13 $M_{\rm Jup}$ deuterium-burning mass limit, and half are not. Therefore, we have adopted 13 $M_{\rm Jup}$ as the median sensitivity mass limit of the survey. The listed brown dwarf companion is a candidate pending astrometric and spectroscopic confirmation.

[a] The target source sample for each work. [b] Median value for the primary stars in the survey.

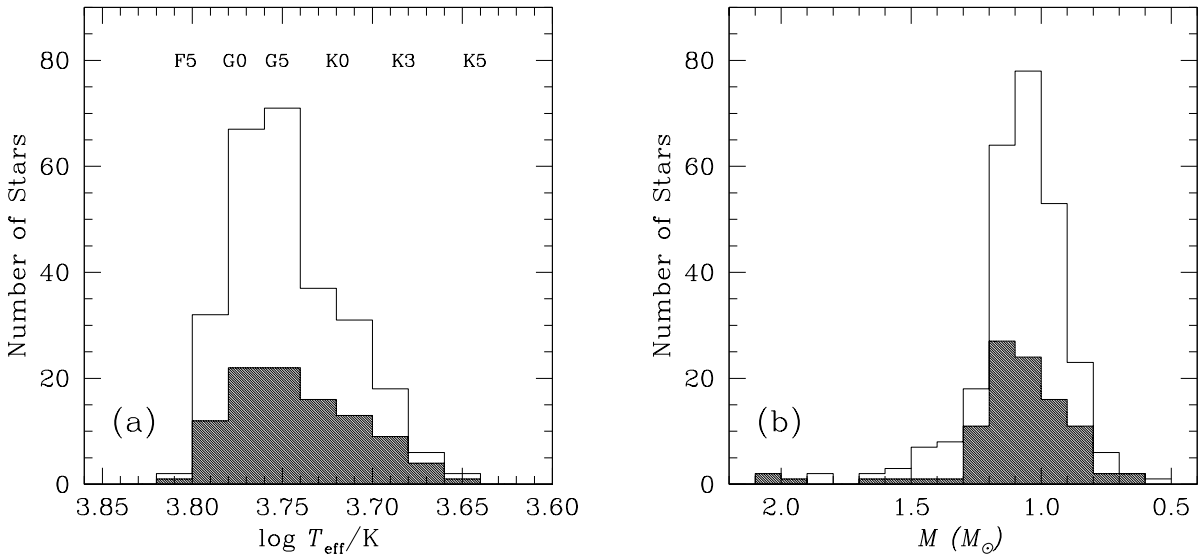

FIG. 1.— Distribution of the sample stars as a function of effective temperature (a) and mass (b). The non-shaded histograms refer to the entire sample of 266 stars, whereas the shaded histograms refer to the deep and young sub-sample of 100 stars. All stars fall in the F5–K5 range of spectral types and the majority are between 0.7 $M_\odot$ and 1.3 $M_\odot$.

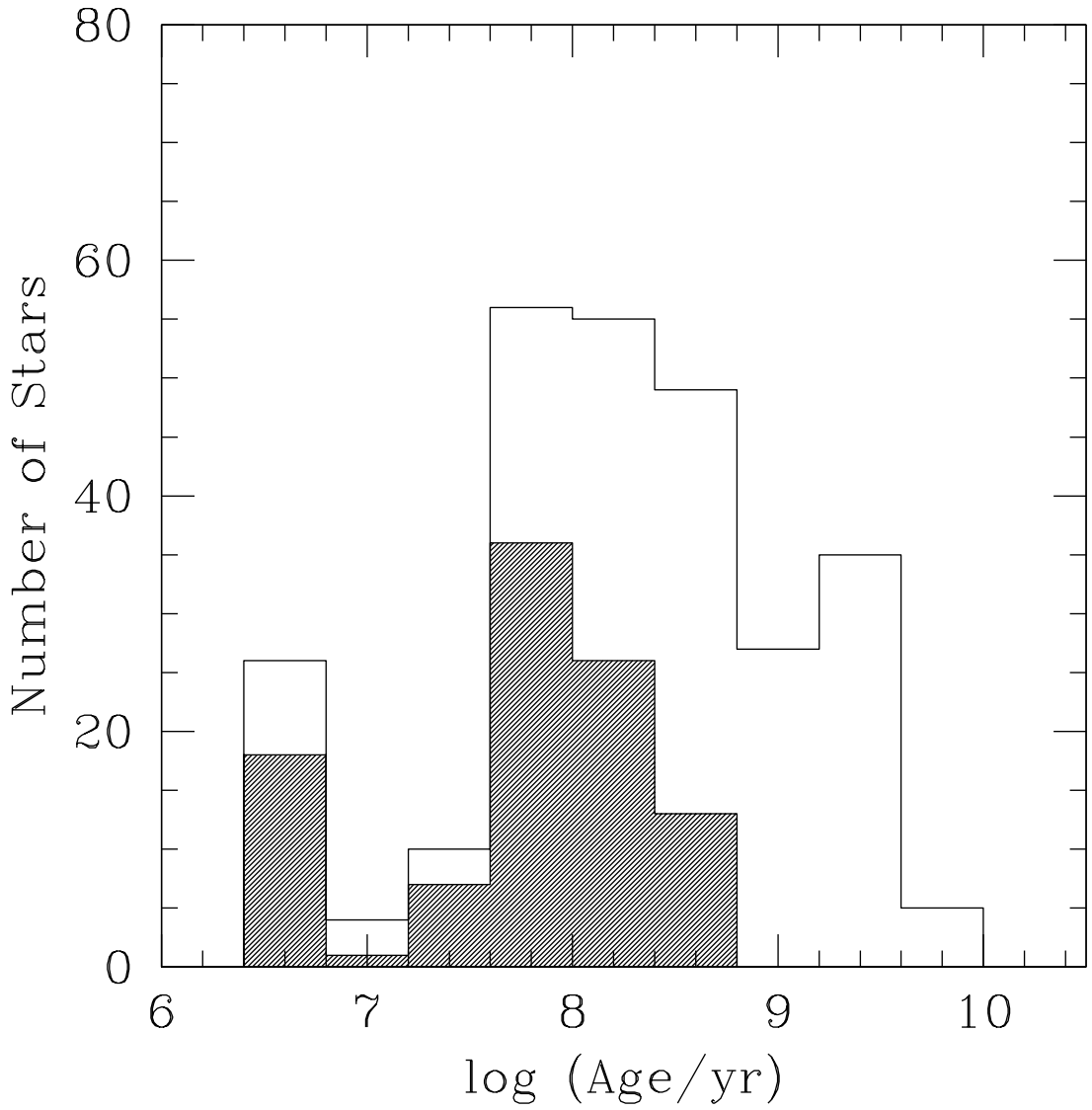

FIG. 2.— Age distributions of the complete survey sample (non-shaded histogram) and of the deep sub-sample (shaded histogram).

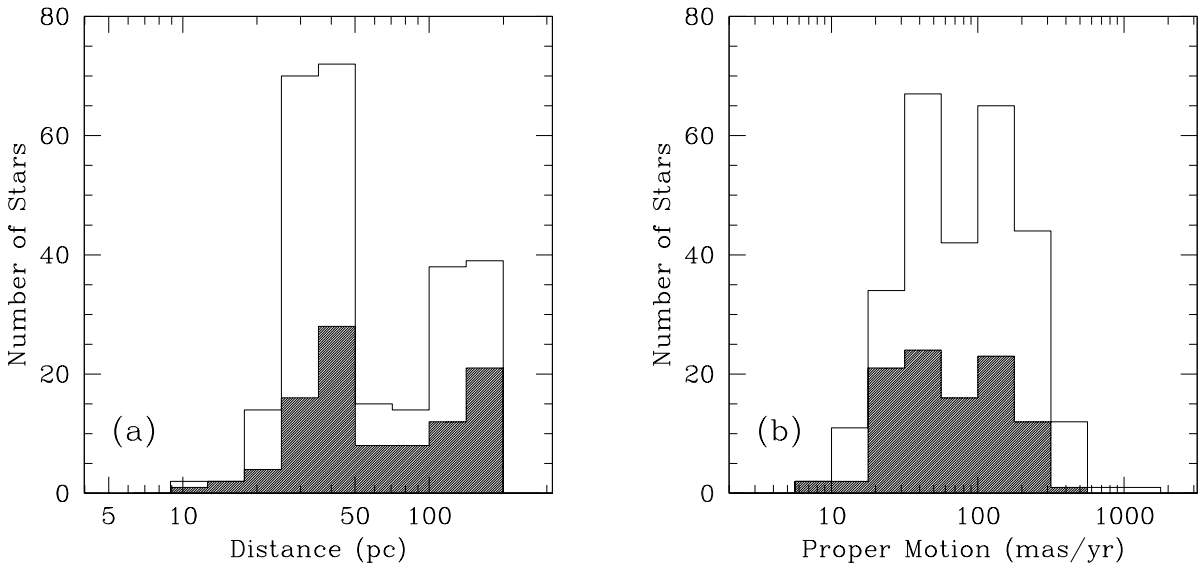

FIG. 3.— Heliocentric distance (a) and proper motion (b) distributions of surveyed stars in the complete sample (non-shaded histograms) and in the deep sub-sample (shaded histograms).

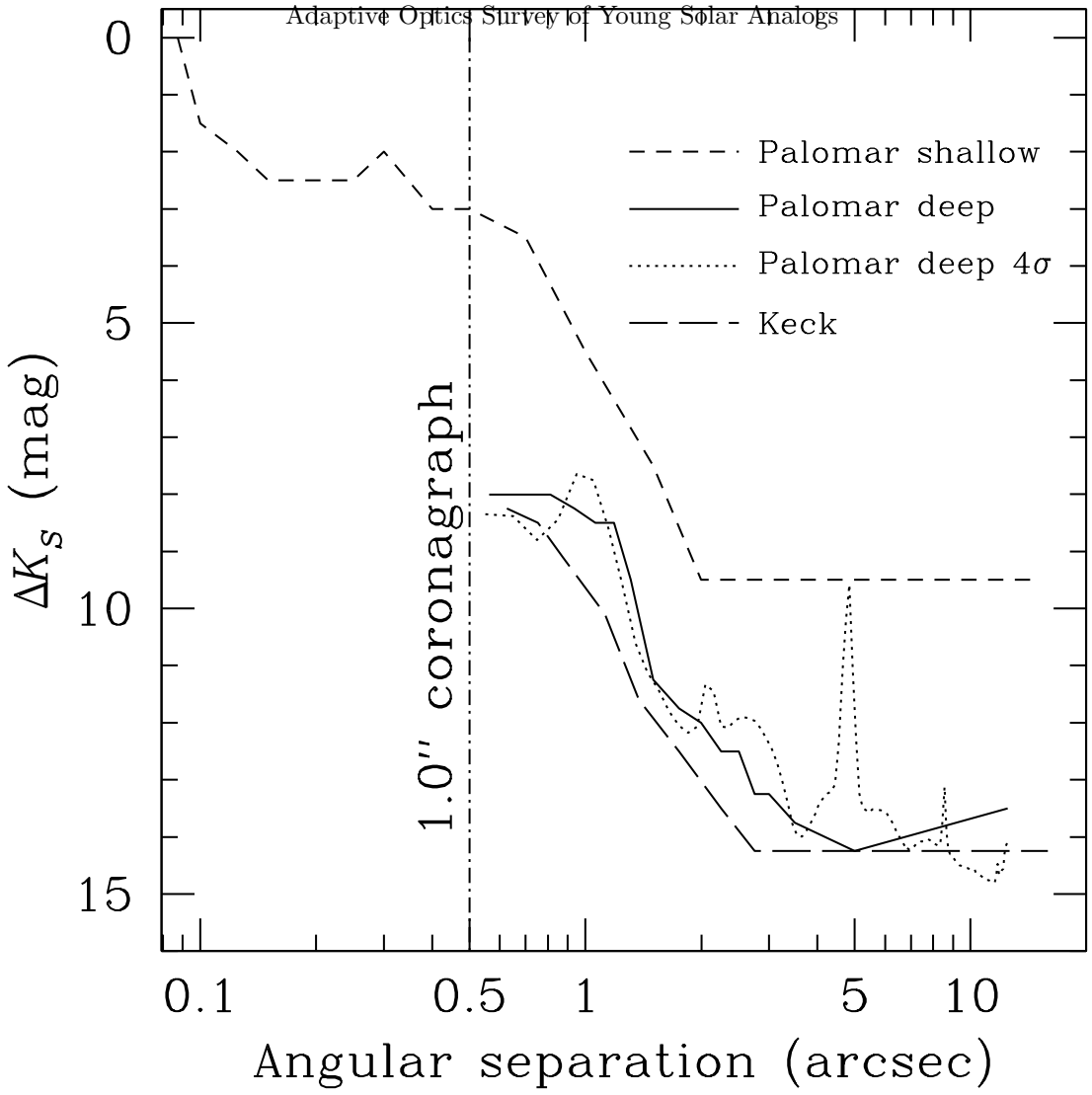

FIG. 4.— Empirical K_S-band contrast limits as determined from artificial star experiments in images of the program star HD 172649 (V = 7.5 mag), taken under good AO performance (≈50% Strehl ratio). The solid and long-dashed curves delineate coronagraphic observations at Palomar (24 min) and Keck (6 min), respectively. The short-dashed line shows the non-coronagraphic component of the Palomar survey. The dotted line represents the 4σ r.m.s. deviation of counts in the PSF halo as a function of separation, normalized to an aperture with radius 0.″1: equal to the FWHM of the K_S-band PALAO PSF. The vertical dash-dotted line shows the edge of the occulting spot at Palomar and Keck. The slight decrease in contrast in the Palomar coronagraphic limits at >5″ separations is due to an additive parameter used to model the decreasing exposure depth toward the edge of the PHARO field, because of image mis-registration among the different CR angles (§ 3.1.1). The contrast degradation is set to vary between 0 mag and 0.75 mag in the 4.″0–12.″5 separation range. The bumps and spikes in the r.m.s. limits correspond to bright features in the image of HD 172649, such as the corners of the waffle pattern at 1.0″ and projected companions to the star at 2.1″, 4.8″, and 8.6″.

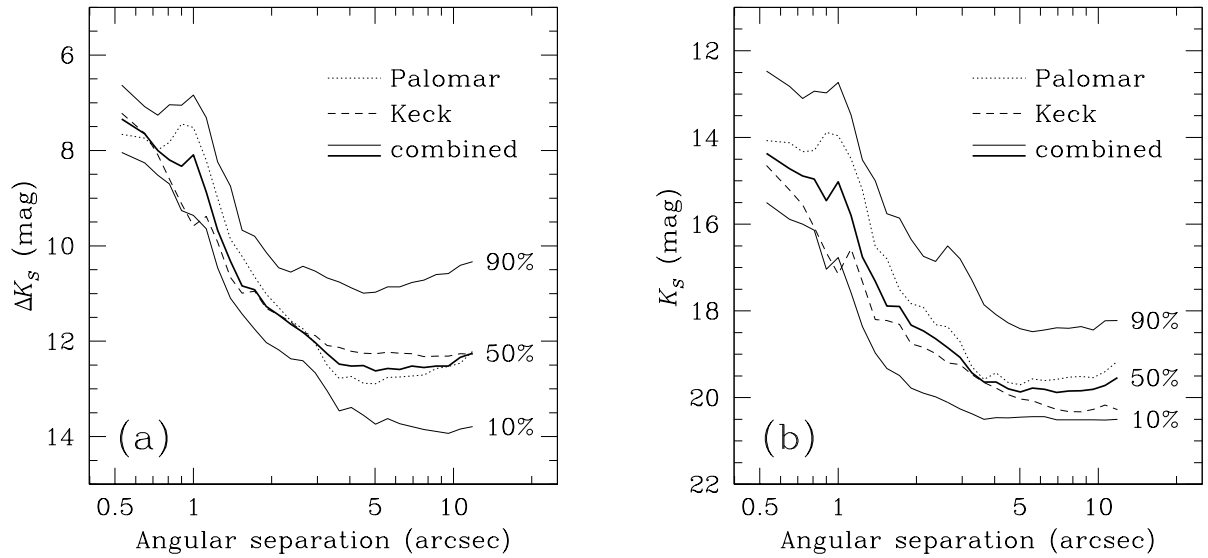

FIG. 5.— Contrast (a) and depth (b) of the deep survey at K_S. The solid lines represent the 10%, 50% (thick), and 90% completeness of the combined Palomar + Keck AO survey. The median (50%) sensitivities of the Palomar (dotted line) and Keck (dashed line) surveys are also shown. The gradual decrease in imaging contrast and depth at Palomar between 4″–12.″5 is partially due to mis-registration of images taken at different CR angles (§ 3.2), and partially to the sometimes smaller depth of observations at 11″–12.″5 separations because of a 0.″5–1.″5 offset of the coronagraphic spot from the center of the PHARO array.

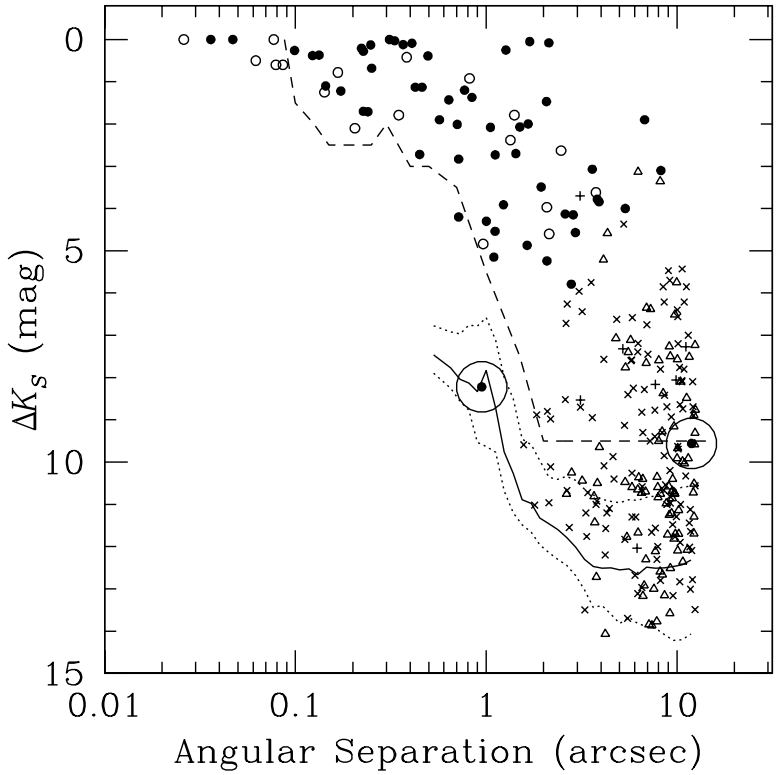

FIG. 6.— Magnitude difference ΔK_S vs. angular separation ρ for all candidate companions discovered in the deep and shallow surveys. The various symbols denote: "•"—astrometrically associated companions; "×"—astrometrically unassociated background stars; and for objects with insufficient astrometric data: "○"—companions associated based on their JK_S photometry; "+"—objects with JK_S photometry inconsistent with association; "△"—undecided objects. The encircled points show the two brown dwarf companions from the survey: HD 49197B (at $\rho = 0.''95$) and HD 203030B (at $\rho = 11.''92$). Detection limits for the shallow (dashed line) and deep (solid and dotted lines) components of the survey are also shown. The solid line shows the median contrast ΔK_S of the deep survey, while the dotted lines delimit the 10–90 percentile region (cf. Fig. 5a). Binaries with separations smaller than the PALAO K_S-band diffraction limit (0.″10) were resolved only at J-band. Correspondingly, the plotted magnitude difference for these companions is the one at J.

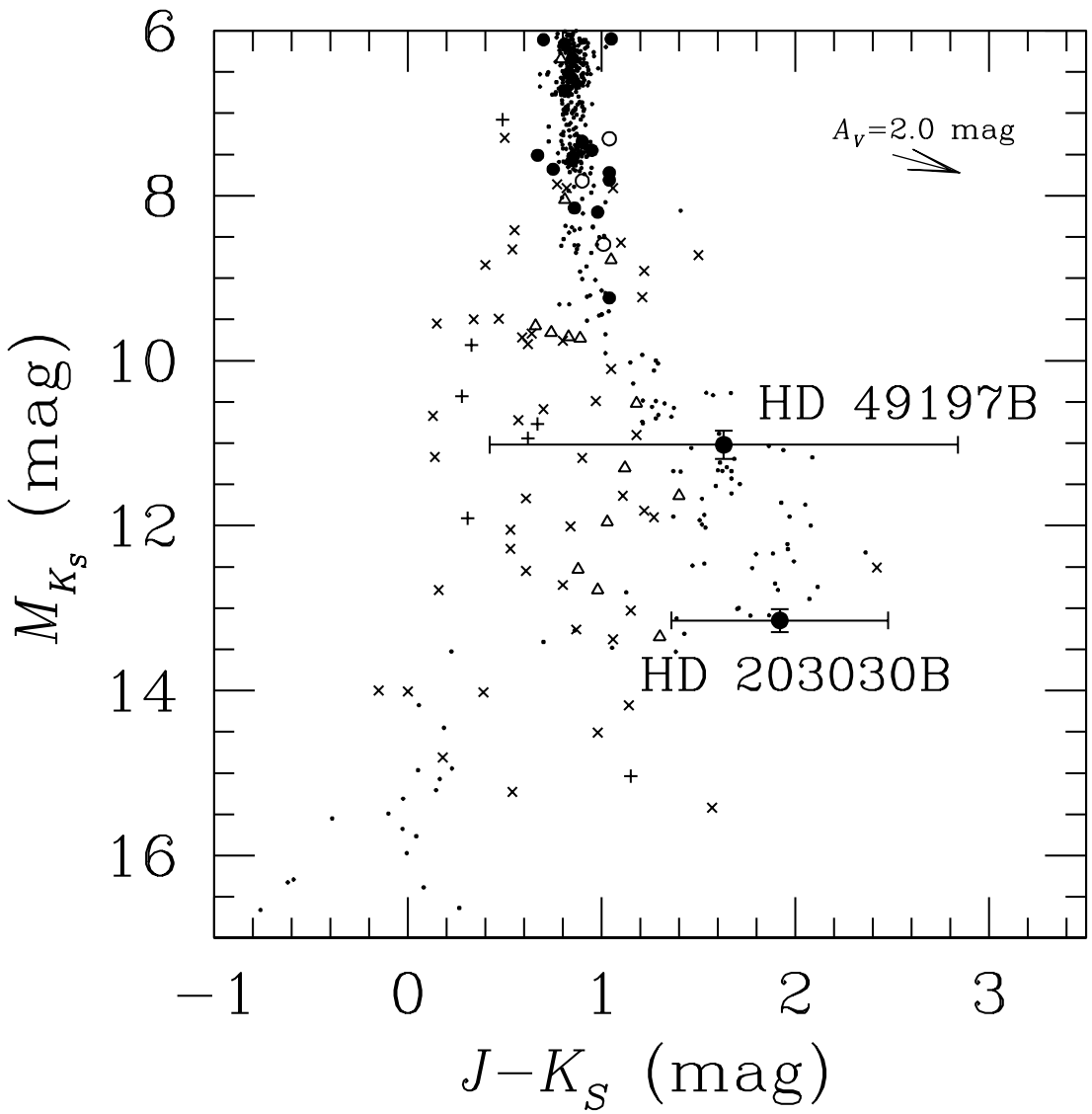

FIG. 7.— M_{K_S} vs. $J-K_S$ color-magnitude diagram of candidate companions for which J-band photometry was obtained. The symbols are the same as in Figure 6. The additional small dots denote M0–T8 dwarfs ($M_{K_S} \gtrsim 4.5$) with parallaxes from Dahn et al. (2002) and Vrba et al. (2004). The points with errorbars represent the two confirmed brown dwarf companions from our survey. The errorbars on HD 203030B are representative of the photometric precision for the faintest ($J \gtrsim 18$ mag) objects in the survey. Brighter objects typically had $J-K_S$ errors < 0.3 mag, except for the large $J-K_S$ uncertainty of HD 49197B, which is unique because of its relative faintness ($\Delta J = 9.6$ mag) and proximity ($\rho = 0\farcs95$) to the primary. The vector in the upper right corresponds to $A_V = 2$ mag of visual extinction, equivalent to a distance of $\sim$3 kpc, or a distance modulus of 12 mag along the galactic plane.

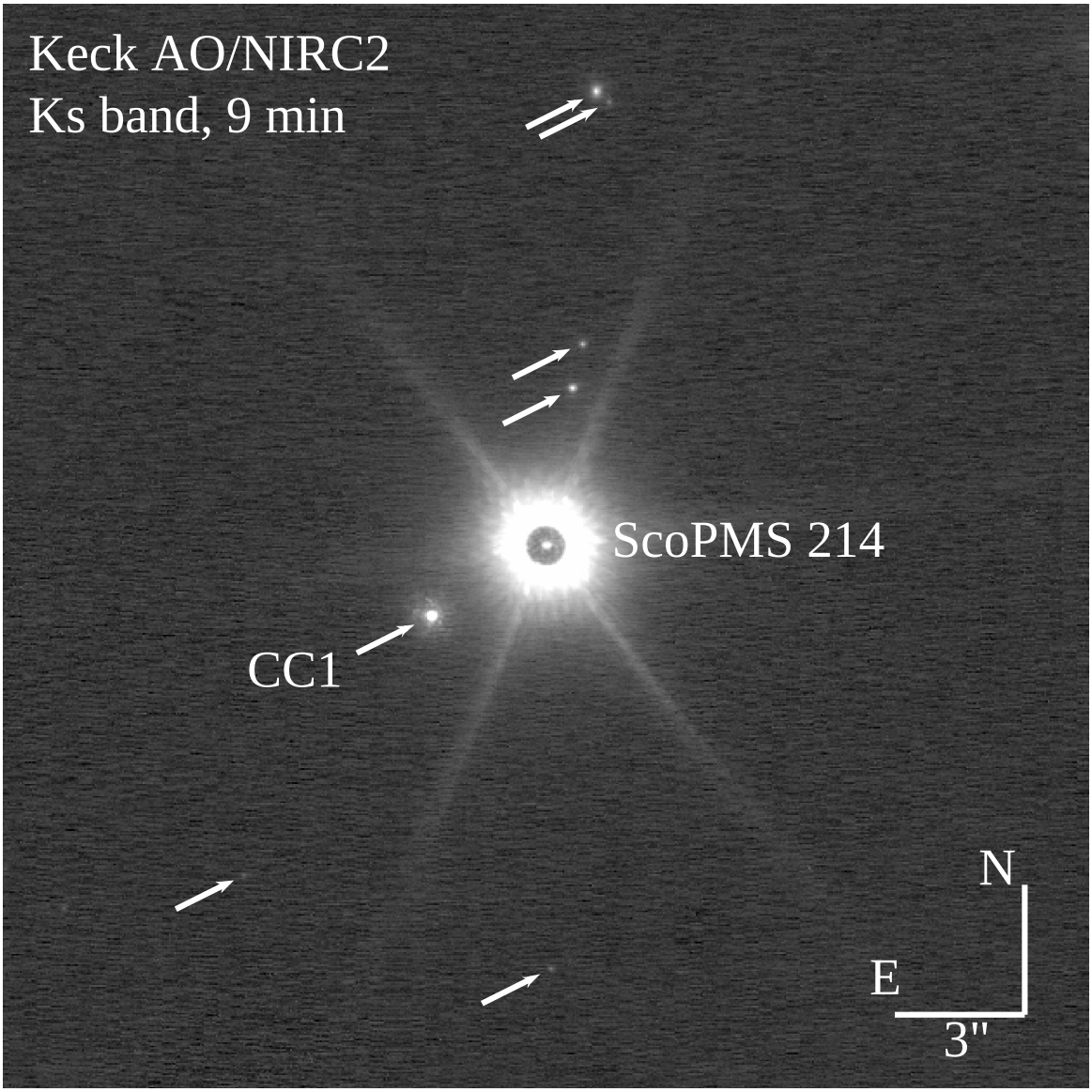

FIG. 8.— K_S-band image of ScoPMS 214 and its candidate companions taken with NIRC2 and the Keck AO system on 5 June 2004. The image is the median of nine 60 s exposures. ScoPMS 214 is occulted by a partially transmissive 1.″0-diameter circular coronagraphic mask. The seven $\rho \leq 12.''5$ candidate companions listed in Table 8 are pointed out with arrows. The candidate proper motion companion CC1 is the brightest of the seven and closest to the star.

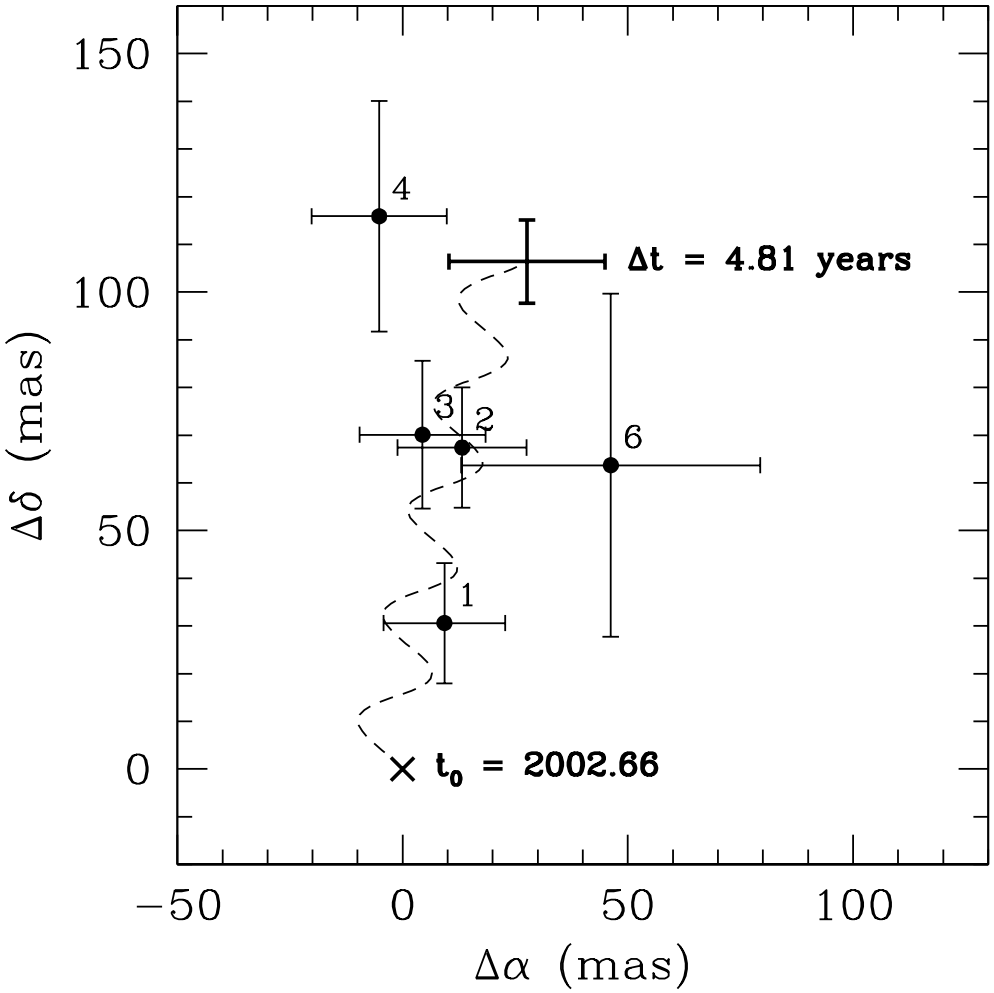

FIG. 9.— Proper motion diagram for candidate companions to ScoPMS 214, spanning the $\Delta t = 4.81$ yr time period between the first and last epochs of observations, between 30 August 2002 ($t_0 = 2002.66$ yr) and 23 June 2007. The dashed line denotes the expected relative motion of a stationary background object with respect to ScoPMS 214 between the initial epoch (marked with $\times$) and the final epoch (marked with thick errorbars without a solid point). The solid points with thin errorbars denote the observed changes in the relative positions of candidate companions 1, 2, 3, 4, and 6. Candidate 5 was outside of the field of view of the medium ($20'' \times 20''$) NIRC2 camera during the last epoch of observations, and candidate 7 was below the detection limit during the initial epoch. Candidate 1 is ScoPMS 214"B", which shares the proper motion of ScoPMS 214 during the 4.81-year time span within 3σ limits and is inconsistent with being a stationary background object (at the 5σ level in declination). Candidates 2, 3, and 4 (and 7, based on observations at intermediate epochs) are all inconsistent with being proper motion companions to ScoPMS 214 and are consistent with being background objects. Candidates 5 and 6 are consistent with being either bona fide companions or unrelated background objects, i.e., their status is undecided.

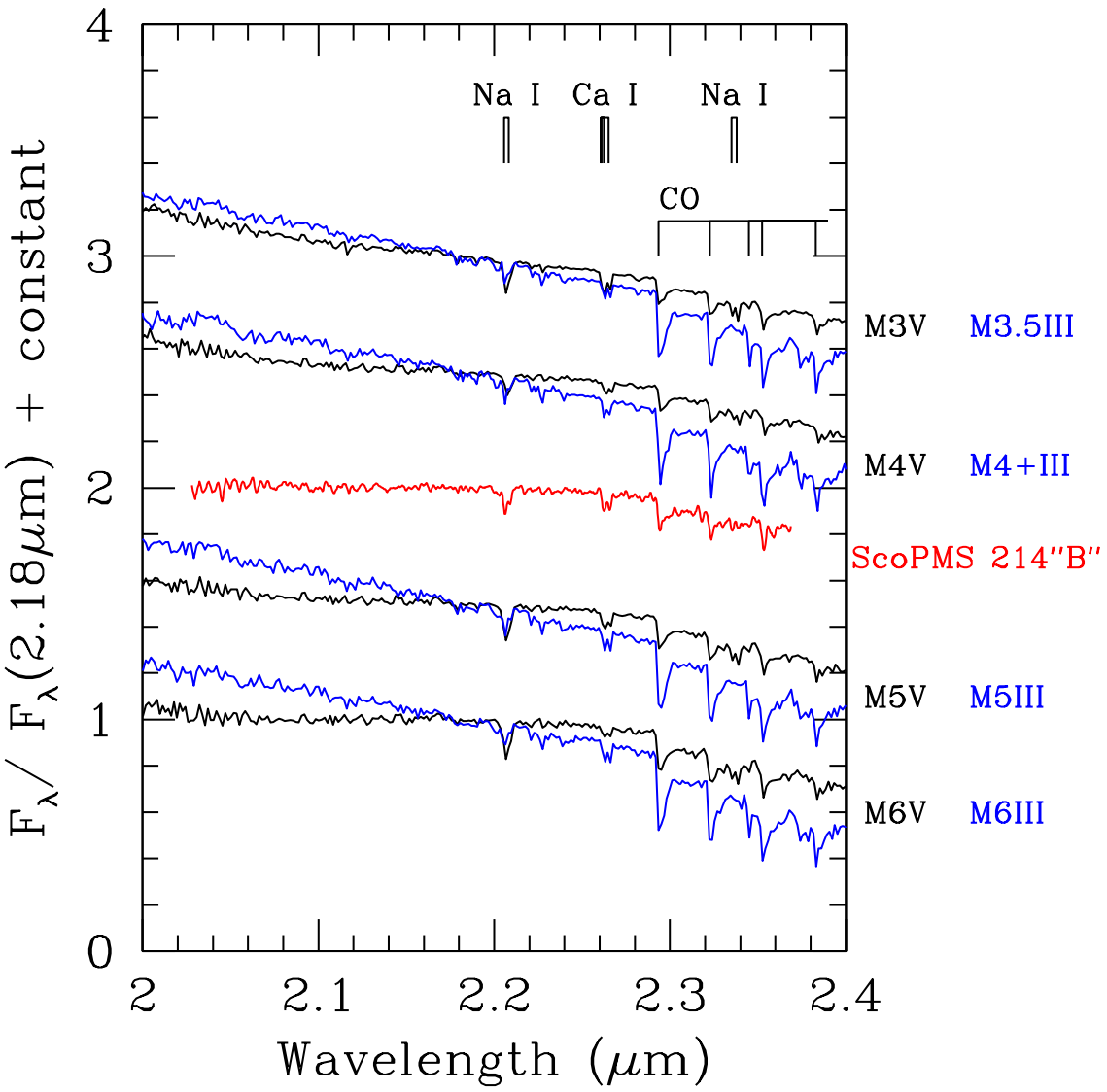

FIG. 10.— K-band spectrum (red) of ScoPMS 214"B" (CC1), compared to spectra of M3–M6 field dwarf (in black) and giants (in blue) from the IRTF Spectral Library (Cushing et al. 2005; Rayner et al. 2008), smoothed to the same $R \approx 1200$ resolution. Dominant absorption features by Na I at 2.21 μm (doublet) and 2.34 μm (doublet), Ca I at 2.26 μm (triplet), and CO bandheads at $\lambda \geq 2.29$ μm are identified. The comparison dwarf spectra are of Gl 388 (M3V), Gl 213 (M4V), Gl 51 (M5V), and Gl 406 (M6V), and the giants are HD 28487 (M3.5III), HD 214665 (M4+III), HD 175865 (M5III), and HD 196610 (M6III).

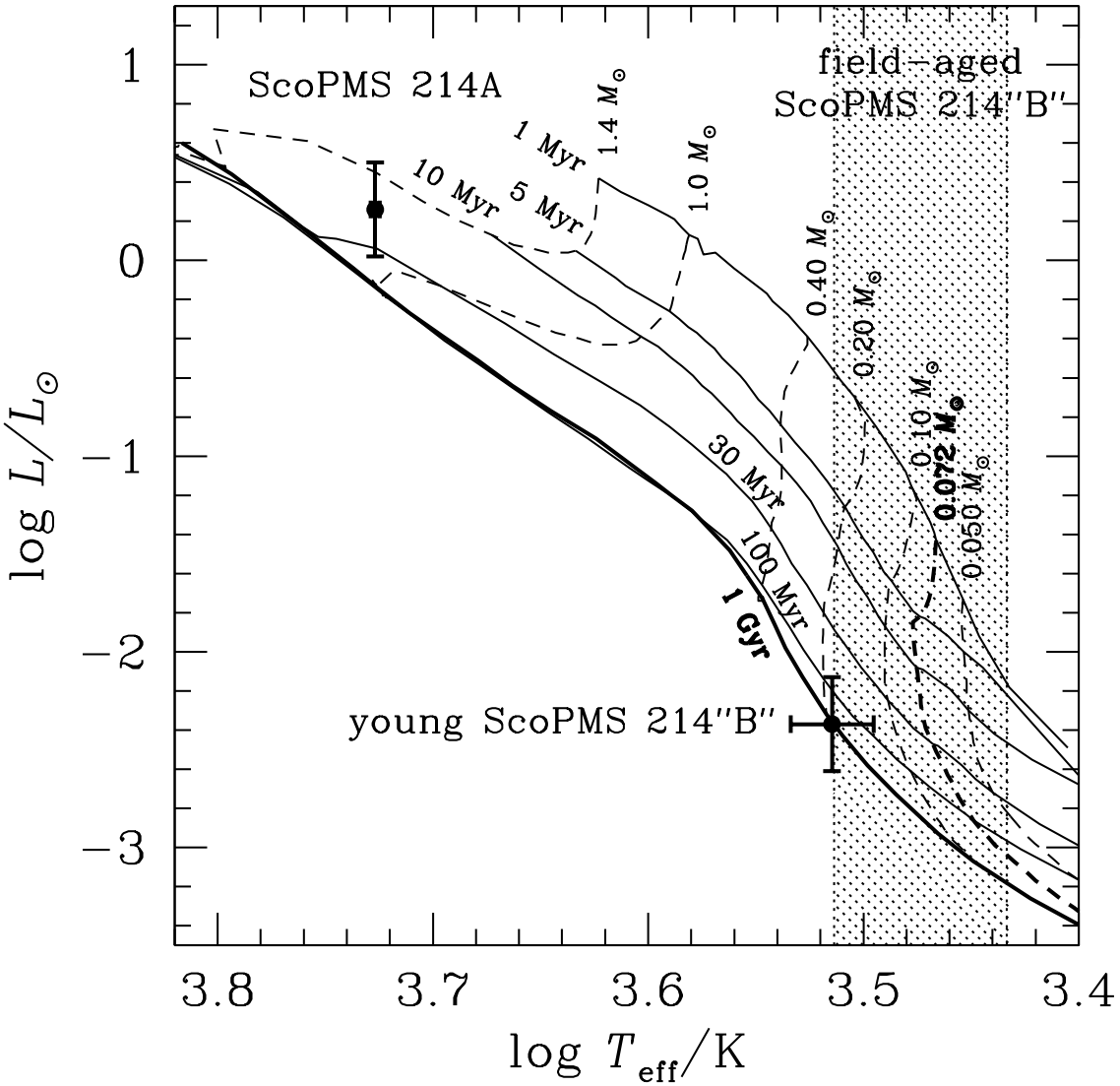

FIG. 11.— HR diagram of the candidate binary ScoPMS 214A"B" with evolutionary models for 0.05–1.4 $M_\odot$ objects from Baraffe et al. (1998). The continuous lines are isochrones and the dashed lines are evolutionary tracks at constant mass. The thick (1 Gyr) isochrone approximates the main sequence, and the thick evolutionary track corresponds to the minimum hydrogen-burning mass. The positions of ScoPMS 214A and "B" under the assumption of equidistance and membership in Upper Scorpius (the "young" ScoPMS 214"B" scenario; § 6.3.2) are shown with solid points with errorbars. The shaded region represents the range of effective temperature allowed for ScoPMS 214"B" if it were an unassociated field-aged (1–10 Gyr) M dwarf. Since in the "young" scenario the candidate binary components do not lie on the same theoretical isochrone, ScoPMS 214"B" is probably not a member of Upper Scorpius. Instead, it is most likely a foreground field M dwarf.

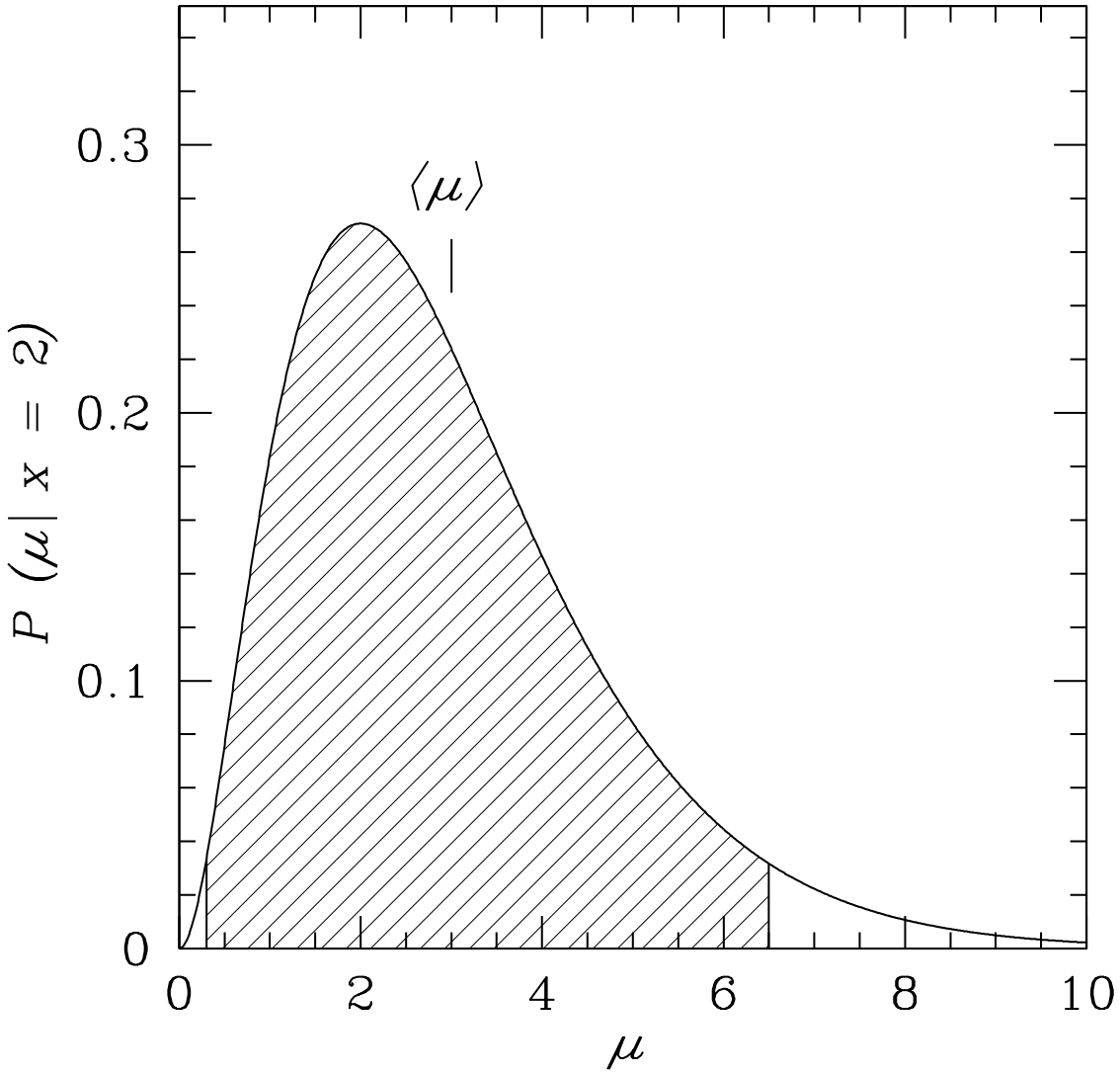

FIG. 12.— Probability density distribution $P(\mu|x = 2)$ for the expected substellar companion detection rate in our survey per 100 stars, given $x = 2$ detections. The curve is a Gamma distribution (Eqn. 5), with a peak at $\mu = \mu_{\rm ML} = 2$, but a mean value of $\langle\mu\rangle = x + 1 = 3$. The minimal 2σ (95.4%) confidence interval on $\langle\mu\rangle$, $0.3 < \langle\mu\rangle < 6.5$ is indicated by the shaded region under the curve.

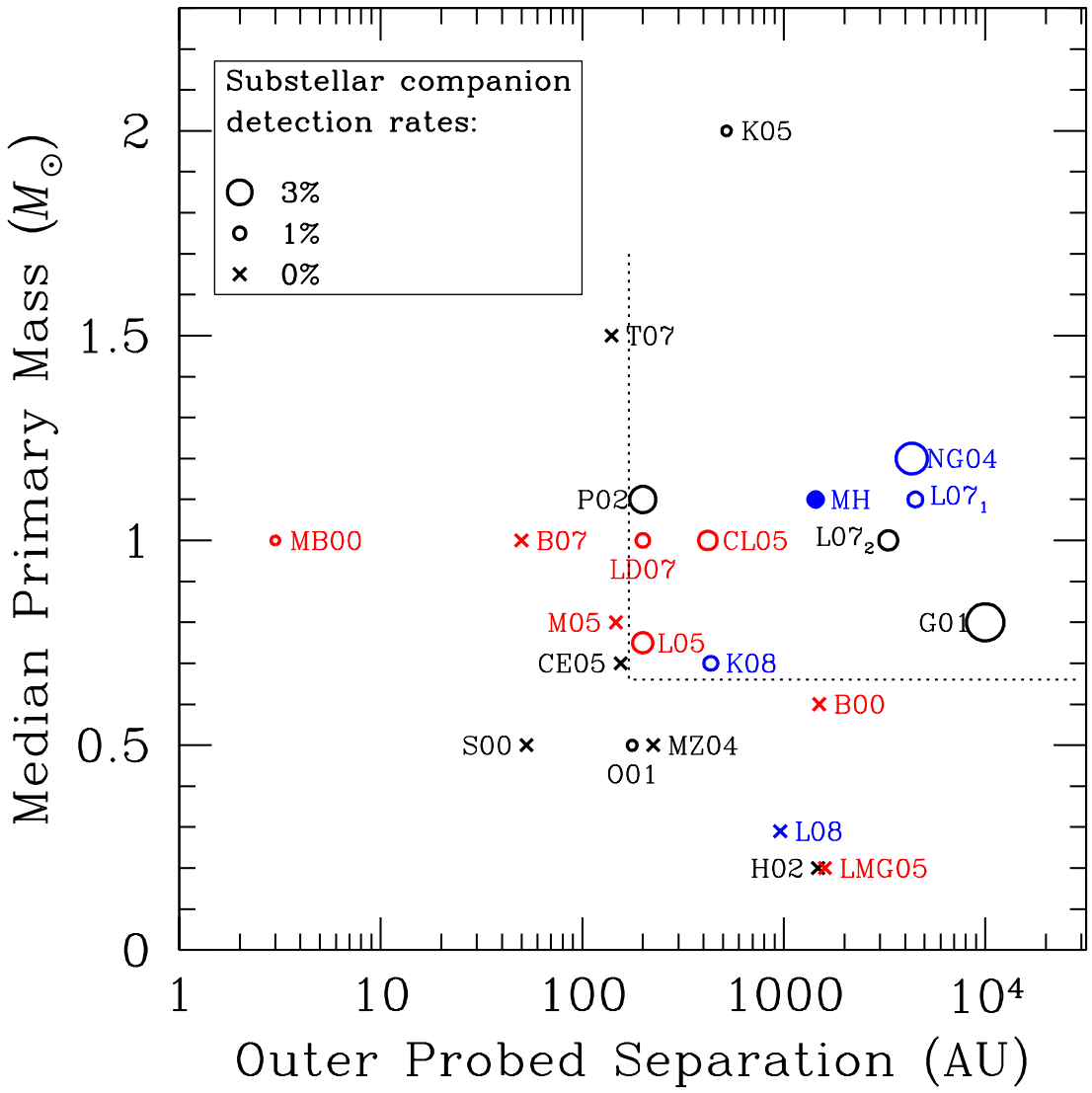

FIG. 13.— Substellar companion detection rates of the published direct imaging surveys listed in Table 12. Circular symbols denote surveys with at least one detection; crosses denote surveys with no detections. The filled circle denotes the present work. The size of the circular symbols is proportional to the survey detection rate prior to corrections for survey incompleteness. Black symbols denote the least sensitive surveys, with $\geq 30 M_{\rm Jup}$ median companion mass sensitivity in the background-limited regime. Blue symbols denote surveys with median companion sensitivities between 13–30 $M_{\rm Jup}$. Red symbols mark surveys with the highest sensitivity, $< 13 M_{\rm Jup}$. The survey labels are as listed in the penultimate column of Table 12. The locus delimited by a dotted line contains only surveys with non-zero detections, with detection rates ranging from 0.5–5%. All surveys outside of this region have detection rates $\leq 0.6\%$.

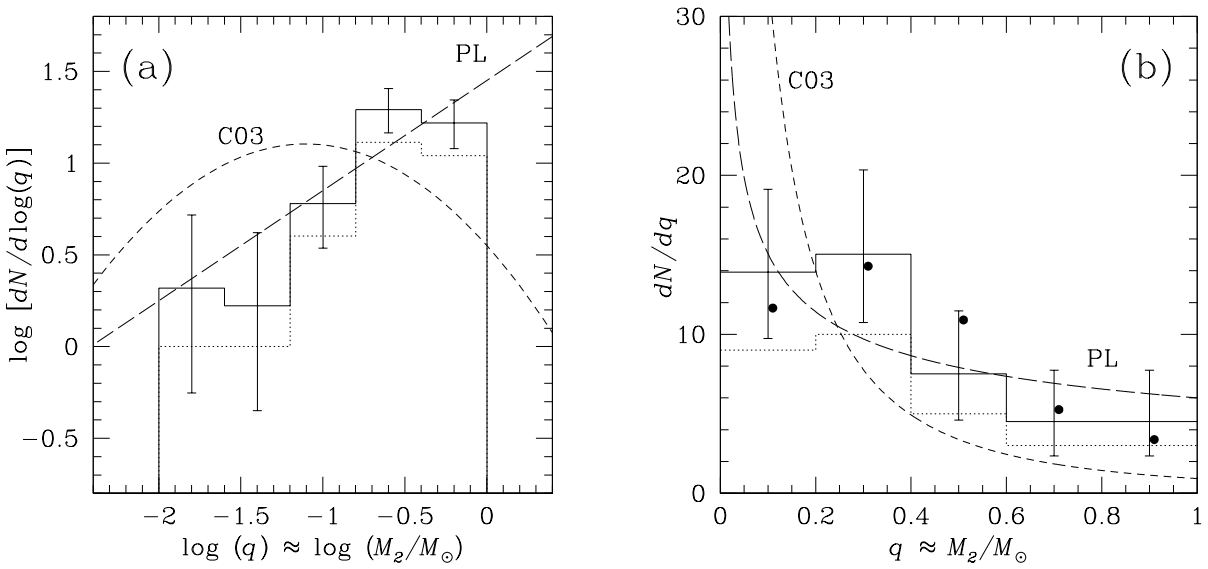

FIG. 14.— Mass ratio distribution for the 30 $\leq$0.5 Gyr-old binaries in our AD_{30} sample (see § 9.1) in terms of $\log(dN/d\log q)$ **(a)** and dN/dq **(b)**. The dotted histogram traces the observed data, while the solid histogram delineates the incompleteness-corrected data. Further incompleteness due to bias against near-equal binary systems exists in the highest mass ratio bin, but has not been taken into account in the present incompleteness correction. The long-dashed line is a power-law (PL) fit to the data, $dN/d\log q \propto q^{\beta+1}$, with an index of $\beta = -0.39 \pm 0.36$ (1σ limit). The short-dashed line represents the log-normal MF of field objects from Chabrier (2003, C03) in units of $M_\odot$, normalized to the incompleteness-corrected data. We note that because the primary masses for stars in our sample are $\approx$1 $M_\odot$, then $q = M_2/M_1 \approx M_2/M_\odot$. The log-normal field MF peaks at $\mu = 0.08 M_\odot$ and has a width of $\sigma = 0.69$ (in logarithmic mass units). The Salpeter index in these units is $\alpha = -2.35$. The solid points in panel **(b)** are the incompleteness-corrected data from Duquennoy & Mayor (1991), normalized to our data. The Duquennoy & Mayor (1991) data have been offset slightly to the right from ours for clarity.

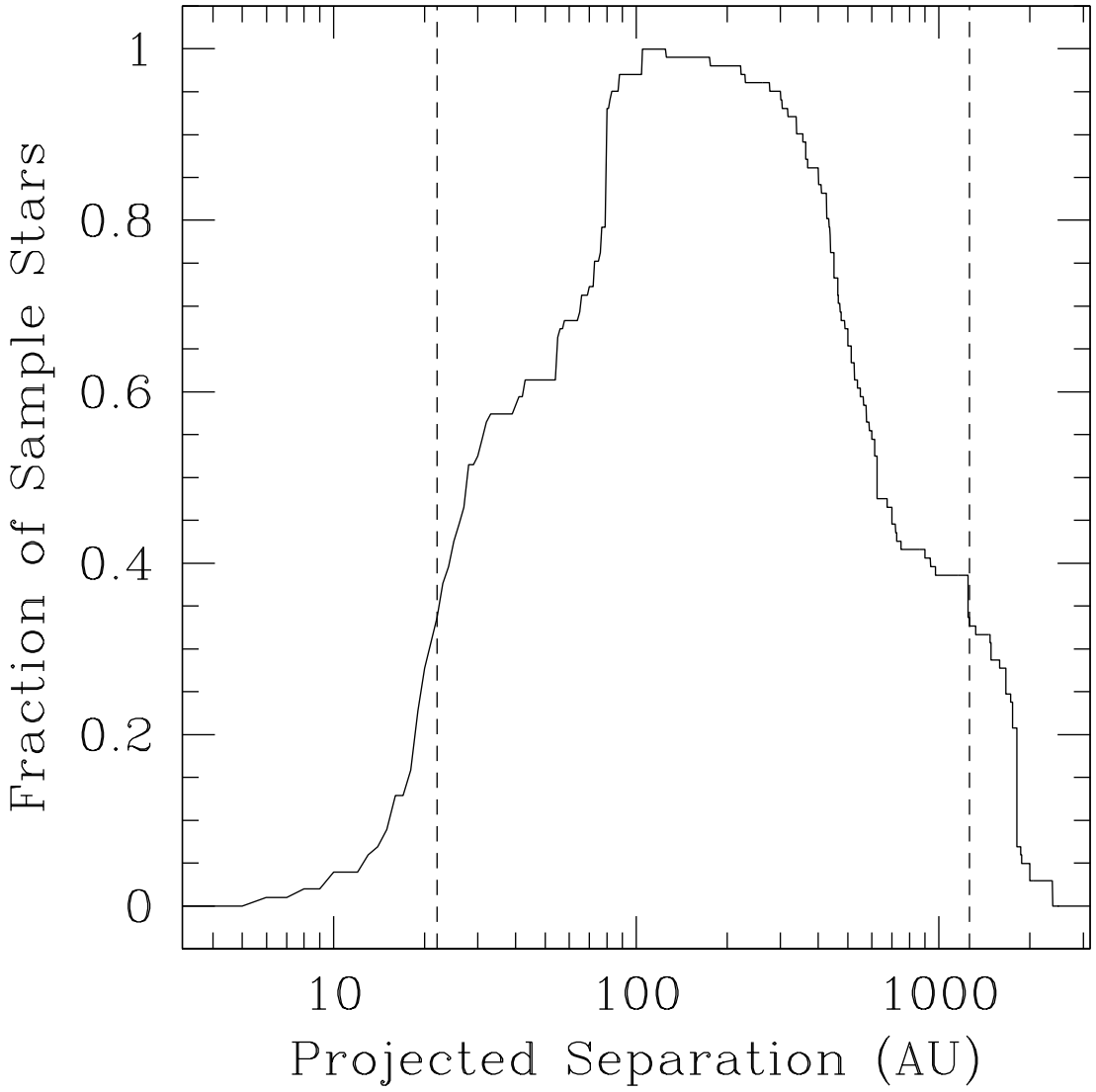

FIG. 15.— Projected physical separations probed in the deep sample survey. The vertical dashed lines delimit the region, 22–1262 AU, in which each 1 AU-wide projected separation interval was probed around at least one third of the stars in our deep sample. The geometrical incompleteness factor for this region is 1.40. That is, 1/1.40 = 71.4% of all companions in the 22–1262 AU projected separation range should have in principle been detected, had their visibility not been limited by contrast.

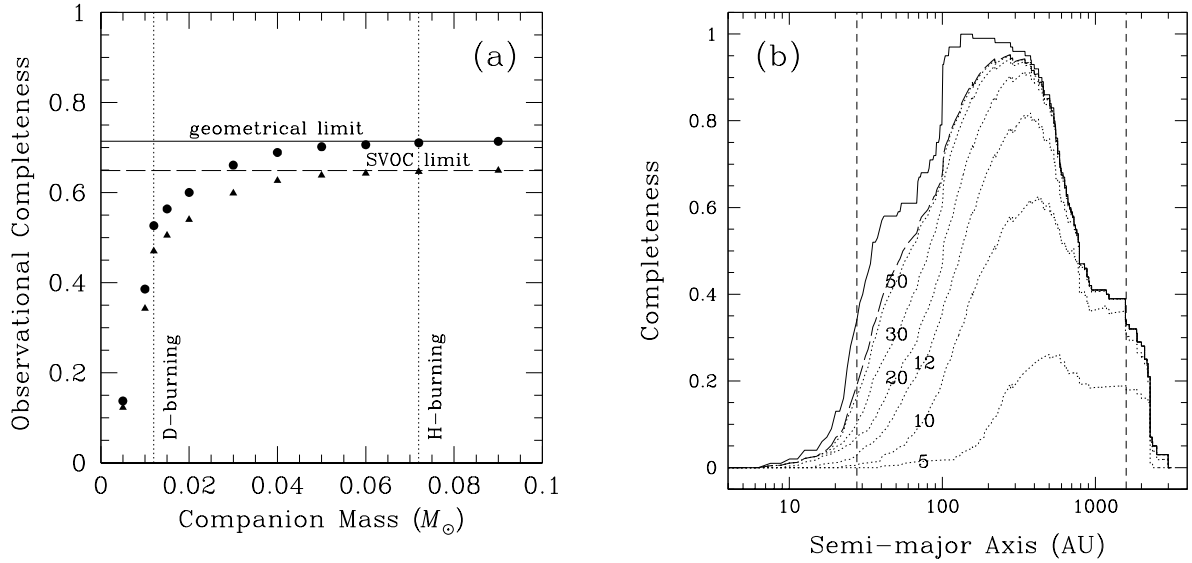

FIG. 16.— **(a)** Observational (circles) and total (triangles) completeness of the deep survey as a function of companion mass. The observational completeness at a given mass is the fraction of companions of that mass that would be detectable within a projected separation of 22–1262 AU from all sample stars (§ A.3.2). The total completeness is defined similarly, but for a 28–1590 AU range of *semi-major axes*, and after consideration of orbital incompleteness (§ A.3.3). Both sets of completeness fractions are calculated assuming a logarithmically flat distribution of companion semi-major axes a (§ A.2). The horizontal lines delimit the maximum possible observational (continuous line) and orbital (long-dashed line) completeness at any given mass over these AU ranges. Our definition of the orbital completeness coincides with the "single visit obscurational completeness" (SVOC; see § A.3.3) defined by Brown (2004). The vertical dotted lines mark the deuterium- (D) and hydrogen- (H) burning mass limits. **(b)** Same as Figure 15, but for the expected semi-major axes (rather than projected separations) of substellar companions and for a range of companion masses. The dotted lines are labeled with substellar masses in units of $M_\odot/100$. The solid curve delineates the geometrical completeness limit and the long-dashed curve, the SVOC limit (cf. panel a). The vertical short-dashed lines have been adjusted from their positions in Figure 15 to correspond to the expected range of semi-major axes, 28–1590 AU, corresponding to the 22–1262 AU projected separations probed by the survey.